An experimental investigation into ALS uncertainty and its impact on environmental applications

GRAHAM STEPHEN STENSON

An experimental investigation into ALS uncertainty and its impact on environmental applications

Thesis submitted for Master of Science

Department of Geography, Durham University

Graham Stenson 2014

i. ABSTRACT

This study takes an experimental approach to investigating the reliability and repeatability of an airborne laser scanning (ALS) survey. The ability to characterise an area precisely in 3-D using ALS is essential for multi-temporal analysis where change detection is an important application. The reliability and consistency between two ALS datasets is discussed in the context of uncertainty within a single epoch and in the context of well known point- and grid-based descriptors and metrics. The implications of repeatability, verifiability and reliability are discussed in the context of environmental applications, specifically concerning forestry where high resolution ALS surveys are commonly used for forest mensuration over large areas.

The study used a regular 10-by-10 layout of standard school tables and decreased the separation from 2.5 metres apart to 0.5 metres in order to evaluate the effects of object separation on their detection. Each configuration was scanned twice using the same ALS scanning parameters and the difference between the datasets is investigated and discussed.

The results quantify uncertainty in the ability of ALS to characterise objects, estimate vertical heights and interpret features / objects with certainty. The results show that repeat scanning of the same features under the same conditions result in a laser point cloud with different properties. Objects that are expected to be present in 40 points per metre^2 laser point cloud are absent, and the investigation reveals that irregular point spacing and lack of consideration of the ALS footprint size and the interaction with the object of interest are significant factors in the detection and characterisation of features.

The results strongly suggest that characterisation of error is important and relevant to environmental applications that use multi-epoch ALS or data with high resolution / point density for object detection and characterisation.

Keywords: LiDAR, Uncertainty, Object Detection

ii. List of Figures

iii. List of Equations

iv. List of Tables

v. Contents

vi. Acknowledgements

I would like to acknowledge the support of Network Mapping for the initial data collection; this was made possible through the funding of One North East and the Friends of Chopwell Wood. Further thanks go to NERC ASRF for the collection of the table study data and the subsequent processing and advice provided. My thanks go to Network Mapping Ltd for the financial support for the project and the invaluable help and insight of my friends and colleagues at Network Mapping whom have listened and supported me throughout this project. Special thanks go to Alex Peters for her motivation and kind words throughout the project. Finally, I would like to express my appreciation of the support and supervision offered by Professor Danny Donoghue who has helped and supported me throughout this project.

vii. Glossary

Accuracy	The closeness of an observation/measurement to its true value (see bias, precision and uncertainty)
ALS	Airborne Laser Scanning, a general term for airborne LiDAR surveys, also the name of the Leica Scanner
ALTM	Airborne Laser Terrain Mapper, the name of the Optech Airborne Laser scanning systems
Bias	The tendency of a set of observations / measurements to over or under estimate the true value (see also, accuracy, precision and uncertainty)
CHM	Canopy Height Model, forested digital surface model with the digital terrain model subtracted. The results are the forest canopy heights referenced above the local ground height.
DBH	Diameter at breast height. A standardised measure of tree trunk diameter
DSM	Digital Surface Model, a model of the uppermost covering of a surface, typically includes trees, buildings and other permanent features. Non-permanent features e.g. vehicles are typically removed
DTM	Digital terrain model, a model of the ground surface, such that all above ground features are removed.

GNSS	Global Navigation Satellite System, the name given to any satellite based positioning system. Examples include GPS, GLONASS and Galileo.
GPS	Global Positioning System, American version of GNSS, the first GNSS and most commonly used.
GSD	Ground Sample Distance, the distance on the ground covered by a single pixel.
GTS	Ground Truthing Site, a ground location surveyed using accurate methods used to calibrate and validate the LiDAR scans.
IMU	Inertial Measurement Unit, a series of gyroscopes and accelerometers for determining the attitude and the accelerations of the aircraft.
Lever Arm	3 dimensional vector in the appropriate reference frame to determine the location of one object to another, for example the GNSS antenna to the IMU
LiDAR	Light Detection And Ranging, a survey technique utilising emitted laser light in order to measure features of interest.
nDSM	Normalised Digital Surface Model, a DTM subtracted from a DSM, giving the relative height of features above the ground surface
NPP	Net Primary Productivity,

PAR	Photosynthetically Active Radiation,
Precision	Precision is the closeness of obervations/measurements to each other. See also accuracy, bias and uncertainty
RADAR	Radio Detection and Ranging,
SONAR	Sound Detection and Ranging,
Uncertainty	The degree to which the measured value of some quantity is estimated to vary from the true value. See also accuracy, bias and precision

1 Introduction

This chapter seeks to outline the premise of the research (Section 1.1), before detailing the importance and therefore the wider implications in the research rationale (Section 1.2). The penultimate section outlines the overarching aim and how this will be met by outlining key research objectives (Section 1.3) before signposting key chapters within the thesis (Section 1.4).

1.1 Research Premise

The study seeks to use a high-resolution LiDAR (Light Detection and Ranging) data set to assess the suitability of LiDAR (also known as Aerial Laser Scanning (ALS)) for deriving environmental metrics by developing and testing simplified models. LiDAR data is regularly used in a number of applications that require precise, consistent and reliable topographic data. Forestry characterisation is a focal area for LiDAR analysis for environmental applications and as such, will be drawn upon to inform the work of this thesis. This thesis will look at the effects of object identification and scan reliability and verifiability in controlled and natural environments. The results from the experiments will inform best practice within laser scanning and environmental monitoring, while the discussion and conclusion will help form the basis of recommendations for the future use.

1.2 Research Rationale

Aerial Laser Scanning (ALS) is now in widespread use for environmental management. Despite this, limited work into object characterisation and repeatability of laser derived datasets is available in the scientific literature. Understanding the uncertainties associated with this form of surveying needs further research. As an example of this forestry is a significant area of interest with aerial laser survey data and as such, this study seeks to link

the uncertainties of environmental aerial laser surveying to applications including forestry. Forestry is economically, environmentally and socially important. The sustainable management of forests is vital. Forest managers need up to date, robust and accurate information to inform decision-making. Current practices rely on labour intensive, potentially dangerous and unreliable techniques. Measures of forestry using local site sampling, as the results are up-scaled to larger areas, create uncertainties in the resultant data. Remote sensing using passive sensors has come some way to answering these criticisms, but in turn can be criticised for its two dimensional approach. Forests are 3-dimensional with the vertical component revealing substantial information, the effective management of these resources relies on the Forest Manager be aware of this information to manage the resource effectively. LiDAR provides a spatially expansive 3-dimensional technique that has the potential to provide reliable, accurate and robust information to Forest Managers, in turn promoting advanced, informed decision-making. Understanding of the areas of uncertainty, reliability and the accuracy of the methodology must be better to progress these applications into mainstream way of working for foresters.

This thesis looks to explore areas of reliability, accuracy and certainty in the data capture and subsequent analysis. To do this, two experiments will be conducted, the first investigates the complex forest environment. This will be simplified and abstracted to look at the behaviour of laser scanning around regular object. The regular object will be 100 exam tables arranged on a flat school field as seen in figure 4-5. This provides a known configuration where objects are regular, consistent and provide the data necessary to assess detection. The controllable and repeatable environment will be used to explore laser-scanning characteristics. The second experiment investigates the repeated scans of the same area to observe differences. In this experiment a gravel hockey pitch will be repeatedly surveyed by the same aircraft within a time period of 1 hour. This ensures that no significant changes will occur within the area and any differences seen in the data are the result of uncertainties. The knowledge gained from this experiment will be interpreted in context of common laser scanning applications,

including engineering and environmental applications. An increased understanding of object detection by aerial laser scanning will inform the many disciplines that use ALS as a survey methodology including forestry.

1.3 Aims and Objectives

1.3.1 Aims

- The aim of this study is to investigate the uncertainty of ALS, relating to object characterisation for environmental applications

1.3.2 Objectives

1. Establish the repeatability of laser scans
2. To establish the suitability of laser-scanning to detect simple objects
3. Investigate the effects of scale and resolution on uncertainty.
4. To investigate the ability of aerial laser data to distinguish and discriminate between objects

The objectives use two experiments. The first looks specifically at object detection by focussing on the exam table study. The second uses the eight overlapping flight lines to establish the scientific rigour and reliability of laser scanning. These experiments are conducted at two sites within the Hookergate School.

1.3.3 Introduction to the Object Detection Objectives

The object detection experiment uses 100 exam tables arranged on flat ground at Hookergate School. The exam tables move from 2.5 metres apart down to 0.5 metres apart in four intervals (2.5 m, 1.5 m, 1.0 m and 0.5 m) as part of the experimental design. This will allow the study to establish the detection, resolution and coalescence of the exam tables. Object detection in this sense relates to the ability of a human interpreter with *a priori* knowledge to determine the objects presence within the dataset. As such, it must have at least one recorded laser strike at an elevation distinguishable from the ground to show its presence

1.3.4 Introduction to the Verification / Repeatability problem

The repeatability and verifiability experiment builds upon the outcomes of the object detection experiment. Repeated flights over the Hookergate school location will be used to assess this. The first assessment will use a flat gravel hockey pitch. Additionally, the same technique will be used on a small sample of forestry and of an urban area. This experiment will investigate the nature of replication/duplication and verifiability of laser scanning over a simple, urban and forested scene. Repeatability refers to the ability to capture the same objects under the same conditions and produce the same results within the uncertainty bounds of the experiment. If a result can be repeated with the same results each time the experiment is conducted, it is verifiable. This work has significant implications to the uncertainty associated with laser scanner derived analysis. Such analysis is commonplace in geographic, engineering and archaeological applications, for example DEM of difference is a common technique that assumes the changes present are real changes within the error bounds of the experiment.

Laser scanning provides a three dimensional model of the landscape scene surveyed. For this to be reliable and verifiable, the scene must be (nearly) identical for a repeat survey of

the same area. Differences because of slightly different point strike locations are expected, but at the scale of the analysis, this should be unobservable. It is important to understand the spatial scales of the artefacts (such as differences in point spacing and density) in order to prevent them affecting the resulting analysis. The artefacts may affect the analysis through the omission of objects or unexpected characterisation of the object. Whilst the laser scanner produces a point cloud, many applications use a gridded raster surface derived from the LiDAR data for the analysis. This thesis will investigate the error associated with point cloud surveys and their resulting gridded products.

A number of safety and policy critical applications have adopted laser scanning as a trusted method of survey. These applications include subsidence monitoring, deformation surveys for mining, and quarrying, deformation studies of dams and bridges, power line studies and highway engineering. As well as the safety critical applications, LiDAR surveys inform policy and management decisions. Forestry, agriculture and archaeological prospection are all activities that regularly use laser scanning.

The problem with the repeatability of a survey is that any analysis performed should be possible to replicate given the same conditions, such that others can repeat the data collection and analysis and verify results. If this basic premise cannot be fulfilled the analysis performed will be based upon data that represents a moment in time. Should a repeat survey provide different results then the confidence in the conclusion of either study diminishes.

This theory provides the rationale to investigate laser scanner behaviour at differing scales and differing landscape complexities. It also provides the motivation to investigate the effects of gridding the point cloud data for analysis

The NERC ASRF data provides an ideal dataset to investigate this topic. The flight over Chopwell Wood and Hookergate School repeated a flight line over forest, urban and school grounds eight times. This provides three ideal landscapes to investigate with eight over flights

using the same parameters and conducted over the period of an hour. Over the period of one hour, the surveyed landscape will not have changed significantly.

1.4 Thesis Structure

The thesis is organised into seven chapters. The first introduces the study and the wider context and implications of the research. Chapter 2 provides a critical review of Aerial Laser Survey applications to forestry. Throughout the thesis, forestry is used as an example of wider environmental applications of Aerial Laser Scanning. Chapter 3 investigates the characterisation, operation and behaviour of aerial laser systems. The study site and methodology are described in Chapter 4, with Chapter 5 presenting the results of the study. The findings are discussed in Chapter 6 and conclusions, recommendations and impacts of the study are presented in the final chapter (Chapter 7).

2 A Critical Review of the use of Aerial Laser Scanning in Forestry

The purpose of this chapter is to introduce the use of ALS for environmental applications, specifically this will focus on forestry. Whilst the experiments do not focus specifically on forestry, this does provide a useful narrative for the implications of uncertainty and error in ALS datasets. Laser scanning is a widely adopted technique for forest modelling and mensuration. As such, it is important to investigate the uncertainties of ALS as a technique and as the application matures, so does the understanding of errors and uncertainties associated with the data collection. Whilst forestry is a core theme to this chapter, parallels with many other complex environments that benefit from surveying with LiDAR are reviewed and discussed. Such applications include the remote sensing of lowland raised bogs (Anderson *et al*., 2010), surveying of geomorphic and hydraulic processes (French*,* 2003) and ecology (Michez *et al.,* 2013).

Sustainable forest management is most effective when informed by good data (Barrett *et al.,* 2016). Forest mensuration is difficult due to the spatially expansive nature of a forest, the difficult access and the inherent remoteness of large forests (Coops *et al.,* 2007). Sustainable management aims to conserve and enhance forest biodiversity (Forestry Commission, 2012). Whilst forest management varies between countries and between organizations, the UK has maintained a Biodiversity Action Plan since 1994 as an outcome of the 1992 Rio de Janeiro Convention on Biological Diversity (JNCC, 2012). After devolution in 1998, a UK wide action plan was no longer appropriate; instead, the countries of the UK had individual plans. Whilst each country recognized the unique landscape that it managed, the reports emphasized the need to work together to enact the plans. July 2012 saw the publication of the UK Post-2010 Biodiversity Framework (JNCC and Defra, 2012). These plans outline the management techniques employed for managing UK Forests. Notably the plan strives for mixed age and type of trees to promote structural diversity. Structural diversity promotes biological diversity, mixing young trees through to mature and deadwood trees creating a range of habitats for

species to thrive (Ishii *et al.,* 2004). Brokaw and Lent (1999) describe structural diversity as a proxy for biological diversity.

2.1 Forest Structure

Forest canopy structure provides a critical insight into the functional processes and characteristics of tree growth, Structural metrics can reveal important information on the forests' response to both natural and anthropogenic forcing at the full variety of scales including individual tree, stand, community, and ecosystem level (Parker *et al*., 2004; Rhoads *et al,.* 2004). Horizontally and vertically, the arrangement of forest canopies can be shown to strongly control the absorption of photosynthetically active radiation (PAR) and subsequently overall stand net primary productivity (NPP) (Chasan *et al.,* 1991; Chen *et al.,* 2004; Hall *et al.,* 2005). Forest structure is an important factor in the suitability of the habitat for a number of birds, mammals and other fauna as well as a control on understorey flora (Franklin *et al.,* 2002; Mackinnon, 2003; Van Pelt and Nadkarni, 2004; Ishii *et al.,* 2004) Structure also plays an important role in the management of forest fires (Morsdorf *et al.,* 2004)

2.2 Remote Sensing for Forestry

Remote sensing has a long history associated with environmental applications. Remote sensing has long been a tool for mapping land use and extracting variables from the landscape not visible to the naked eye. Aerial photography provided the initial spark of interest during the application of airborne espionage during the First World War, over the next 60 years remote sensing developed to produce satellite imagery, multispectral imagers, hyper-spectral imagers and active sensing techniques including SONAR, RADAR and LiDAR (Campbell, 2007).

2.3 LiDAR

2.3.1 LiDAR Applications

Light Detection and Ranging (LiDAR) is a remotely sensed topographic mapping technique using a laser fired from a platform and measuring the return to work out the distance. LiDAR is a form of active remote sensing in that it creates the energy source that it measures (Campbell 2007; Lillesand *et al*., 2008). It takes direct contactless measurements of the incident surface using a laser pulse. ALS has an extensive history in applications involving high-resolution terrain models; these applications include but are not limited to the large spatial extent, national elevation models such as the Swiss National Elevation Dataset (Federal Office of Topography 2012).

At a regional extent, LiDAR has many applications such as city modelling (Axelsson, 1999), flood inundation mapping (Neal *et al*., 2009; Neal *et al*., 2011), forest canopy height models (Gaveau and Hill, 2003; Pitkänen, 2004), digital terrain models (Ussyshkin and Theriault 2011) and archaeological prospection (Devereux *et al*., 2005; Challis, 2006 Chase *et al*., 2011). Looking at the sub regional and local scales, high-resolution, low spatial extent data applications include digital documentation (Barber, 2007) and many engineering applications. Such applications notably include power line engineering (Usshikin *et al.*, 2011) but also with applications to the rail industry (Hardy *et al.,* 2012), roads and oil and gas processing plants. LiDAR has also shown use in disaster planning and response such as the recent use of bathymetric LiDAR for the planning and delineation of shipping lanes for Port Au Prince Harbour, Haiti (Roe, 2010) and in tsunami hit Fukushima, Japan (Butcher, 2011) and in the planning and preparation for tsunami (Aguiar, 2010).

Aerial laser scanning has a relatively short history from the discovery of the laser to the common mapping technique used today. Throughout this history, it has rapidly evolved to

become a useful and powerful mapping tool with many end applications. These applications each require the accuracy and spatial expansiveness that aerial laser surveying provides.

2.4 Aerial Laser Scanning for Forestry

This section provides a critical appraisal of the literature on forest structure analysis using aerial laser techniques. Initial exploration of the mechanics of laser interaction with the forest canopy are discussed, these factors are relevant regardless of analytical approach. The importance of spatial scales are considered and explored with individual tree versus stand based modelling techniques described and reviewed. Methodological differences in processing are highlighted through the exploration of point cloud filtering literature. This chapter concludes with a breakdown of the current state of laser scanning for key forest variables.

2.4.1 Interaction of the Laser with the Forest Canopy

The forest canopy represents a complex structure for the laser footprint to strike, should the whole footprint not strike a single object, part of the beam may be reflected back to the scanner with the remainder travelling onwards ready to reflect off a more distant object (Baltsavias, 1999; Wehr and Lohr, 1999; Amable *et al*., 2004). This is not the only factor affecting the interaction of the laser with the forest canopy. Harding *et al.,* (2001) and Hofton *et al.,* (2002) found that increasingly dense vegetation tends to cause multiple scattering and absorption of the LiDAR pulse resulting in fewer ground returns, this effect is seen to increase with increased canopy closure, canopy depth and complexity, due to the obscuring of the laser pulse. Gaveau and Hill, (2003) showed that small footprint LiDAR (less than 1m) tends to penetrate the crown before returning. Ground returns decrease as scan angle increases, due to the increasing depth of canopy the laser seeks to penetrate (Kalogirou, 2006). Laser beam divergence affects penetration with narrower beams tending to penetrate the canopy

where larger footprints reflect off the surface of the canopy (Naesset, 2004). The altitude of the scanner above the forest also has an effect, altering the distribution of laser returns from the top of the canopy and within the canopy (Naesset, 2004). The distribution of the laser returns also alters with changes to the pulse repetition factor (Chasmer *et al*., 2006). A practical demonstration of the above factors was shown by Goodwin *et al.,* (2006) in a study using three different altitudes above ground (1000, 2000 and 3000 meters), two scan angles at 1000m (10^{o} and 15^{o}), and three footprint sizes (0.2, 0.4 and 0.6m at nadir) for three Eucalyptus Forest test sites. The study found that higher altitudes result in a lower combination of first and last return couples and as such found higher altitude flights to be less suitable for determining forest structure. As increased altitude results in a lower point density, it also results in a lower likelihood of a crown strike; shown by the underestimation of tree heights seen at higher altitudes. Other factors also have an effect on scanning the forest structure but cannot be changed easily in the flight planning stage. The method of echo detection used, trailing edge, leading edge or constant fraction discriminator can all affect the likelihood of over or underestimation of the forest structure parameters (Wagner *et al.,* 2004). Full waveform scanning will overcome some of these challenges, allowing the user greater control over the detection algorithm used (Stilla and Jutzi., 2009), however, the expensive data storage and significant processing overheads prevent this being used as a mainstream technique. System design is an important aspect with the sensitivity of the laser receiver, wavelength of the emitted laser pulse and laser power all having an effect (Baltsavias, 1999) The characteristics of topography have an impact, particularly through backscatter characteristics (Baltsavias, 1999). Transmissivity (the degree of impedence to transmission) of the laser pulse is dependent on system transmissivity and atmospheric transmission characteristics (Wagner *et al*., 2006)

2.5 Individual tree versus Stand based approaches

LiDAR investigations into forestry takes two distinct approaches, the individual tree approach and the multiple tree or stand approaches. With the increasing resolution of scanners, a move

from the holistic landscape approach to a more reductionist individual tree approach can be seen (Lim *et al.,* 2003)

Individual tree characteristics are best described using their dimensions and attributes. Common metrics include tree height, diameter at breast height, and upper diameter (*e.g*. diameter of tree at 4 metres), height of crown base (such as lowest green branch), species, age, location, basal area, volume or leaf area index (Hyyppa *et al*., 2009). These metrics are traditionally taken in the field using Hypsometers, DBH tapes and borers. LiDAR based approaches typically look to finding tree locations, tree locations with crown size attributes or full crown delineation (Poulieot *et al*., 2002). Tree locations can be detected using local maxima filtering (Friedlander and Koch, 2000; Brandtberg *et al.,* 2003). Minima filtering Perrson *et al*., (2002) or segmentation approaches can be used for additional details about the tree crown attributes (Hyyppa *et al*., 2009). Full crown delineation using region growing techniques and reconstruction of the point cloud is another method (Hyyppa *et al.,* 2009).

Stand based analysis typically uses larger reference data sets and lower density data. In areas of dense forestry, individual tree approaches can lead to an underestimation of stem counts. Stand based analysis typically relies on larger reference data sets and statistical inference techniques (Hyyppa *et al*., 2009). Stand based characteristics typically include, tree densities (number of trees per hectare) mean diameter, basal area per hectare, mean diameter, mean height, dominant height (typically the mean height of the 100 trees per hectare with the largest diameter at breast height). Lorey's mean is another method used that weights the measures based on the cross sectional area of the tree, as such larger trees have a dominant weighting (Hyyppa *et al.,* 2009)

Villika *et al.,* (2007) used a novel approach to improve the quality of an individual tree based inventories, using laser height distribution characteristics of individual trees combined with more traditional parameters of individual tree recognition such as height and diameter at breast height measures for improving the prediction of individual tree stem volume. This study

did use approximated tree height and crown diameters for the constructed models (direct measurement and Finnish Standard model) but the lower height quantiles and corresponding crown densities hold some additional statistical explanation for the tree characteristics.

The two most often used ground-captured variables to characterize the vertical and horizontal canopy structure are canopy closure and leaf area index (LAI). Canopy closure, defined as the fraction of the sky no longer visible due to foliage within a stand (Lefsky *et al.,* 1999). Whilst being a relatively fast technique and computationally simple, this method is subjective and imprecise (Rhoads *et al.*, 2004). LAI ($m^2\ m^{-2}$), is typically defined as the ratio of the single sided surface area of leaves to the projected ground area (Barclay and Goodman, 2000; Lefsky *et al*., 1999) and has proved useful in measuring the impacts of natural and anthropogenic disturbances on forest ecosystems (Rhoads *et al.,* 2004). The direct measurement of LAI can involve destructive sampling of the canopy (Gower and Norman, 1991), the use of litter fall traps, and the measurement of individual leaf area using planimeters (Rhoads *et al.*, 2004)

2.5.1 Models and Point Clouds

Different techniques make use of different models. Typically digital terrain Models (DTM), digital surface models (DSM), normalised digital surface models (nDSM) and canopy height models (CHM) are used. The DTM represents the bare earth terrain with all above ground objects removed; this is where LiDAR is particularly strong being able to return a ground model from beneath a forest (Baltsavias, 1999; Wehr and Lohr, 1999; Pfeifer and Mandlburger, 2009). DTMs can be expressed as a raster structure (a regular grid), or using triangular irregular networks (a vector structure) or using the last return of the point cloud, or ground filtered point cloud. The DSM gives a representation of the above ground surface, typically taking the order of a first return model or alternatively using the highest point within a grid, again to produce a raster grid or triangular irregular network. A normalised DSM is the DSM minus the DTM (equation 2-1) as such it is the difference model of the DSM to DTM.

This has the advantage that all features within the model are referenced relative to ground height rather than the height above the datum. As such, tree crowns are extracted as tree height.

$$nDSM_{xy} = DSM_{xy} - DTM_{xy}$$

Equation 2-1 shows the per pixel location subtraction that takes place to produce a normalised digital surface model.

2.5.2 Ground Filters

Differentiating point clouds between ground and non-ground allows for effective derivation of the digital terrain model. Ground detection is typically an automated algorithm used to filter the ground points. A variety of ground filters exist, from the simplistic to the complex (Pfeifer and Mandlburger, 2009). At its simplest, a ground filter may filter the last and only returns of the LiDAR scanner. This is problematic, as the last return does not always refer to the ground; it may be lower vegetation, a building, an open manhole cover or have undergone the effects of multipath error. Multipath error is the effect of a signal reflecting from a surface giving an apparent path length that is longer than the direct path length. As such, more complex filtering is necessary. Rasterisation provides the basis of some techniques; this seeks to turn the irregular point cloud into a raster structure, allowing the operation to come into the more familiar image-processing realm. Rasterisation results in a loss of precision through the generalisation process (Axelsson, 1999). The rasterisation divides the irregular point cloud into regular cells. This results in the need for some generalisation by averaging of the elevation counts for that cell, maximum height, minimum height, mean height or median height all provide a solution, the complexity of the gridded terrain being the control on the degree of

error being introduced. Morphological filters provide an alternative, using maximum admissible height differences in the ground model over a set distance, taking a Pythagorean approach to deriving planimetric distance. The maximum admissible change in height over that distance provides a filter of whether the area represents ground. Larger planimetric distances permit larger changes in filter height, and the converse is true for smaller planimetric distances (Vosselman, 2000).

Progressive densification provides an alternative means of ground classification. The filter works by iteratively using the lowest cell that is not classified as ground as its start point and progressively densifying the ground point network through subsequent iterations, the densification is governed by limits of the angle between ground points (similar to the morphological filter) (Axelsson, 2000; Kobler *et al*., 2007; Pfeifer and Mandlburer, 2009).

Surface Based filters work in an opposing way to progressive densification, these filters assume all points belong to ground and work to filter off the none ground points. As such, the DSM is constructed and eroded to leave the DTM.

Segmentation based filters provide a further alternative. These work by building segments of point cloud that are homogenous and analysing segments as opposed to the individual points. The segmentation approach then uses a region growing technique to grow the ground model. The region growing is defined by setting a change in height over distance or through setting parameters on the normal vector that defines the segments. Filin and Pfeifer (2006) provide an example of this filter that runs on flat terrain in the first instance before filtering the rougher terrain in subsequent iterations. The ISPRS Working Group III conducted tests presented in Sithole and Vosselman, (2004). The evaluation used qualitative and quantitative analysis of twelve datasets processed using eight different filters. The test found that all filters worked well in relatively flat rural areas, and ran into an increasing number of problems in complex urban areas. The test also shows that the filters are insensitive to point densities for the given range within the test.

2.6 Forest Metrics

This section introduces practical forest metrics that are increasingly derived from LiDAR data. The use of these techniques relies upon accurate and reliable ALS data.

2.6.1 Tree Counting

Friedlaender *and Koch*., (2000) used discrete return small footprint LiDAR to map crowns using a local maxima filter, and subsequent minima filters to identify areas of single crowns, this technique works well on dominant crowns, but the filter can omit sub dominant trees. A more recent attempt that uses a stand-based approach is presented by Tesfamichael *et al*., (2009) who used a semi variogram approach to estimating stems per hectare for a eucalyptus forest. The study found that the use of the semi variogram technique is very scale dependent. The study sought to identify the ideal window size for local maxima filtering of the CHM. Using spatial resolutions of 0.2, 0.5 and 1m for the CHM, results in accuracies of 73%, 56% and 41% respectively, showing the predictive capacity of the semi variogram to increase with finer spatial resolutions. The study showed that the technique typically underestimated the number of stems per hectare, probably due to problem of identifying the sub dominant crowns. The main advantage of this approach is the elimination of the need for prior knowledge regarding the tree stocking of the plantation.

2.6.2 Tree heights

Derivation of tree heights is highly dependent on correct local filtering (Vosselman, 2000; Lim *et al*., 2003; Hyyppa *et al*., 2009). Takeda, (2004) showed that in dense forests the digital terrain model might be 10 to 20 m out. Tree height estimates typically use the local maxima that identify tree height and subtract the DTM at that point to produce the tree height. Most studies find tree heights are underestimated (Persson *et al.,* 2002; Yu *et al.,* 2004).

Underestimation relates to the point density, the higher the density the closer to the true value. Current thinking links this higher density to the increasing likelihood of a crown strike (Hyyppa *et al*., 2009). Given the complexity of factors including sensor, system design, flight altitude, forest type and ground detection algorithm, it is unlikely that a universal correction factor can be established (Hyyppa *et al.,* 2009). Even with these limitations Naesset and Okland, (2002) assert that laser derived tree heights are more accurate than existing non-destructive methods.

2.6.3 Canopy Height

Canopy height is a stand-based characterisation that extracts different tree heights, different studies have used non-parametric or regression models for estimation of tree height, basal area and stem volume (Naesset, 1997; Lefsky *et al.,* 1999; Means *et al.,* 1999; Naesset, 2002). Naesset, (2002) estimated a series of canopy height and density metrics using a two stage field procedure, looking at the use of the percentile of the first pulse for canopy heights, and the proportions of first and last laser pulse hits to look at density. Canopy tree height forms a strong predictor of other forest attributes, such as biomass and volume (Lim *et al.,* 2003)

2.6.4 Forestry and Uncertainty

The study of forestry structure and measurement using aerial laser survey techniques is advanced and provides significant benefit to the users of the data. Many of the studies report good accuracy and precision of their studies and techniques and as such, LiDAR is reported as a suitable tool. Many studies however do not take into account the sources of error associated with the data used. The studies assume that laser scanners behave in similar

ways and that derived datasets such as digital terrain models are produced consistently by different software or data providers. Chapter 3 explores this in more detail.

2.7 ALS in Forestry and uncertainty studies

The literature reviewed within this chapter show that the work on forestry applications for aerial laser surveying is well developed. The work is gaining complexity, moving from simple approaches of stem counting and subsequent allometric extrapolation, towards more complex structural metrics. As the complexity of the application increases, so too does the need to understand the data being used for the analysis. Work towards this understanding is beginning to emerge with Luscombe *et al.,* (2014) providing an interesting analysis of 0.5 metre LiDAR derived DSM's for the investigation of upland ecosystems. Fisher and Tate (2006) showed that the digital elevation models are a fuzzy concept, with need to consider both the conceptualisation of the surface being measured as well as the accuracy of the measurement. Chu *et al.*, (2014) extend this work looking at stochastic simulation to identify the effects of uncertainty of spatial features with respect to sample size. However, the work to date concentrates on the derived surface models and the uncertainty rather than the point cloud uncertainty. This study will focus on the effects of point cloud uncertainties.

3 Sources of uncertainty in Aerial Laser Survey data

This chapter focusses on the specifics of ALS methodology and metrology. LiDAR techniques are rigorously reviewed and described in order to identify sources of uncertainty. The LiDAR system is described through its component subsystems: the sensor head; Global Navigation Satellite System (GNSS); and Inertial Measurement Unit (IMU). Processing and filtering techniques are described and appraised with respect to their influence on uncertainty.

3.1.1 LiDAR Components

The LiDAR scanner consists of three component parts, a Global Navigation Satellite System (GNSS), an Inertial Measurement Unit (IMU) and a scanner head (Baltsavias, 1999). Figure 3-1 shows a diagrammetric representation of these systems. GNSS such as GPS provide a constellation of satellites that provide signals that once decoded by the receiver can locate the receiver in 3-dimensional space. Differentially post-processing the signal against a base station can provide an accurate (circa 0.02 m) 1 Hz kinematic GPS track. The IMU works using a series of accelerometers to measure the roll, pitch and yaw of the aircraft at a high frequency (typically 200 Hz). The IMU and post processed GNSS tracks are filtered using a Kalman algorithm before being merged to provide a trajectory for the rover, which is the aerial platform. The accuracy of this trajectory is a function of the GNSS quality and the IMU performance characteristics (Wehr and Lohr, 1999; Petrie and Toth, 2009; Wehr, 2009; El-Sheimey, 2009).

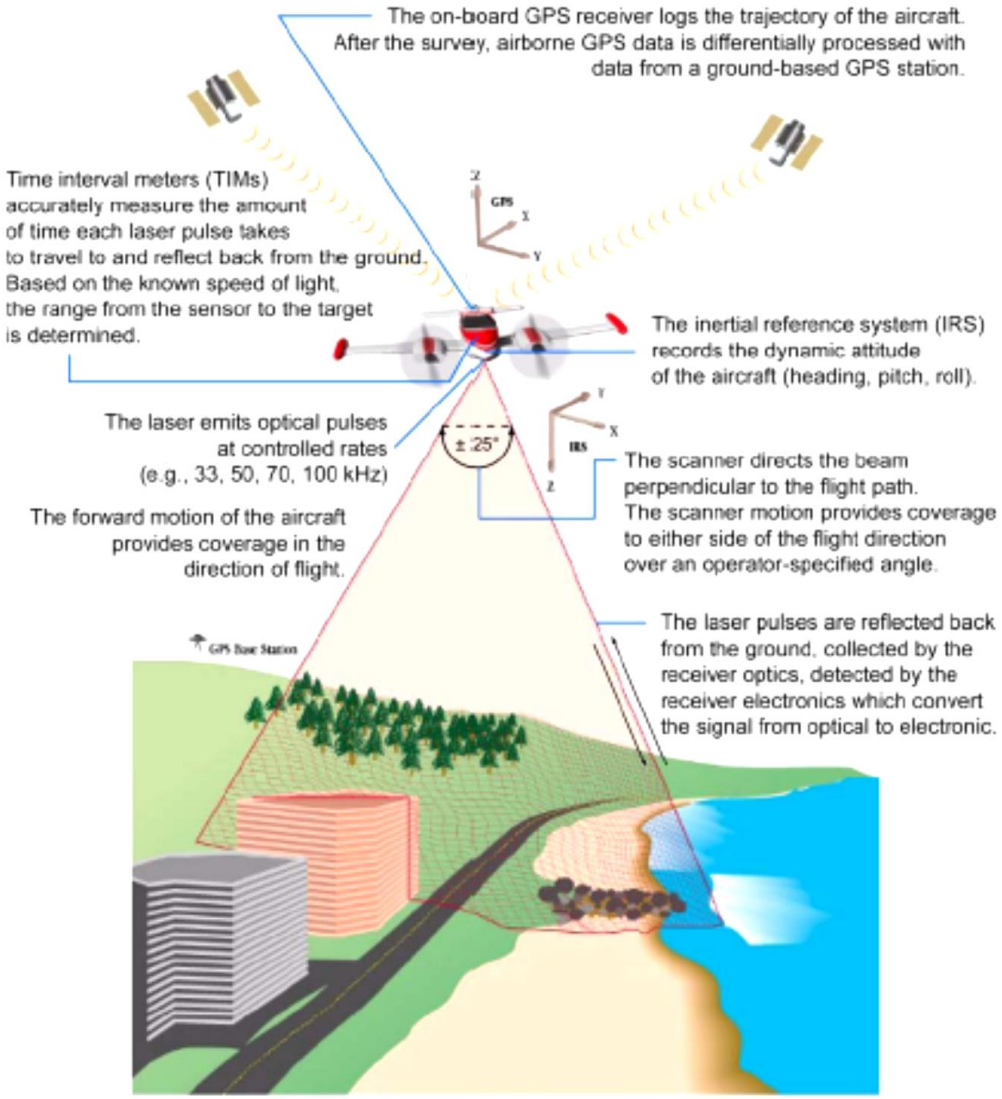

Figure 3-1 Diagram representing an Aerial Laser Scanner. Note the Inertial Reference System is a synonymous term with Inertial Measurement System. Optech Incorporated (2006).

3.2 Sensor Head

The sensor head provides the mechanics of pulse emission, recording and direction. Whilst it does not take positional data from the aircraft, it does record a time stamp for each pulse

that correlates with the GNSS timing signals. The sensor head varies between manufacturers, but includes a laser, a mirror or fibre optic arrangement along with a pulse-recording unit.

3.2.1 Pulse Emission

Pulse emission is the result of firing a laser beam. The laser is typically in the order of 1064 nm in order to provide optimal spectral response from the landscape limiting the laser energy lost to absorption and backscattering (Baltsavias 1999). A variety of methods of pumping the laser to emit the energy can be used. Diodes typically which use Q switching is a popular method of producing sufficient energy. Q switching uses a shutter to delay the release of energy stored in the pulse until it reaches a very high power (Petrie and Toth, 2009). Figure 3-2 shows the schematic form of the pulse emission system.

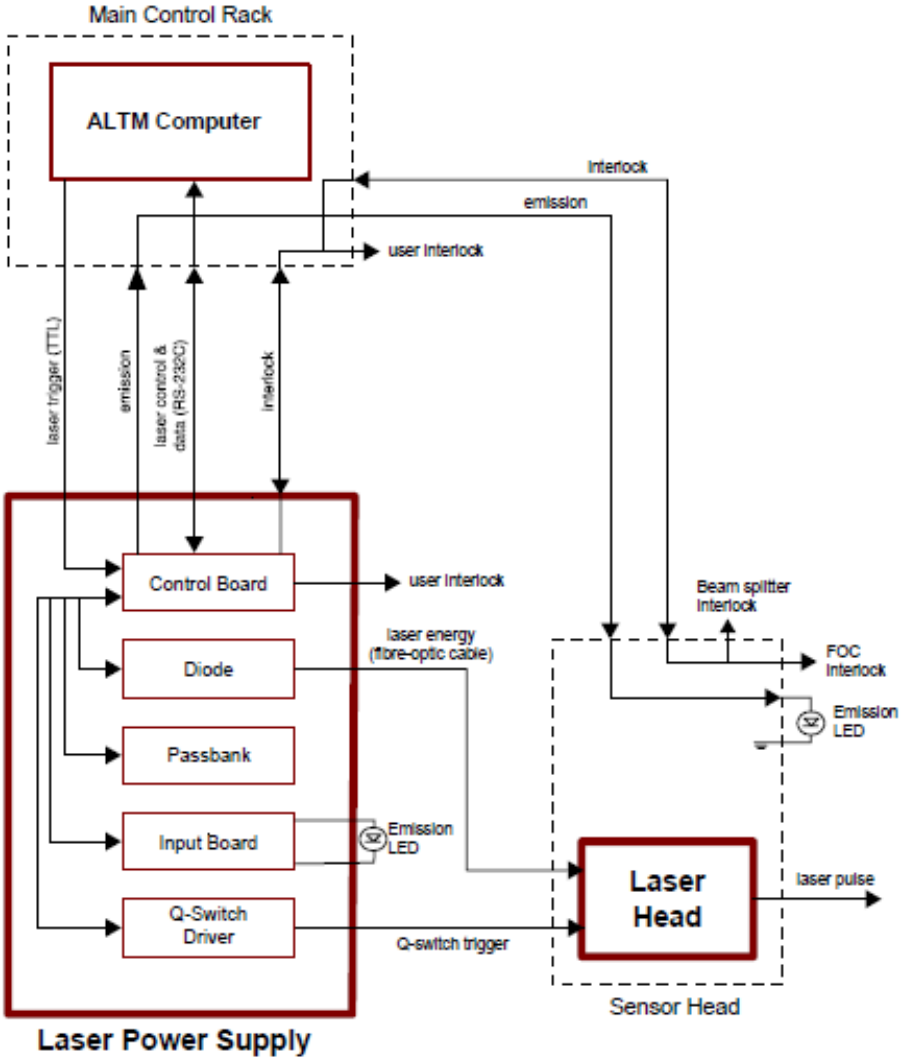

Figure 3-2 Diagram showing a typical arrangement of laser pulsing technology. Note the Q switching used to achieve higher emission energies. Source Optech Incorporated 2004

3.2.2 Mirror Operation

The mirror arrangement subtends the emitted laser pulse through a series of angles to give a larger field of view. The mirror system used depends on the manufacturer. Different mirror arrangements allow for different scan patterns on the ground. Oscillating mirrors produce

fewer scans at nadir and an increasing number as the angle approaches zenith, this can be modelled using simple harmonic motion (Baltsavias, 1999). Oscillating mirrors fall broadly into two categories: saw tooth patterns, and, sinusoidal patterns (Petrie and Toth, 2003). These patterns are the result of mirror movement patterns but the names are the result of the characteristic scan pattern seen in the data. An alternative pattern is Palmer scanning; this nutating (a rocking motion) rather than oscillating mirror system provides scans fore and aft of the scanners location resulting in redundant measurements. This system is not a common scan pattern despite the scientific merit of sampling each area twice to provide a redundant and thus more reliable point cloud. Figure 3-3 and figure 3-4 provide a diagrammatic overview of the alternative mirror systems.

The aim of laser scanning is to take measures from the area of interest. This area of interest is typically nadir of the aircraft (especially in corridor applications). The oscillating mirror systems provide fewest points at nadir concentrating the point density instead at zenith. The zenith point is furthest away from the area of interest and is where accuracy suffers from the limb effects of high scan angles. High scan angles have a greater path length through the atmosphere and strike the surface with an elliptical footprint that has a greater surface area than its nadir counterpart.

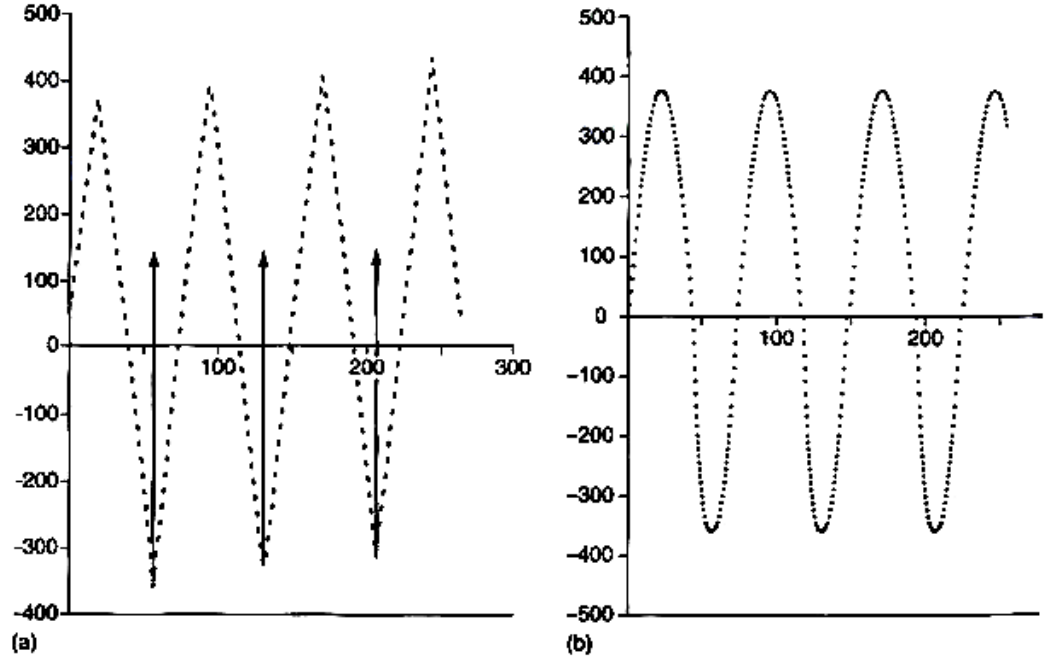

Figure 3-3- Showing a comparison of the scan patterns between a saw tooth (Optech) pattern (left) and Sinusoidal (Leica) pattern (right). Taken from Petrie and Toth (2003) pp 44

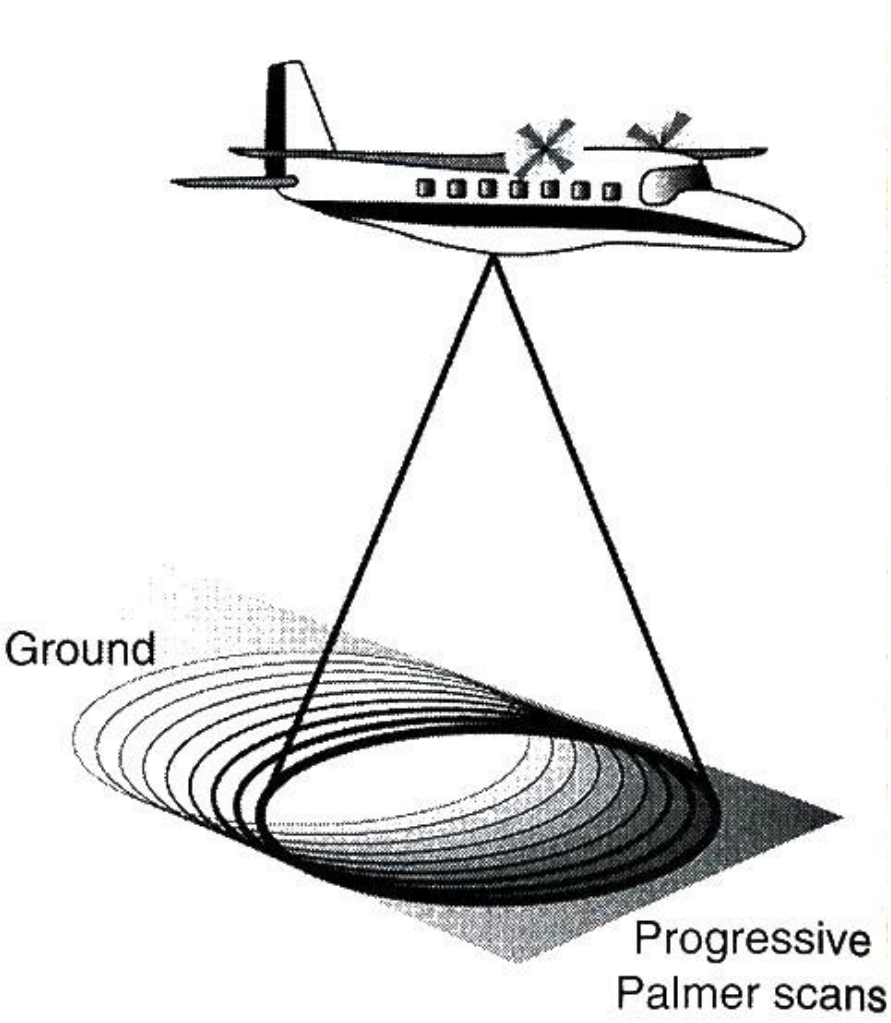

Figure 3-4 Showing the scan pattern produced by a rotating mirror resulting in redundant scan measurements. Taken from Petrie and Toth (2009) pp 46

3.2.3 Pulse Measurement

An emitted pulse provides the energy to interact with an object; the subsequent returned pulse is measured as either a comparison of the phase difference of the emitted and returned light, or the time of flight of the laser pulse. Phase difference scanners are highly accurate but only operate over a short distance, typically less than 100 m, although ScaLARS, the University of Stuttgart research scanner is a notable example of phase based aerial laser scanning (Petrie and Toth, 2009 ; Wehr and Lohr, 1999); as such for topographic mapping the time of flight

measurement is used (Petrie and Toth, 2009). The phase comparison works based on the principle that a measurement wave at a lower frequency is modulated by a higher frequency carrier wave. This modulated wave is reflected back to the scanner where the signal is deconstructed through a process known as demodulation. This allows for a comparison between the emitted and returned signal to identify a phase offset. Thus, the distance is solved using ambiguity resolution calculations synonymous with those used in GNSS carrier phase calculations to give the integer number of wavelengths plus the final phase angle difference that results in the scanner to target distance. The frequency of the modulated signal varies based on controller information to allow the increase in precision of the result aiming for an exact integer waveform count.

Time of flight laser systems emit a short pulse of light; the length of this pulse affects the precision of the return with longer pulses providing lower precision (Baltsavias, 1999; Wehr and Lohr, 1999; Beraldin *et al*., 2011). This is the method employed by airborne scanners. This requires the scanner to output discrete pulses of light. In its simplest form the time taken for the pulse to reflect back from the object to the scanner is used to calculate the distance the pulse travelled based on the constant speed of light, this is then halved to give the time of flight to the object equation 3-1. A diagram showing the difference between the methods can be seen in figure 3-5.

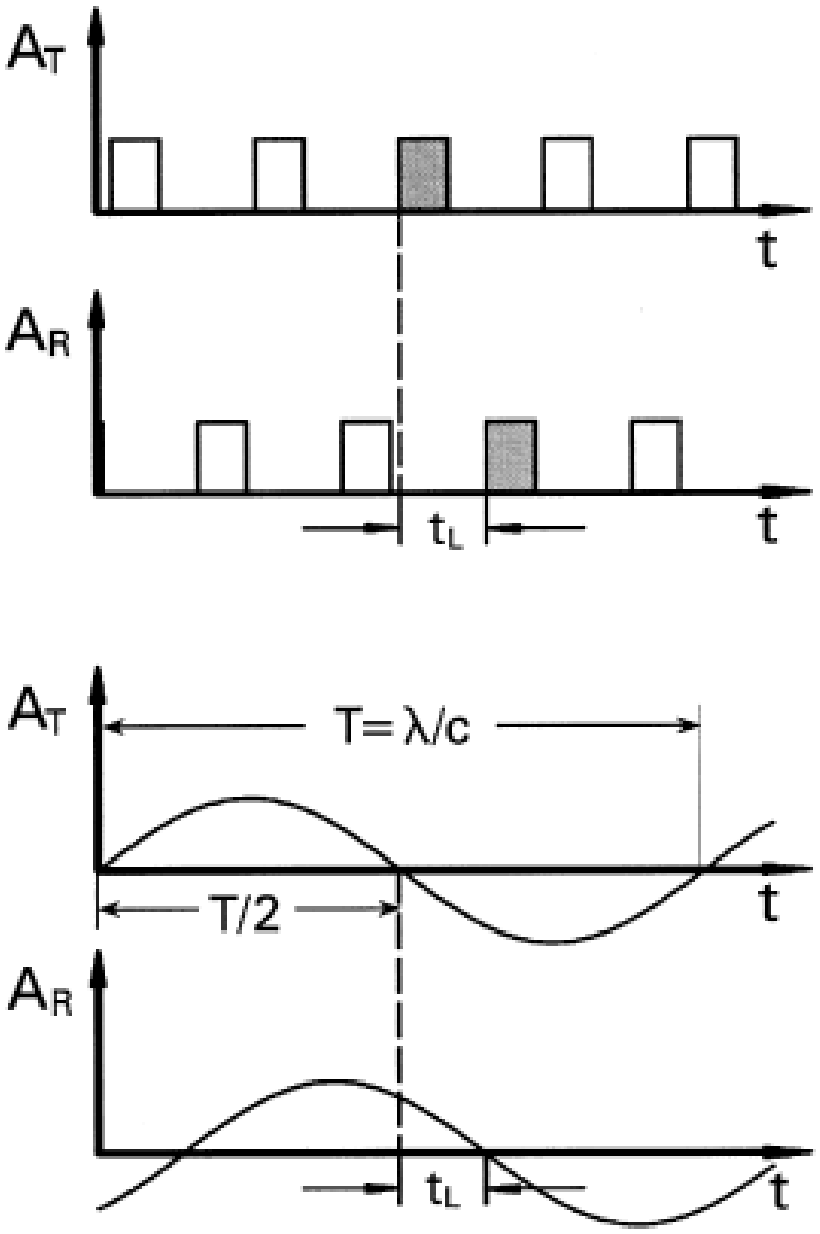

Figure 3-5 Diagram showing the difference between the time of flight method (top) and phase difference method (bottom) of determining an objects distance from the scanner. Source Wehr and Lohr, (1999) page 71

Thus, the equation can be considered as:

$$\mathrm{R} = \mathrm{c}\frac{\mathrm{t}}{2}; \Delta\mathrm{R} = \mathrm{c}\frac{\Delta\mathrm{t}}{2}$$

Equation 3-1 showing the time of flight equation. R = range, c is speed of light, t is time.

The equation 3-1 shows the principle of time of flight measurements. This combined with scan angle gives the location relative to the aircrafts perpendicular axis, for an oscillating mirror as:

$$x = \frac{c\ t}{2}\sin\theta\ ; or\ simply\ as\ x = R\sin\theta$$

Equation 3-2 showing the relationship between scan angle and the distance from nadir. Assuming flat ground and aircraft perpendicular to ground surface where t is time, c is the speed of light and R is the range of laser scan.

Alternatively, for a given flying height, the change in point spacing in the aircrafts x axis (wing to wing axis) can be given as:

$$X = h\ tan\theta$$

Equation 3-3 showing the distance from nadir for a given scan angle and flying height. Assuming flat ground and aircraft perpendicular to scanned surface.

The pulse length affects the precision of any recorded laser pulse. The pulse must be sufficiently long to give a reflection from the target of interest yet not be too long as to affect the ranging calculation. The effect is shown in equation 3-4.

$$Vertical\ Precision = \frac{pulse\ length}{c}$$

Equation 3-4 showing the relationship between vertical precision and pulse length.

Therefore, for a vertical precision of 0.01 m the pulse time would need to be 33.356 picoseconds.

Vertical precision depends in part on the pulse length but is also affected by footprint dynamics and sensor location systems (GNSS and IMU).

3.2.4 Footprint

The sensor footprint is the instantaneous field of view (iFOV) of the scanner. This important parameter determines the area sampled. The footprint is dependent upon laser aperture, beam divergence, scan angle and incident surface (Baltsavias, 1999; Petrie and Toth 2009). Figure 3-6 shows the effect of aperture, divergence and distance to target.

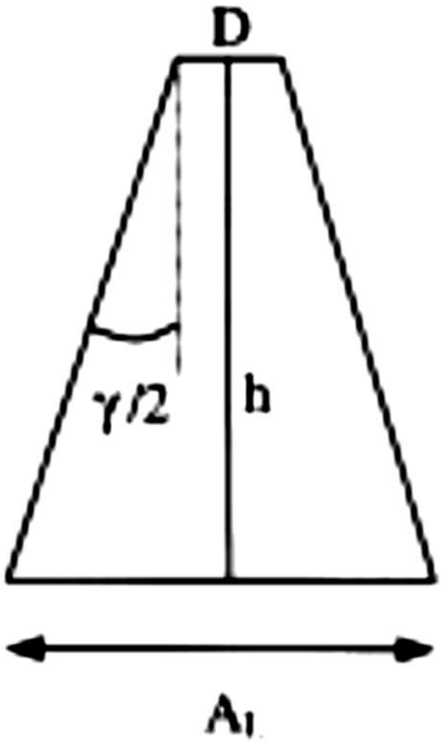

Figure 3-6 Diagram showing the effect of aperture (D), beam divergence (γ) and height (h). When the incident surface is flat. Source Baltsavias, 1999.

This gives rise to equation 3-5, showing the relation between aperture, beam divergence and flying height.

$$Footprint\ size = \ D + 2h\tan\frac{\gamma}{2}$$

Equation 3-5 showing the relation between footprint size, aperture (D), Height above ground (h) and beam divergence (gamma). Source Baltsavias, 1999.

Where the iFOV intersects with a non-perpendicular plane, the angle of incidence must be taken into account, thus giving equation 3-6:

$$Footprint = \frac{(\cos(\theta + i) + \sin(\theta + i)\tan\left(\frac{\theta + i + \gamma}{2}\right) * (2\ h \sin\frac{\gamma}{2})}{\cos(\theta - \frac{\gamma}{2})}$$

Equation 3-6 showing the relationship between instantaneous scan angle, incident plane angle (defined away from the laser beam) (i), and beam divergence (gamma). Adapted from Baltsavias, 1999

Footprint size affects the incident energy intensity on a target; as such, a larger footprint will return a less intense reflection than a narrow footprint. For a given point-density, large footprints sample a greater proportion of the ground as such a trade-off is necessary between precision and sample size.

The energy distribution across the laser footprint is not even, the peak intensity is at the centre of the footprint with the energy decreasing towards the edge. This forms a two dimensional (axis) Gaussian distribution of energy within the footprint, the circular Gaussian loss is known as a Van Mieses distribution. A diagram showing this can be seen in figure 3-7.

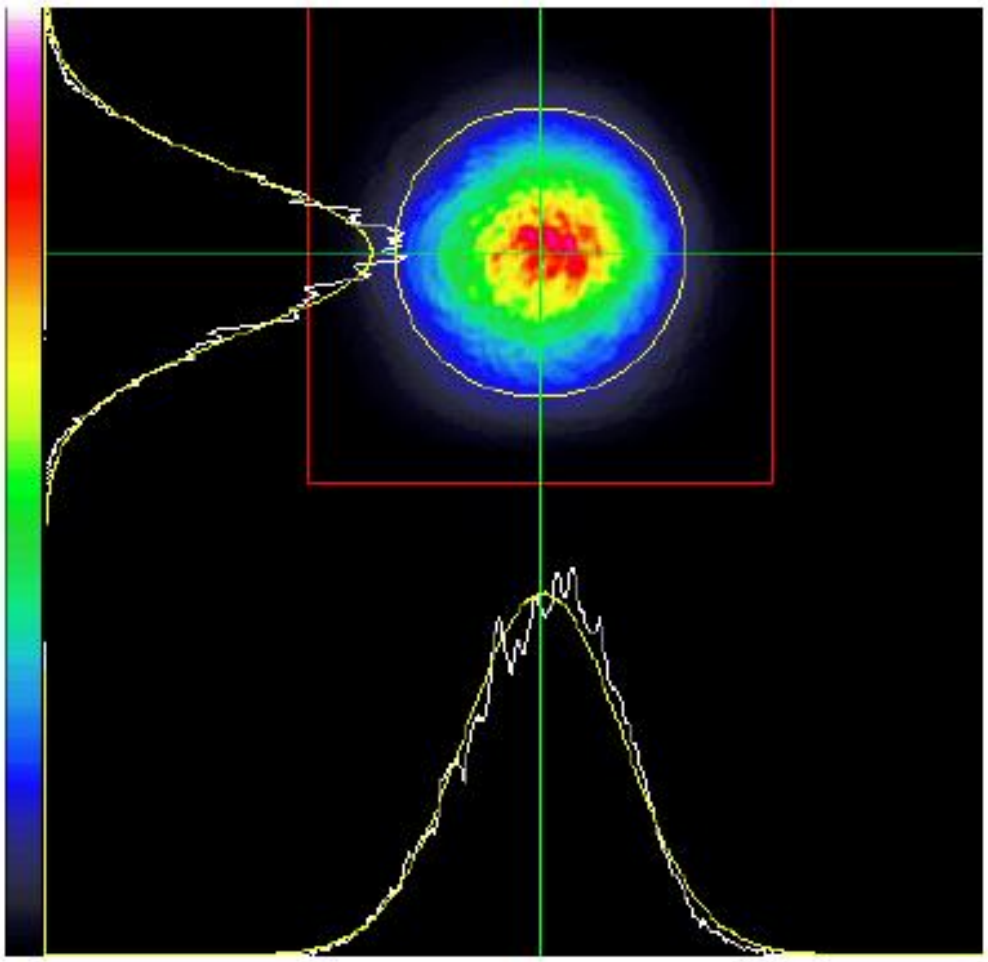

Figure 3-7 showing the Van Mieses distribution seen within a laser footprint. Source Ussyshkin (2009)

3.2.5 Pulse – Object interactions

LiDAR pulses interact with an object of interest as the reflected energy from that interaction is recorded at the scanner. The nature of the interaction between the incident laser light and the object of interest is complex. Many factors affect the interaction including reflectivity, relative beam size, incident angle, directional reflectance and emitted wavelength.

The wavelength of the emitted light is important; the wavelength should allow for atmospheric transmission and for reflection by the objects of interest, these windows are shown in figure 3-8. Whilst this spectral response is well understood within passive remote sensing, the collimated coherent light source of a laser scanner does not conform to the bidirectional models established (Harding, 2009). Although most objects are diffuse, very rarely are they truly Lambertian (Campbell, 2007; Harding, 2009) resulting in uneven reflectance patterns. A number of studies have noted the increase in laser reflectivity when the phase angle approaches 0^{o} (Kaasalainen and Rautiainen, 2005; Kaasainalainen *et al.,* 2006; Harding, 2009).

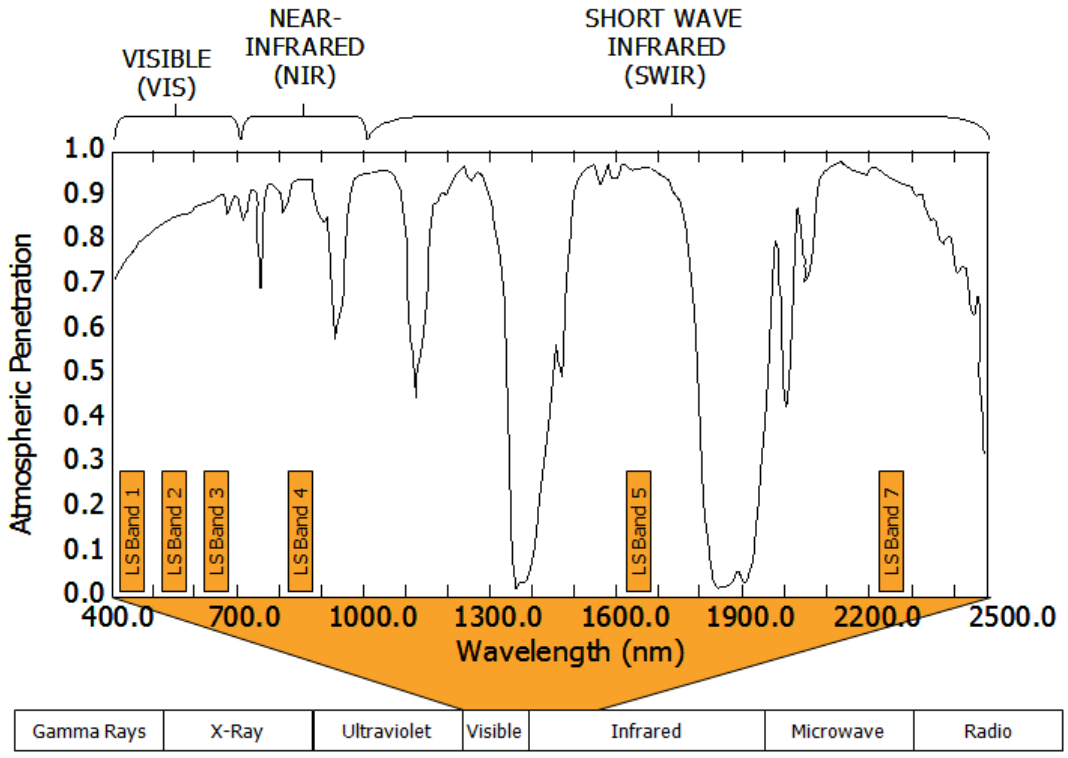

Figure 3-8 showing the transmission of energy through the atmosphere at different wavelengths. Note the high transmission at 1064nm. Source Exelisvis (2014)

Object reflectivity represents an important control on the ability to detect the object (Baltsavias, 1999). Usshykin and Smith, (2007) go further to provide approximations for

reflectivity, range, scan angle and linear target diameter. Figure 3-9 provides a visualisation of the linear target problem.

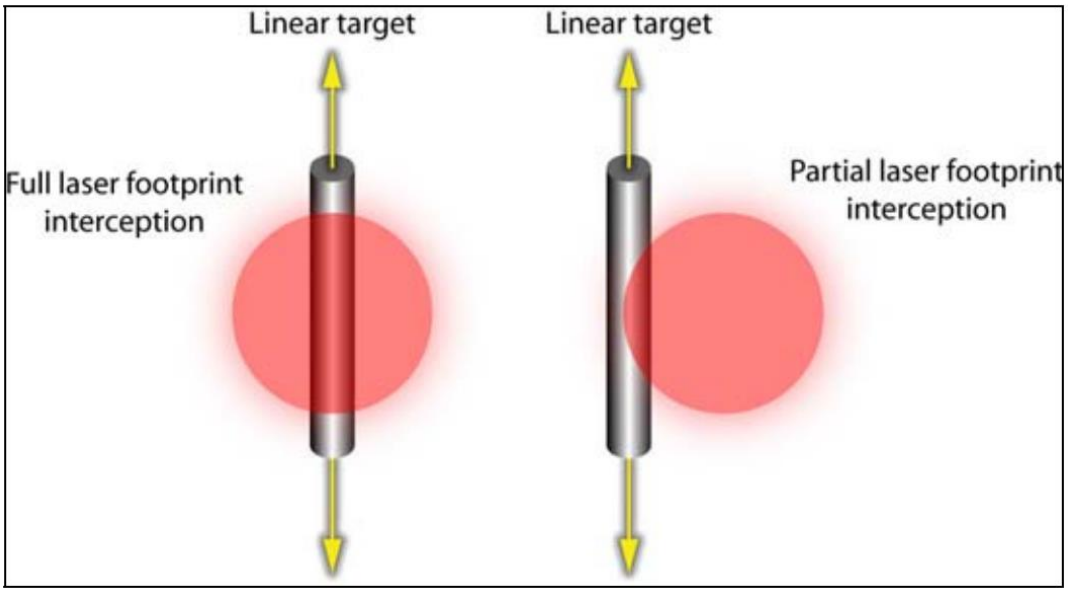

Figure 3-9 Diagramatic representation of footprint interaction with object of interest. Source Ushykin and Smith, (2007) page 8

$$\boldsymbol{P_{area} \propto \frac{\rho_{area}}{R^2}}$$

Equation 3-7 Power returned from an area acting as a Lambertian scatterer where ρ is reflectivity and R is range. Source Usshykin and Smith, 2007

$$P_{linear} \propto \frac{\rho_{linear} D}{\theta R^3}$$

Equation 3-8 power returned from a linear target (where target size is smaller than footprint size) where Ro is reflectivity, D is diameter of object, theta is scan angle and R is range. Source Usshykin and Smith, 2007

Equation 3-7 and equation 3-8 demonstrate the comparative difficulty in detecting an object at or below the footprint size, such that it reflects back an increasingly decreased energy for a small change in size, or where the beam does not fully strike the object of interest.

3.2.6 Waveforms and discrete returns

The returned pulse may be simple or complex, as the laser strikes the first reflective surface, depending upon the size of the footprint relative to the reflective surface. All of or some of the energy is returned, whilst any non-reflected or absorbed energy continues on to the next reflective surface, creating the potential for multiple returns. Two methods of recording these reflections are commonplace. The first is to record all received energy as a function of time creating a histogram of energies known as a waveform. The alternative method that is more commonplace discretises the returned energies into pulses and records discretised pulses.

Discrete return scanners can record up to a set number of pulses. Early scanners are able to measure two pulses, later scanners four pulses, and recent announcements by Optech suggest seven pulse systems are coming (Gelhar, 2010), this is even higher in other systems such as Leica. The pulses returned depend on the manufacturers set logic, for a two return system, the first and second pulse may be recorded, alternatively the first and last pulse may also be chosen as the logical pair to record (Petrie and Toth, 2009; Gelhar, 2010). The last return is the last reflective surface struck by the scanner; this is typically the ground surface.

The returned pulse is often complex, being a composite of the surfaces that the pulse struck and interacted with, as such the returned pulse is not represented by a quantised pulse, it is instead often considered to be a series of Gaussian curves that need to be discretised to single pulses . A variety of pulse detection methods are in use, the most common types being leading edge detection, constant fraction discrimination, trailing edge detection or

thresholding. Most LiDAR manufacturers use the thresholding technique in addition to detection of a point on the pulse to provide the discrete return (Harding, 2009).

The alternative and increasingly popular method is the recording of the full waveform. In this case, the scanner records the returned energies for set time bins. The smaller the time bin the more complex the waveform can be recorded (higher temporal resolution) and the more precisely it can be located. Larger bins allow greater energies to be recorded that may be useful in areas of poor reflectivity. The waveform is decoded during post processing yielding significant information about the nature and complexity of the topography. Figure 3-10 provides a comparison of the two methods.

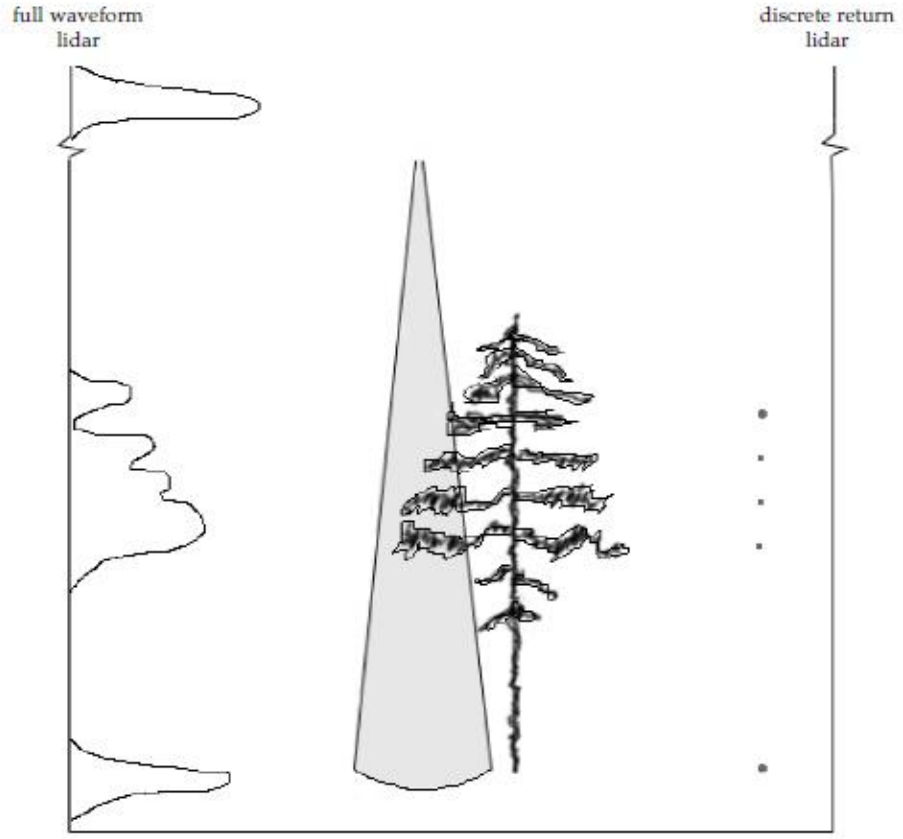

Figure 3-10 showing the difference in pulse recording between Full wavefom (left) and discrete return (right) taken from Lim *et al.,* (2003) page 92

The energy returned from the reflection is recorded by both methods; this is known as the intensity. The intensity value can be recorded based on the integral of the returned pulse complex, that is the energy under the curve, or alternatively by taking the energy return value at the point the pulse is recorded (Petrie and Toth, 2009; Wehr, 2009)

Whilst waveform data yields greater information, it is difficult to analyse and greater storage needs prevent its greater uptake. Ussyshkin and Theriault (2011) provide an overview of the advantages and disadvantages of each system, Gelhar (2010) takes the work further suggesting discrete return data from high vertical resolution scanners can yield very similar data to a full waveform system when intensities are accounted for.

3.3 GNSS Navigation

Global navigation satellite systems provide a means of fixing a precise location within the Earth's terrestrial reference frame. Many techniques for positioning can be utilised with GNSS ranging from 0.02 m accuracy to 15 m accuracy. Code based positioning using the coarse information contained within the emitted signal provides a low accuracy rapid means of location, when augmented by a broadcast known signal accuracies of 1m are possible. This suits applications such as navigation. For survey grade applications carrier phase measurements are required to meet the typical accuracies required (Wehr and Lohr 1999).

In order to calculate a position, the receiver must interpret the signals provided by the numerous satellites, each signal provides a distance from the satellite but no further information and as such, the satellite provides a sphere about which the receiver may be positioned. The receiver is located at the intersection of these spheres, a process known as trilateration calculates this. Trilateration is a 3D spherical approach that is similar to the

familiar, straight-line triangulation approach. Trilateration works for both code and carrier phase positioning techniques.

TYPICAL GPS RANGING ERRORS			
Error Source	**Autonomous GPS**	**Differential GPS**	**RTK**
User Range Errors (URE)			
SYSTEM ERRORS			
Ephemeris Data	0.4 – 0.5m	Removed	Removed
Satellite Clocks	1–1.2m	Removed	Removed
ATMOSPHERIC ERRORS			
Ionosphere	0.5 – 5m	Mostly Removed	*Almost All Removed*
Troposphere	0.2m – 0.7m	Removed	Removed
Subtotals	*1.7–7.0m**	*0.2 – 2.0m*	*0.005 – 0.01m*
User Equipment Errors (UEE)			
Receiver	0.1–3m	0.1–3m	*Almost All Removed*
Multipath	0–10m	0–10m	*Greatly Reduced*

Table 3-1 Showing typical values for error sources found in the space and user segment of a GPS system. Source Trimble 2007

Carrier phase differencing is necessary to achieve the accuracies required for aerial survey (Wehr and Lohr 1999; Petrie and Toth 2009). Carrier phase positioning uses the short wavelength (L1 0.023 m, L2 0.019 m) waves to compute a position. Figure 3-11 shows the principle. The counting of integers of the two waves and then performing an ambiguity resolution calculation upon the signal allows for centimetre level accuracies.

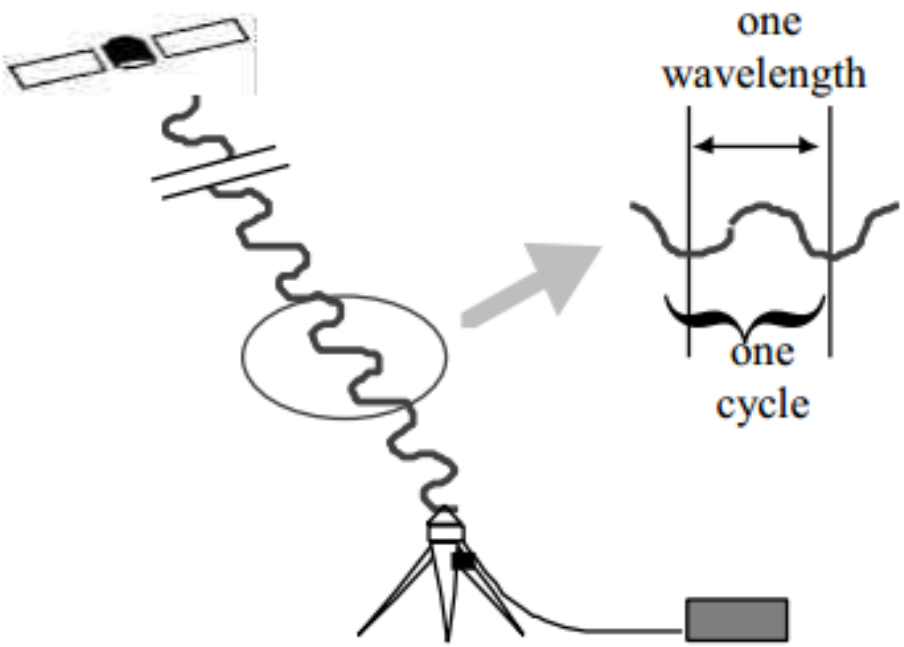

Figure 3-11 Showing the carrier phase signal to be calculated. source Trimble 2007.

Code or carrier phase positioning relies on the user segment being capable of resolving its position with as little uncertainty as possible. The number of satellites and their geometry used in the calculation can affect the uncertainty significantly. Satellites rely on good signals received from different views form the user segment, the ideal geometry places satellites at relatively low elevations (circa. 25 degrees) relative to the receiver and one satellite overhead, this results in a very small solution space, as such small uncertainty. This geometric arrangement is well understood, and for any location on earth, a forecast of that geometry can be made. Geometry predications allow the calculation of the dilution of precision of the satellite constellation for any given time and location. As such, a high dilution of precision gives a lower accuracy reading. The dilution of precision is expressed in terms of positional, time or the combined geometric dilution of precision. Equation 3-9 shows the calculation of the positional dilution of precision, as the root of the sum of the location variances of the horizontal and vertical components. GNSS systems calculate position, time

and subsequently velocity as core calculations. TDOP, the time dilution of precision is given in equation 3-10. To give an overall precision for the system, the geometric dilution of precision is calculated as the root of the sum of the location and timing variances, this is expressed in equation 3-11

$$PDOP = \sqrt{\sigma_x^2 + \sigma_y^2 + \sigma_z^2}$$

Equation 3-9 Positional Dilution of Precision equation, taking the variance of X, Y and Z

$$TDOP = \sqrt{\sigma_t^2}$$

Equation 3-10 Dilution of precision of the timing element of the system

$$GDOP = \sqrt{PDOP^2 + TDOP^2}$$

Equation 3-11 Geometric dilution of precision equation, showing the link to the time and positioning elements

3.3.1 Inertial Measurement Unit

Inertial measurement units record the attitude and acceleration of the aircraft; in order to do this they contain a series of gyroscopes and accelerometers. A very high measurement interval is used (typically 200 Hz) to record rapid and small changes in the aircrafts attitude and acceleration (El-Sheimy, 2009). Whilst very sensitive the IMU suffers from drifts over time, in part due to the rotations of the gyrospcopes aligning, or in ring laser gyroscopes

decohering. In addition as the IMU navigation uses an additive approach, summing the last recorded vectors to the sum of the previous recorded vectors, known as Dead Reckoning, this error increases over time (El-Shiemy, 2009) as such is not suitable for long periods of time.

3.4 Integrated Positioning Solution

LiDAR systems need to be able to know their position at any instant in time. This is necessary to directly georeference the emitted laser pulses. A typical laser system records a GNSS location every second (1 Hz), and an IMU location every 200th of a second (200 Hz). Neither system provides sufficient information to accurately locate the aircraft at any moment in time, by merging the two navigation solutions. For any moment in time, the aircraft position is calculated as:

$$POS = \begin{pmatrix} X_{GNSS} & Y_{GNSS} & Z_{GNSS} \\ X_{IMU} & Y_{IMU} & Z_{IMU} \\ \omega_{IMU} & \varphi_{IMU} & \kappa_{IMU} \end{pmatrix}$$

Equation 3-12 Showing the 9 parameter matrix for the instantaneous position of a Laser Scanner. Note GPS positions are in the mapping frame, All IMU positions are in aircraft frame and need translating prior to solution. Source El-Shiemy, 2009

Equation 3-12 is only valid when all the measurements occur simultaneously (same epoch and resolution), because the IMU captures at a significantly higher rate, the data must be filtered and merged.

The integration of the two sources of positional information helps to eliminate the shortcomings of each individual technique, (low temporal resolution and not attitude

information for GNSS, no absolute measurements and drift problems for the IMU) (Schwarz, 1993). Several techniques exist for the integration of this data, but each uses a hind and forecasting filter that takes the position and error estimates to establish a best estimate travel path, this filtering is known as Kalman Filtering (El-Shiemy, 2009).

Two approaches to the integration of the data are possible; the first offers a tightly coupled approach, taking the GPS and IMU data simultaneously. Figure 3-12 shows the block diagram input of this system. The technique has been implemented with success by Knight, (1996), Scherzinger and Woolven, (1996), Moafipoor *et al*., (2004) and is integrated in the latest Trimble post processing software PosPac MMS (Scherzinger and Hutton, 2006). Boba *et al.,* (2008) demonstrate the effectiveness of tightly coupled processing approaches for LiDAR data.

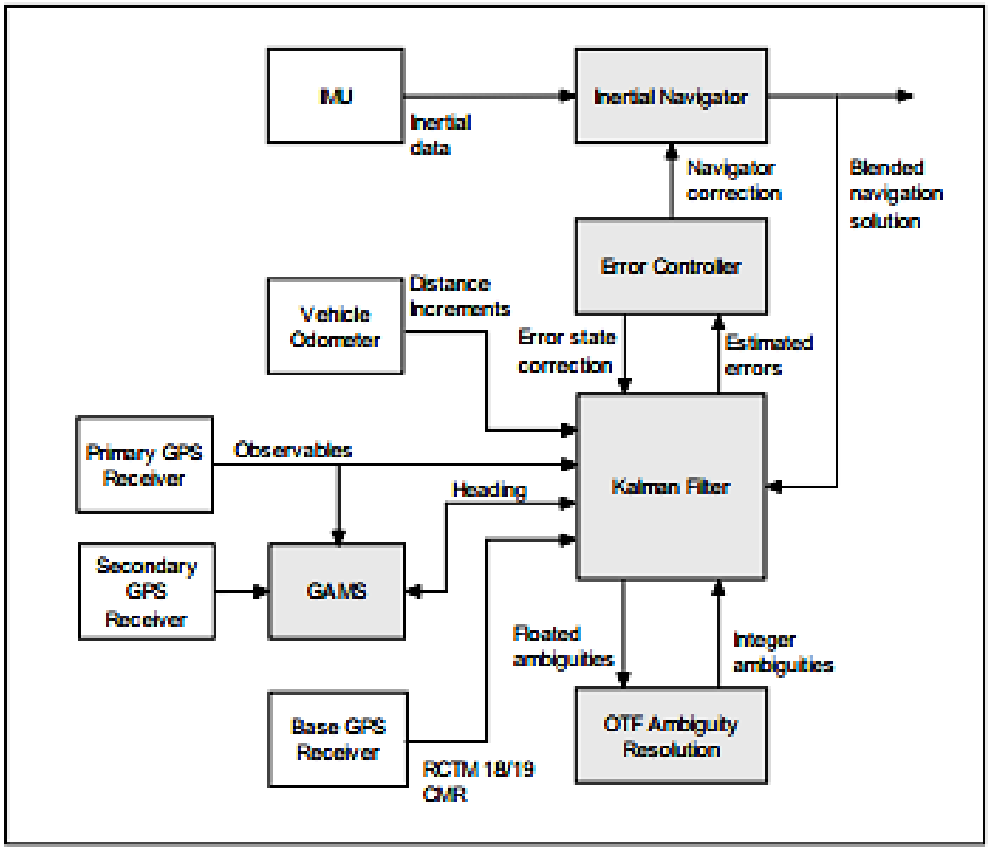

Figure 3-12 Diagram showing the inputs and processes of a tightly coupled navigation solution. Source Scherzinger and Hutton 2006

For a tightly coupled solution, the state vector at any point can be considered as the vector sum shown in equation 3-13.

$$x = (\boldsymbol{\varepsilon}, \delta \boldsymbol{R}, \delta \boldsymbol{V}, \boldsymbol{d}, \boldsymbol{b}, \delta \boldsymbol{N})^t$$

Equation 3-13 State vector for a tightly coupled solution, where ε is the attitude errors, R position errors, V, velocity errors, d, gyro drift about the gyro axes, b, is the accelerometer bias and N the GNSS ambiguity vectors all vectors are with respect to time. Source El-Shiemy 2009

In equation 3-13 , all components are vectors defined within the same reference frame, where each vector has 3 components (XYZ or ω,φ,κ) except N, which has components equal to the sum of satellites visible – 1 components.

Loosely coupled solutions consider the IMU and GPS filtering separately prior to merging the data; this has advantages when the incoming data is of poor quality or from multiple sources. Using the nomenclature from equation 3-13, the loosely coupled state vectors can be considered for the GNSS and IMU as equation 3-14 and equation 3-15 respectively.

$$X_{GNSS} = (\delta \boldsymbol{R}, \delta \boldsymbol{V}, \boldsymbol{\delta N})^t$$

Equation 3-14 showing the state vectors for GNSS errors. Source El-Shimey 2009

$$X_{imu} = (\varepsilon, \delta \boldsymbol{R}, \delta \boldsymbol{V}, \boldsymbol{d}, \boldsymbol{b})^t$$

Equation 3-15 showing the state vectors for IMU errors. Source El-Shiemy 2009

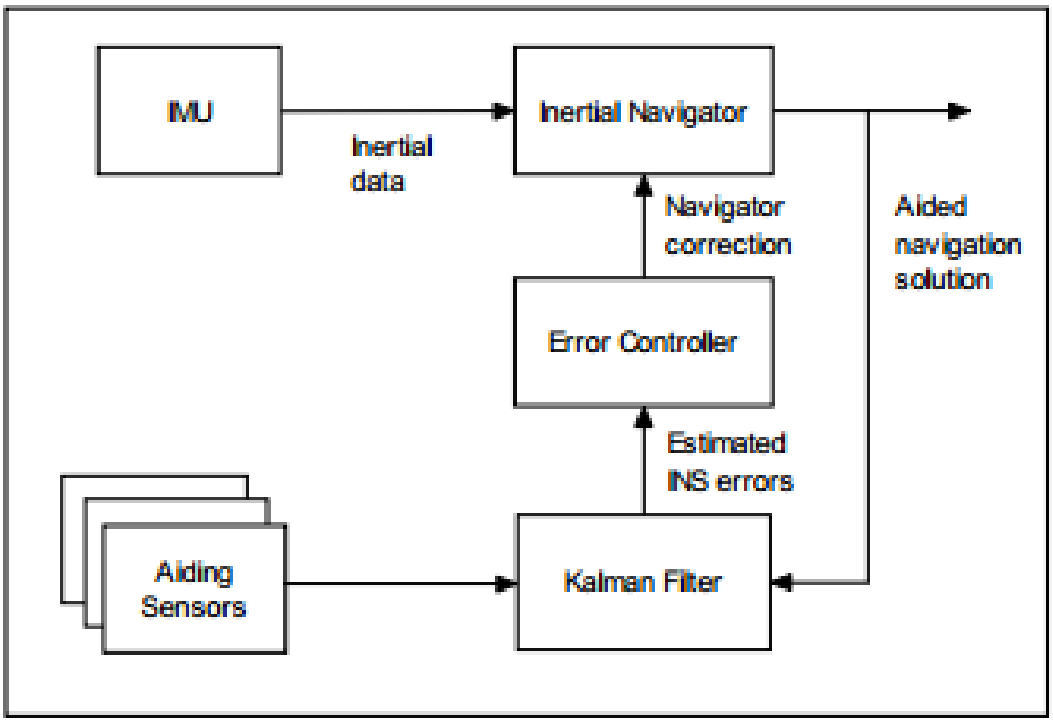

Figure 3-13 showing the generic architecture of a loosely coupled filter. Source Scherzinger and Hutton 2006

The main advantage of the loosely coupled approach is that any blunder in one stream has a desensitised effect upon the other data stream (El-Shiemy, 2009).

Georeferencing of LiDAR point clouds requires the understanding of several reference frames. Firstly the sensor frame; this maps all data relative to the position of the sensor, the IMU frame which maps data relative to the alignment of the IMU, the aircraft frame provides a framework relative to the aircraft, and the mapping frame relative to an arbitrary terrestrial reference frame. In order to provide information in the final mapping frame it is necessary to translate, rotate and scale the data appropriately to correspond to the final mapping frame.

Georeferencing of the point cloud is decoupled from the navigation optimisation. The navigation is provided in the mapping frame, typically as a series of longitudes, latitudes and

ellipsoidal elevations relative to WGS84. Georeferencing can be seen within the mapping frame as an implementation of equation 3-16.

$$\boldsymbol{r}_i^m = \boldsymbol{r}_s^t(t) + \boldsymbol{R}_s^m(t)\begin{pmatrix} -dsin\alpha \\ 0 \\ -dcos\alpha \end{pmatrix}_i^s$$

Equation 3-16 showing the georeferencing with respect to time, where r(mi) is the posion vector of an object in the mapping frame, r(ms) is the transform between the S and M frames, and the final matrix the position vector for an object (i) in the sensor frame. Source El-Shiemy 2009

LiDAR uncertainty is a complex and difficult subject, a number of factors aggregate to produce the overall error budget, some factors are mutually exclusive of other values whereas others are dependent upon other values, this makes quantitatively expressing the uncertainty at any given point very difficult. The effect of this uncertainty is less well understood, this table study seeks to enhance the understanding of uncertainty estimates on aerial laser scanning mapping and object detection.

4 Materials and methods

This section will describe the methodology, study location and outline the reasoning of the method and location with respect to the experiments. The experimental design and controls are discussed and evaluated in this chapter. The experiments are at Hookergate High School, located 10 miles southwest of Gateshead. The school provides a variety of target surfaces for the study as well as providing a series of tables for the table study. The school is adjacent to Chopwell Forest, an ancient woodland site, this area has been captured by the LiDAR flight passes.

4.1 Study Site

The study is located at Hookergate School, Rowlands Gill near Gateshead. Hookergate school is a large secondary school providing a range of terrain to scan. This includes a flat hockey pitch, a concrete area that the table study can be located and grassy fields. The school also kindly provided students to assist with experimental set up and configuration. The school is located at 54.9277482 N,1.7746738 W. The map of the area is shown in figure 4-1.

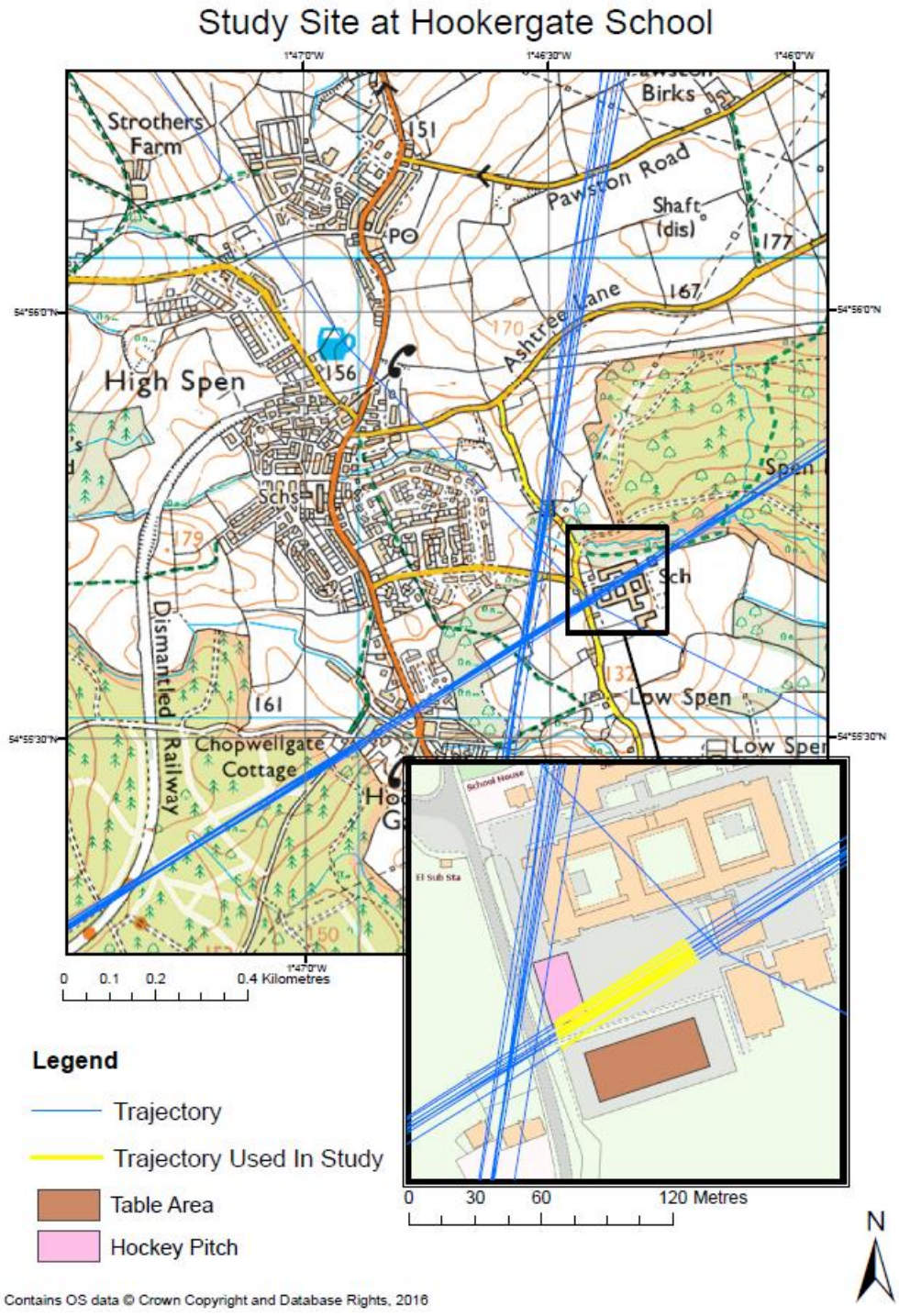

Figure 4-1 Map showing the study area with inset map showing the detailed view of the study area and the trajectory of the aircraft for the data used in the study

4.2 Data description

The LiDAR data for this project will be conducted by NERC's Airborne Science Research Facility (ASRF). The NERC data collected using a fixed wing Dornier 228 aircraft using a Leica ALS50 scanner with an attached multispectral scanner. The research will use a variety of techniques, focussing on point cloud data rather than derived surfaces. The techniques are likely to include surface differencing to produce an nDSM, manual object identification, and statistical analysis and display of the data.

The Leica ALS50 scanner uses a 1064nm laser with a pulse repetition factor of 87 KHz, returning up to four pulses per emitted pulse, the vertical resolution between pulses is 2.8 meters and Leica uses the constant fraction discriminator to discretise pulses. The data was captured at 800m above ground level.

4.3 LiDAR Plan and Capture

The survey was captured using the NERC ASRF Leica ALS 50 system. The system was fitted to a Dornier 228 fixed wing aircraft (D-CALM). The system is fitted with a full waveform digitiser and discrete return digitiser. Figure 4-2 shows the Leica ALS50 mounted in the Dornier 228, as used for the capture of table study data. Figure 4-3 shows the trajectory of the aircraft relative to the study areas.

Figure 4-2 Leica ALS-50 System used for capture. IMU and data control in the foreground and the laser sensor is mounted in the grey box towards the background.

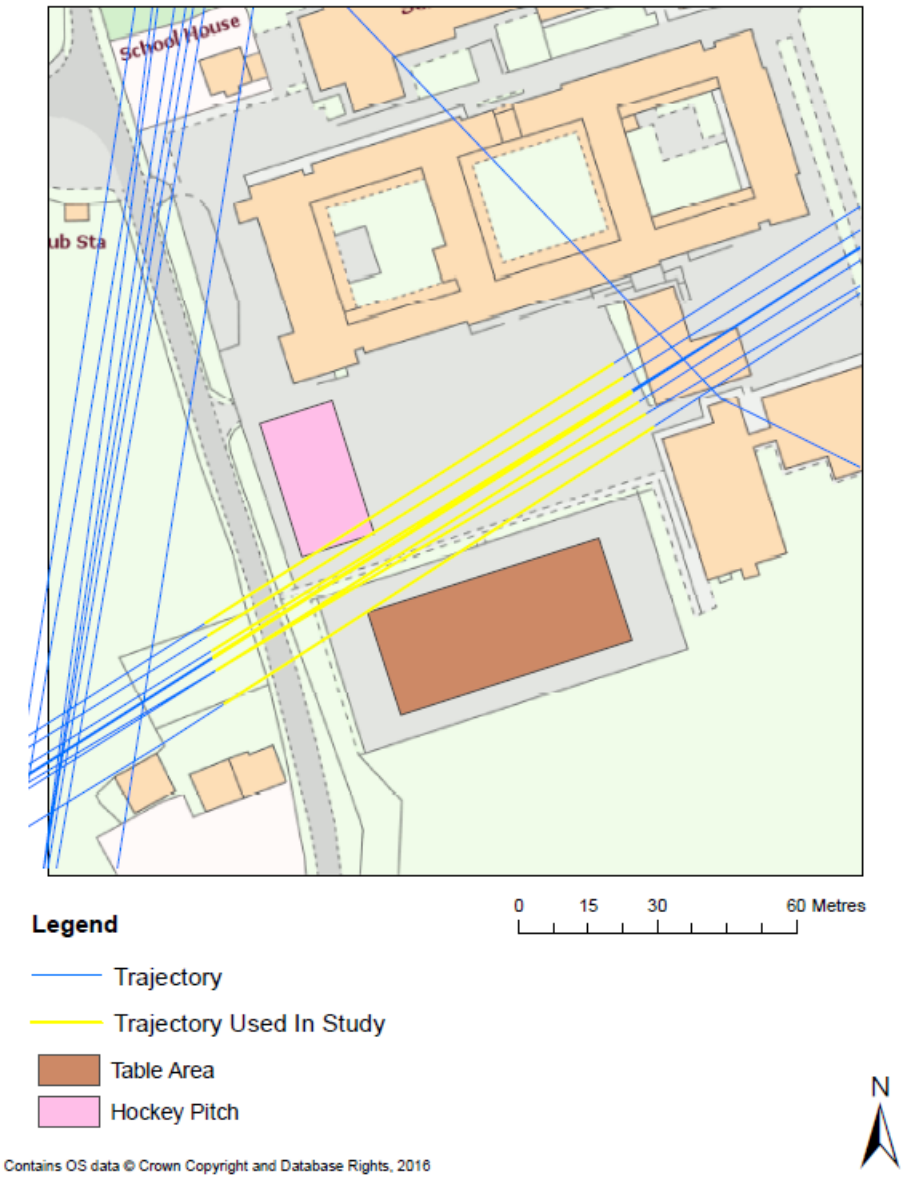

Figure 4-3 map showing the area of trajectory used for the table and hockey pitch studies

4.4 Table Study Experiment Design and Methods

Figure 4-4 showing the NERC ASRF aircraft at Newcastle Airport (mobilisation site for the study).

Figure 4-5 showing the table arrangement.

Flight planning was undertaken using Google Earth and ALTM NAV. NERC ASRF converted these into Leica ALS flight plans. A Leica GPS 1200 base station was set up 300 meters from the study site. This gives an exceptionally short base-line and will constrain differencing errors to 0.005 m. The base station is shown in figure 4-6

Each table has black plastic wrapped around the legs in order to prevent a laser strike penetrating beneath the table and giving difficult or inaccurate readings (although this was subsequently tested and showed to have no impact on the 1064 nm wavelength light). The capture day proceedings can be seen in figure 4-4, figure 4-5, figure 4-6 and figure 4-7.

Figure 4-6 Leica GNSS base station set up for differential processing of the flights. Note the tables in the background showing the very short baseline used in processing.

Figure 4-7 showing the tables with polythene wrapped around to prevent laser strikes under the table legs

The table study will be used to provide experimental results to aid the understanding of a laser scanning performance and characteristics. The data will be used to study the effects of vertical resolution, object definition, identification and characterisation, point cloud gridding techniques, and scan patterns. The aim is to work towards a better understanding of laser scanning and the commissioning of laser scanner data collection.

Object characterisation is often the primary purpose of a survey, in the fields of archaeology, as-built engineering, forestry and prospection surveys. For these surveys, correct definitions of the objects of interest are integral, failure. Other surveys hold topographic representation as their aim, for this characterisation of a landscape at a given scale is paramount. The

gridding study will seek to expose the differences that subtle changes in processing technique can produce and the artefacts that may be introduced through such techniques. These findings will inform the use of these point generalisation techniques.

The processing steps outlined are utilised to produce data for the experiments as outlines in the following section. Where specific processing has occurred, these steps will be outlined in the sections below.

4.5 Table Experiments

The table experiments simplify the complex forest canopy into regular objects spaced at repeating distances, this allows for the investigation of the effects of uncertainty and accuracy. In the context of this study the use of uncertainty refers to the ability to predict the likely outcomes through scientific approaches, for example, the use of repeatability to assess the certainty with which overlapping flight lines of the same area record features in similar ways. Accuracy refers to the closeness to which the recorded data matches the real world scene it captured. Determining accuracy and uncertainty within this experiment is likely to be through use of comparative and observational methods. The use of numeric techniques is limited by the nature of the captured dataset.

4.5.1 Point cloud Experiment 1

This experiment will produce a footprint of the laser beam using established formulae (Baltsavias 1999), project these footprint diameters to the area covered. Produce statistics relating to area illuminated and table illumination. This will allow a comparison to the concepts of point spacing and point density as parameters to consider when commissioning a LiDAR survey.

4.5.2 Point Cloud Experiment 2

A comparison of data for the same table spacing. Each table spacing was covered with two flight passes; this creates a test of verifiability of the point cloud. The scan reproducibility is an important factor to consider in many different applications. This work will be valuable in the decision making process to scan an area twice for point density requirements, or to fly lower and slower to achieve the same point density in a single pass. The former being an often cost effective and safer method.

4.6 Table experiment controls

It is integral to the experiments that variables are controlled and changed systematically in order to explore their effect upon the experimental outcomes. The tables represent a systematic approach to understanding object detection and characterisation using laser scanning. The variables controlled were terrain, aircraft speed, table orientation, table type, scan setting and altitude. The two variables considered are table spacing and flight direction.

The terrain was flat over a hockey pitch, whilst some of the tables at the larger configurations were on a gentle slope; this effect was removed using ground level subtraction. The degree of slope is minimal and unlikely to have a significant effect on the table detection.

The tables were exam style tables used by the school, each table had the same dimensions (W: 0.6 m, L: 0.6 m, H: 0.7 m), the tables were equally spaced and black plastic bags were used to prevent laser strikes under the table (experimental results later showed the black bags are effectively transparent at 1064 nm so had no effect). The table surface was not uniform across each table so this may become a variable at a later stage; this will be investigated in the results section. As the tables were moved between configurations, each

table kept it respective position, as such should a table occupy position F4; it will remain as F4 for each table configuration.

The scan settings remained constant for each over flight; the aircraft speed naturally varies slightly as it moves, but the pilots intended to keep the same altitude, attitude and speed. Given the small area that the tables occupy, the aircraft can be considered to be at a constant speed, checks on the aircraft trajectory show that the aircraft held a constant speed over the site.

Table spacing was systematically altered over the flights. This is the primary variable investigated. The tables, initially spaced at 2 metres apart were moved closer towards the centre by 0.5 metres each configuration, this configuration.

Each table configuration was overflown twice. The flights were from opposing directions but otherwise the variables remained the same. This will allow for an increased point density overall as well as investigation into how multiple overflights can capture different details.

4.7 Pre Processing for the Point Cloud Experiments

The registered LiDAR data points must be manipulated into a format fit for analysis and processing. The Point cloud contains massive amounts of information, notably each point includes easting, northing, height, intensity and echo number. This information is stored in the LAS (LiDAR Archive Format), the open format from the ASPRS designed for LiDAR point cloud information. This format is the industry standard. The LiDAR point cloud is produced per flight strip, each strip being an individual file and needing to be agglomerated into a dataset covering the area of interest. The point cloud is loaded into Terrascan to form a project; this provides the facility within Terrascan to deal with mass point cloud data. The area of interest is split into blocks of 500 m^2. The LiDAR point cloud is then stored in one of

the 500 m^2 blocks allowing for overlapping flights to be stored as well, albeit with an identifier showing the flight it is related to. Point cloud filtering techniques are applied to the point cloud; this routine seeks to eliminate noisy and spurious points to a separate class, classify the ground using a combination of progressive densification filtering and morphological filtering and to classify points by their respective position above the ground surface. This last step allows for easier visual interpretation of the point cloud.

4.7.1 Relative and Absolute accuracy assessments

Each LiDAR strip will show small variances in height; this is a result of tropospheric changes, sensor heating and performance degradation through operation. As such, two adjacent strips may show a small vertical error. This is expected and Terramatch software is used to adjust each point cloud to match its neighbours. This adjustment is performed by creating a TIN of the classified ground points, these points are likely to be stable and unchanging over a short period, other features such as vegetation may sway in the wind or objects such as vehicles may move. The ground however is assumed at this point to be constant. The software works to adjust the two TIN surfaces to match; this uses a least squares adjustment procedure. Once the point clouds match, this ensures their relative accuracy to each other; such that measuring from strip 1 to the top of a tree covered in strip 2 as well will yield the same result.

4.7.2 Absolute Accuracy

In order to check the point cloud is in the correct position relative to its projection and datum, it must be checked against conventional survey data. The first survey used a car park at the north east of Chopwell Wood, surveyed using stop go GPS differencing techniques, the second data set is fitted to the first dataset to provide control, additionally the GPS base

station set up at Hookergate School will be used to verify the adjustments. The adjustment is performed as a single block adjustment across the LiDAR project, this is due to the shift being systematic and the dataset already being adjusted for internal inconsistencies.

The LiDAR data is initially processed into the appropriate UTM zone, this provides a base projection for the registration to work to as a mapping frame, however needs to be referenced against Ordnance Survey Great Britain National Grid. This is a Transverse Mercator projection based on an old terrestrial reference frame. The frame is no longer valid and as such, a rubber sheeting transform has been approved, this is known as OSTN02. The transform cannot be applied using a simple 7-parameter Bursa-Wolfe projection or 9-parameter time dependent projections (as is common when translating between many coordinate systems). This transformation was carried out using Terrascan and verified adjusting the ground truthing data in Leica Geo Office (LGO). The OSTN02 transform also transforms the WGS84 ellipsoidal heights (based on GRS80) to heights based on the Newlyn datum.

4.7.3 Verifiability Study Design and Methodology

The experimental is designed to maximise the information that can be gathered from multiple overlapping flight lines with all other variables kept constant. The experiment keeps the flight parameters and platform constant, repeats the survey many times over a short time period and uses statistical visualisation techniques and descriptive statistics to describe and compare the datasets.

In order to assess objective one, the ground surface will be classified for the same overlapping areas using the same algorithm, the ground surface is exported with a flight line identifier producing a point cloud of the derived ground surface with each overlapping flight line identified. There are eight flight lines overlapping each scene, flown in the same direction and within a short time period.

The data over the areas of interest will be tiled into grids at 10m, 20m and 50m. The difference between the tile sizes will show the sensitivity of the point cloud to aggregation techniques. For the gridded digital terrain model experiment, a single grid per flight line will be made using the full area of interest.

It is an assumption of this methodology that once temporary objects such as cars and people are removed from a scene, that scene will not change significantly over the short time of the flight.

The resulting point cloud for each area will be processed using a Python script, making use of the MatPlotLib library for graphing. The graphs will show the resulting violin plot for each flight line.

Violin plots provide an overview of the data distribution and descriptive statistics. Providing the median, inter quartile range and a descriptor of the distribution of the data they make an ideal plot for comparing the complex and variable LiDAR data.

5 Experimental Results and Analysis

This section displays all relevant information regarding the uncertainty experiment through a range of photographs, graphs and statistics to help achieve the aim of the research. The results will be described in this section before being discussed and examined in chapter 6.

The tables were configured with 4 separations, the aim of moving the tables closer together after the repeated scans is to determine how close regular discrete objects can be before coalescing in a scan scene. The results of the scans were surprising, with tables left undetected and a range of laser strikes on tables. This changed the direction of the study towards an analysis of uncertainty in laser scanning. The results shown are those relating to laser scanning uncertainty.

The tables are equally sized and as such each table would expect to receive a similar number of hits for a given point density. Point density is determined by the number of points per square metre; as such, a table of 0.36 m^2 would expect to receive 0.36 times the point density in strikes. This is under the assumption of a uniform distribution of points, the literature clearly shows that a number of variables can affect the distribution of points across a laser scan, these first order controls are scan pattern, scan frequency, footprint size and object reflectivity, second order controls include the pulse digitisation, system transmissivity and sensor performance characteristics.

Although each table is expected to receive the same number of strikes, it is expected that the ability to determine tables as discrete objects will diminish as the objects are brought closer together.

The tables are arranged in a grid as can be seen in figure 4-7

The table spacing's are outlined in Table 5-1.

Table Configuration	Distance between tables
Table 1	2.5m
Table 2	1.5m
Table 3	1.0m
Table 4	0.5m

Table 5-1 Table showing the spacing's between tables for each table configuration

The tables did not alter their relative position within the grid, as such, each table could be assigned an alphanumeric reference that remained constant throughout the survey, the positions of the tables changed as the tables moved closer together but the neighbour tables remained the same respectively. The tables are given an alphanumeric reference to describe their relative location within the project grid as shown in figure 5-1.

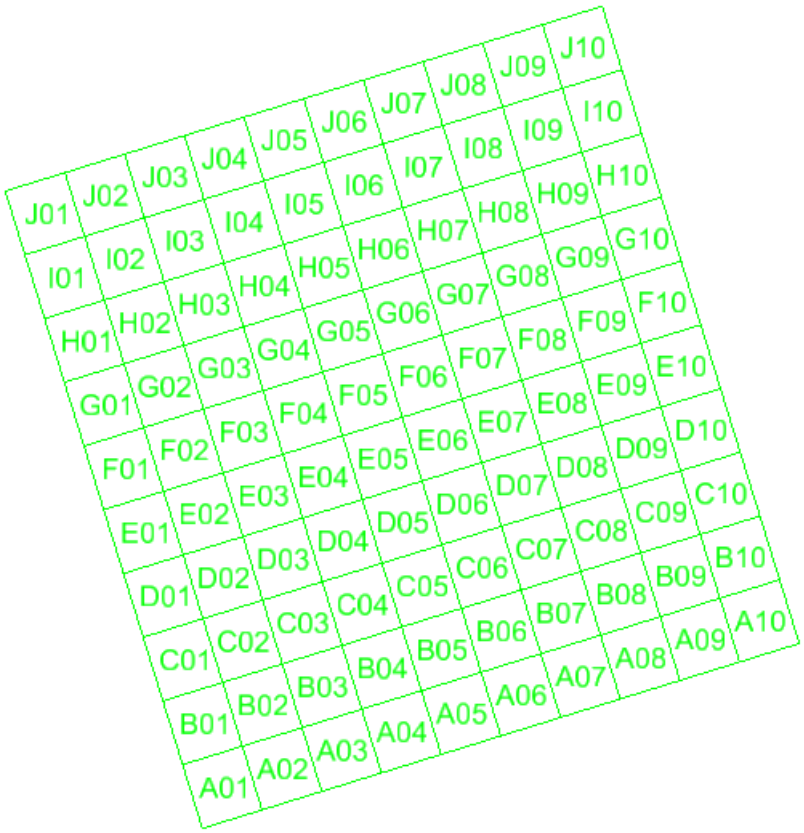

Figure 5-1 Alphanumeric grid to identify each table

The table uncertainty study has revealed many interesting factors regarding aerial laser survey techniques. Large-scale mapping performed as part of the table study has revealed

significant sources of uncertainty and raised questions regarding the repeatability of LiDAR studies for large-scale applications.

The results are split by table configuration; each table configuration shows a LiDAR point cloud representation of the tables with the separate overpasses showing disparate results. Each ALS over pass was conducted on the same flight, thus the variables were minimised such that the tables and the scanner parameters remained constant.

ALS survey parameters are characterised using point density and point spacing metrics. Thus, it is then assumed that should an object of size X be larger than the point spacing it shall be recorded during an ALS study. The flight parameters for the table study are 4.5 points per square metre per over flight. Thus, equation 5-1 gives a point spacing of 0.47 m.

$$Q = \frac{1}{\sqrt{d}}$$

Equation 5-1 deriving point spacing from point density for an idealised point cloud. Q is point spacing and d is point density

Given a beam divergence of 0.22 mrad, the footprint size is derived to be 0.13m diameter, giving a footprint area of 0.0132 m^2. Figure 5-2 shows the idealised representation of the point cloud including the objects chances of illumination percentage. It is clear that for an object near the point spacing of a point cloud, significant variations (by a factor of ten) can occur. This calculation assumes a uniform energy distribution across the footprint. When modelled as a Van Mieses distribution, the intensity drop off is similar to a 2-dimensional Gaussian distribution as shown in figure 5-3.

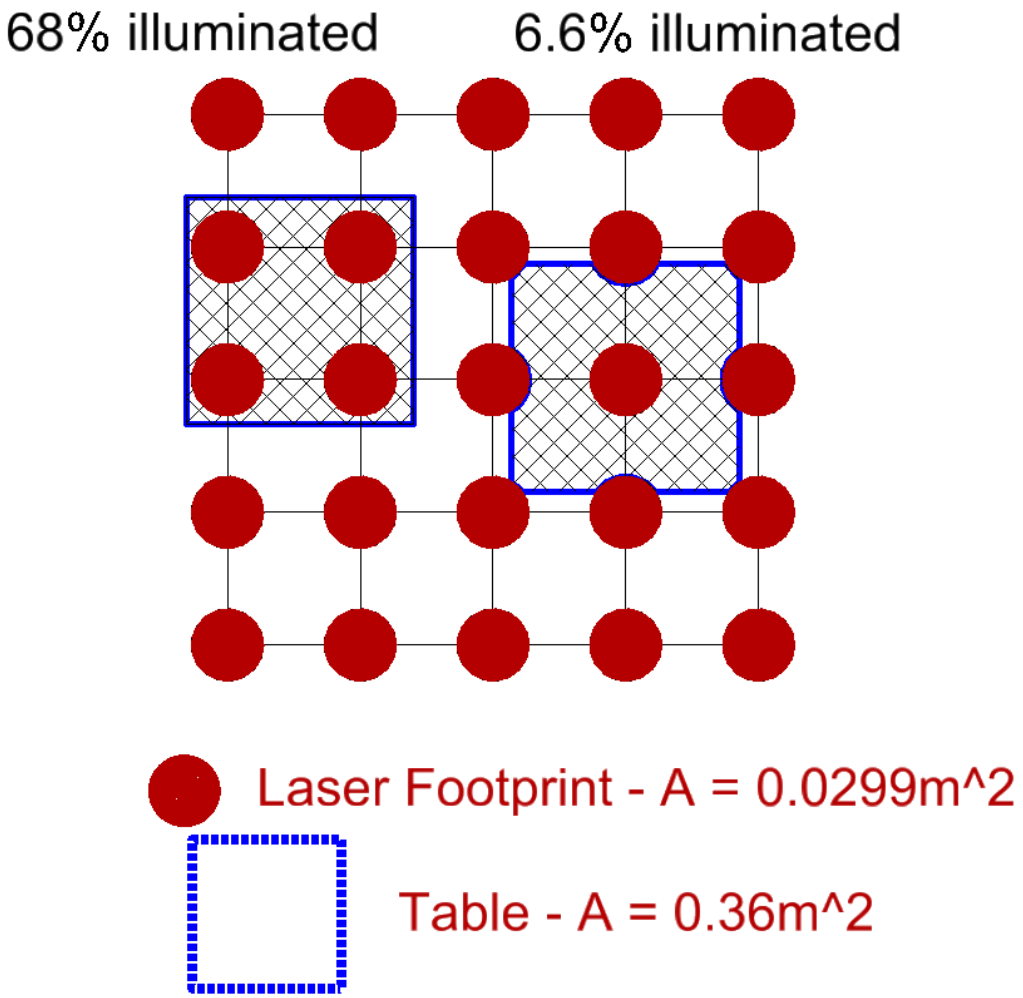

Figure 5-2 showing the different illumination an object can achieve for the same scan pattern

Figure 5-2 is a scale diagram showing the laser footprint near nadir in an idealised gridded pattern, the footprint is projected using equation 3-5. Clearly, a table can undergo a situation where four strikes occur on the table significantly increasing the chance that the table is picked up and likely to characterise the shape of the table. Where the centre of the table has a laser strike, the neighbouring eight pulses intersect almost tangentially. Figure 5-3 expands this to show that under a real distribution, this is a very low intensity part of the laser footprint that greatly reduces the likelihood of a return. This effect is further exacerbated by the very strong ground return likely to occur from those pulses that may "swamp" the digitiser removing the

likelihood of detection further. This diagram shows LiDAR is an under sampling approach that can have a significant effect on the ability of the survey to detect objects. Where the object is close to the point spacing size, the object illumination is very sensitive to small changes in the scan characteristics. No modelling of irregular or linear objects has been performed. It would appear that these features pose an even greater sensitivity to detection

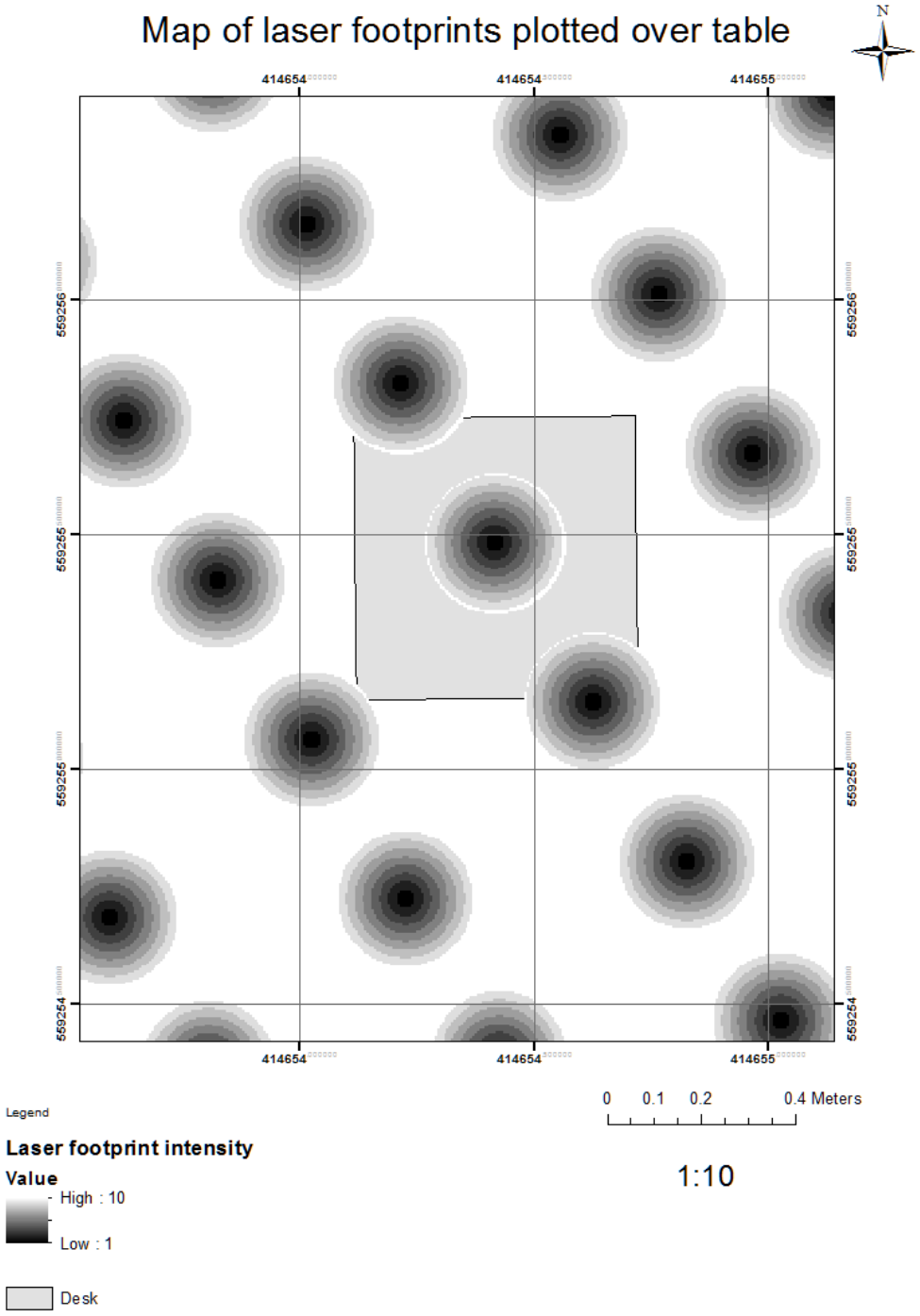

Figure 5-3 Map showing the laser footprints coloured by intensity and a mock up table placed within the survey area

5.1 Experimental conditions

The experiment conducted using the NERC ASRF aircraft planned to cover the tables in four flight orientations. Due to an unforeseen change in plan on the day of the flights, the table study location was moved to a different area of the school, as such, the study site was covered by opposing direction flights trending northeasterly and southwesterly but the perpendicular flights did not cover the table area. The flights over the table area can be seen in figure 5-4.

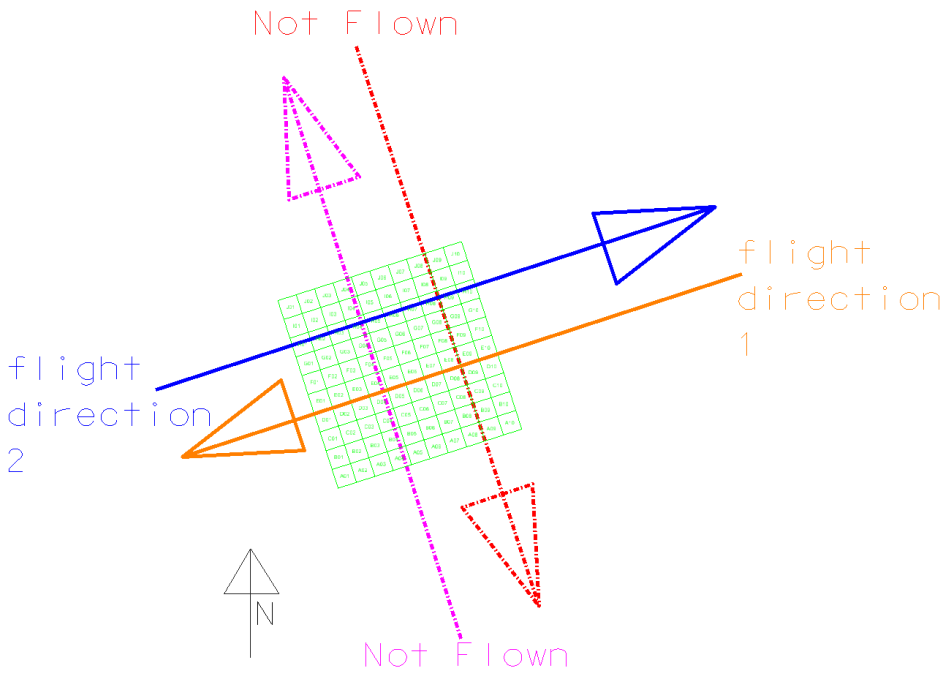

Figure 5-4 Diagram showing the flight directions as planned, and annotated to show what was flown for the table study

shows the change in elevation over the project area, it can be seen that the variation within the project area is approximately 3 metres; this is not expected to have a significant impact on the experiment outcomes.

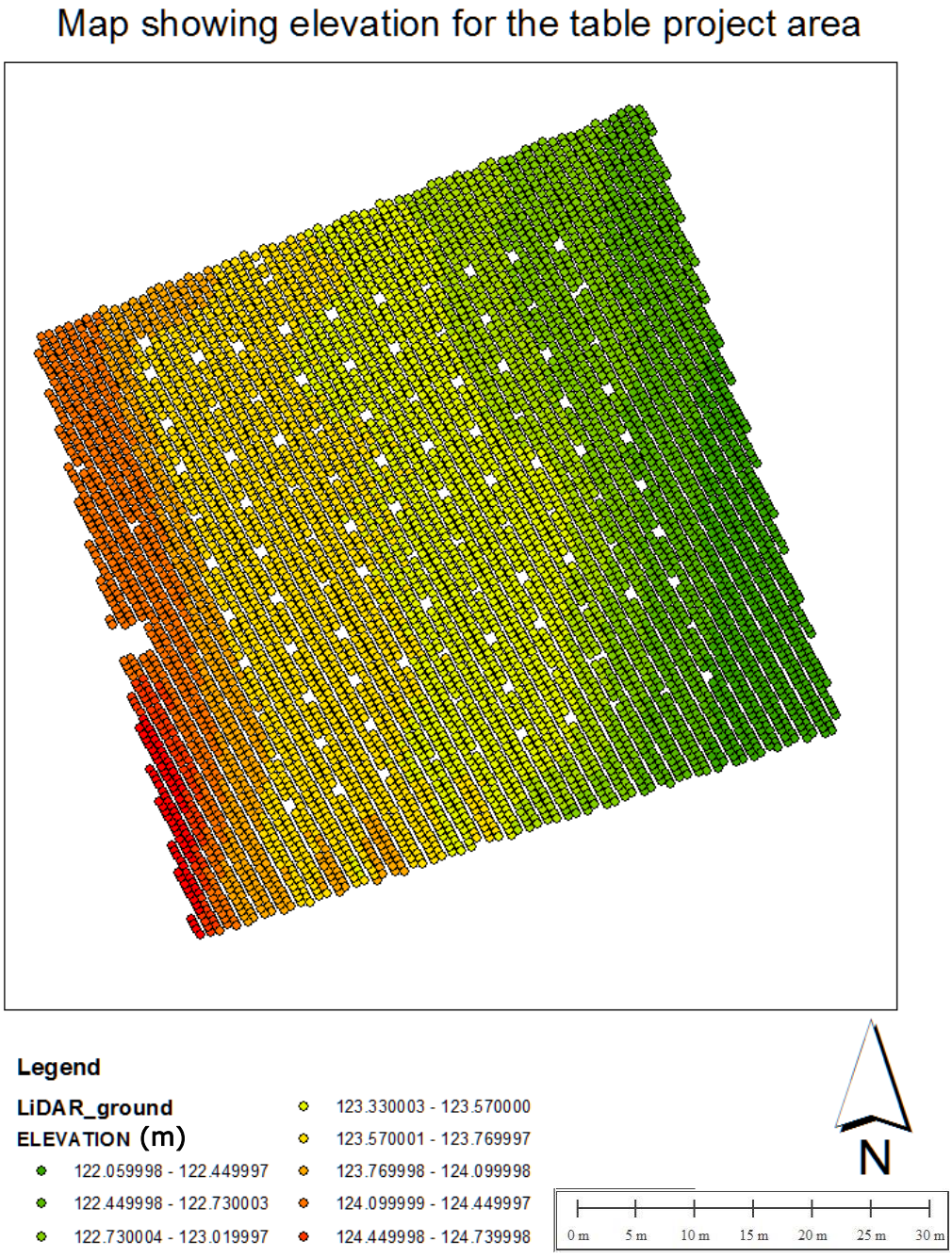

Figure 5-5 Map showing the change in elevation of the bare ground over the project area

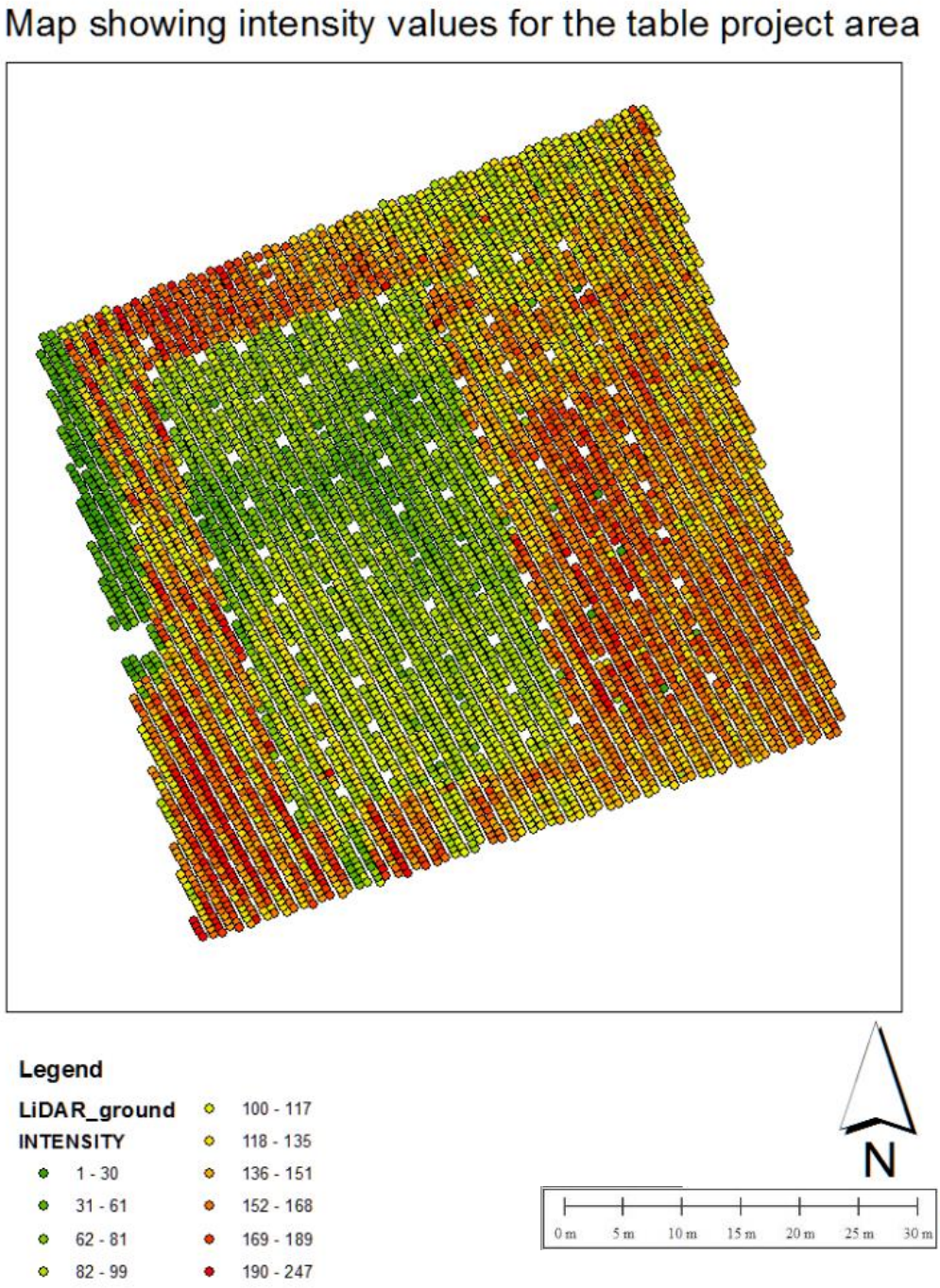

Figure 5-6 map showing the LiDAR intensity values over the project area

Intensity values are shown in these vary over the project area; it is probable that the lower intensity shots are the second returns where part of the incident beam that was reflected came from a table or other object. The higher intensity values are very prevalent outside the table area (white missing areas), these are where no interaction other than the ground has occurred. Figure 5-7 shows the change in scan angle over the project area, scan angle is expected to be a fundamental control on footprint size, incident radiation and increase error through limb effects. The scan angle was controlled to very nadir values and varies by 4 degrees. The scan angle is defined relative to motion towards the right wing, as such negative scan angles show the angle subtending from nadir to the left wing.

It can be seen that the experimental variables have been closely controlled; the data was processed in accordance with the steps laid out in the methodology.

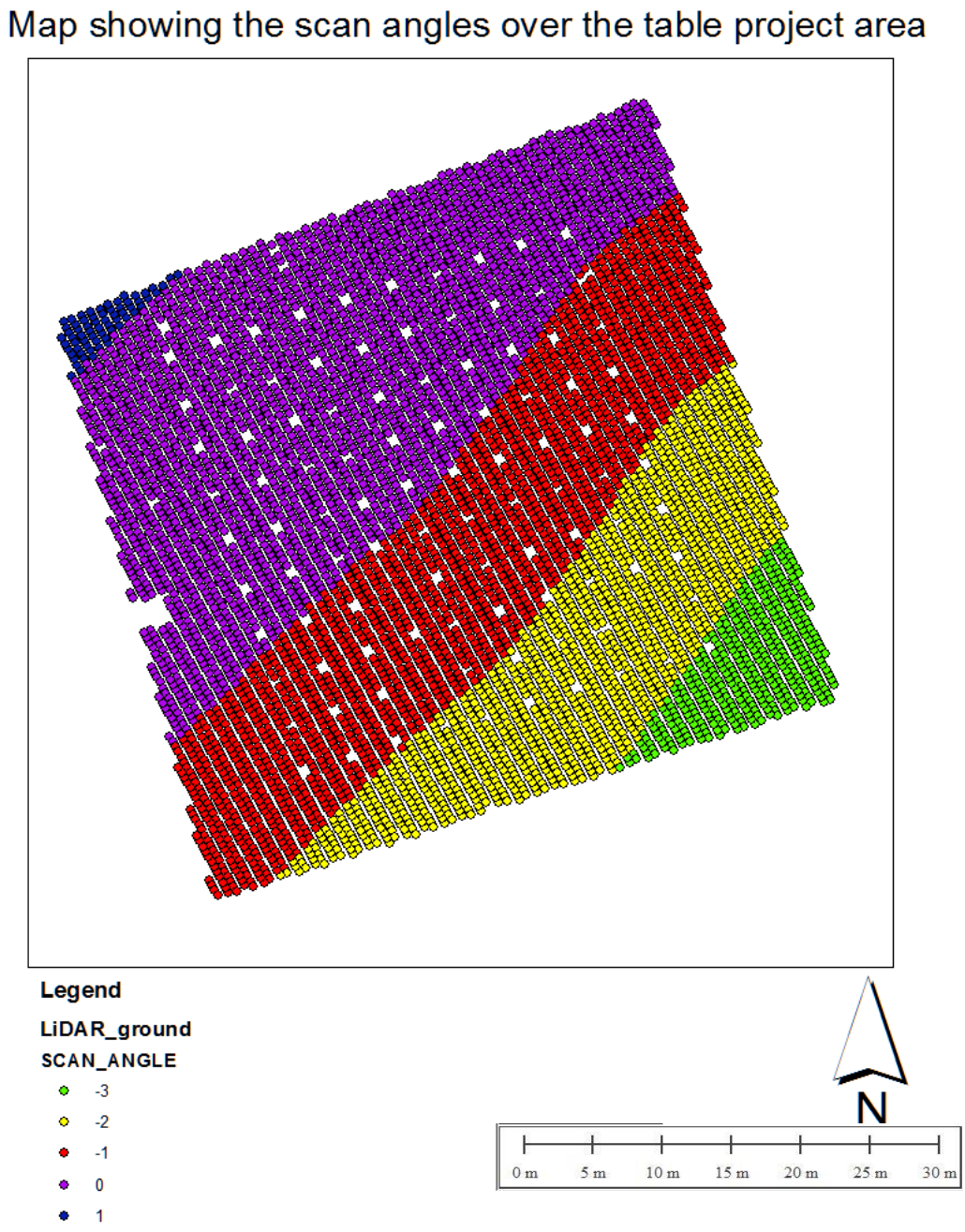

Figure 5-7 Map showing the typical scan angle range over the project area. Scan angle is measured in degrees from nadir

5.1.1 Spatial Modelling

In order to convert the LiDAR point cloud into a surface, interpolation of the points must occur to form the surface. Interpolation can be performed using a number of methods, from the very simple inverse distance weight method through to complex modelling techniques such as Kriging. Three methods were investigated for the table surfaces. These were natural neighbours, ordinary kriging and inverse distance weighting. Natural Neighbours uses the surface to construct Delaunay Triangles, calculating their dual to give Veronoi diagram and weighting the neighbours based on the area of the interpolated surface within the intersecting areas of the surface and the nearest neighbours. Ordinary Kriging uses kriging with an assumption of a constant mean to derive the surface interpolation, given the flat ground and regular tables the constant mean is a fair assumption over the surface area. Inverse distance weighting uses the simpler approach of linearly interpreting a position based on its distance from surrounding points. Figure 5-8 shows a map of the different interpolation methods. The tables are clear in each image; the surface under the tables within the interpolated area is very similar across the interpolation methods. Once the surface extrapolates beyond the table surfaces significant changes between the techniques can be seen.

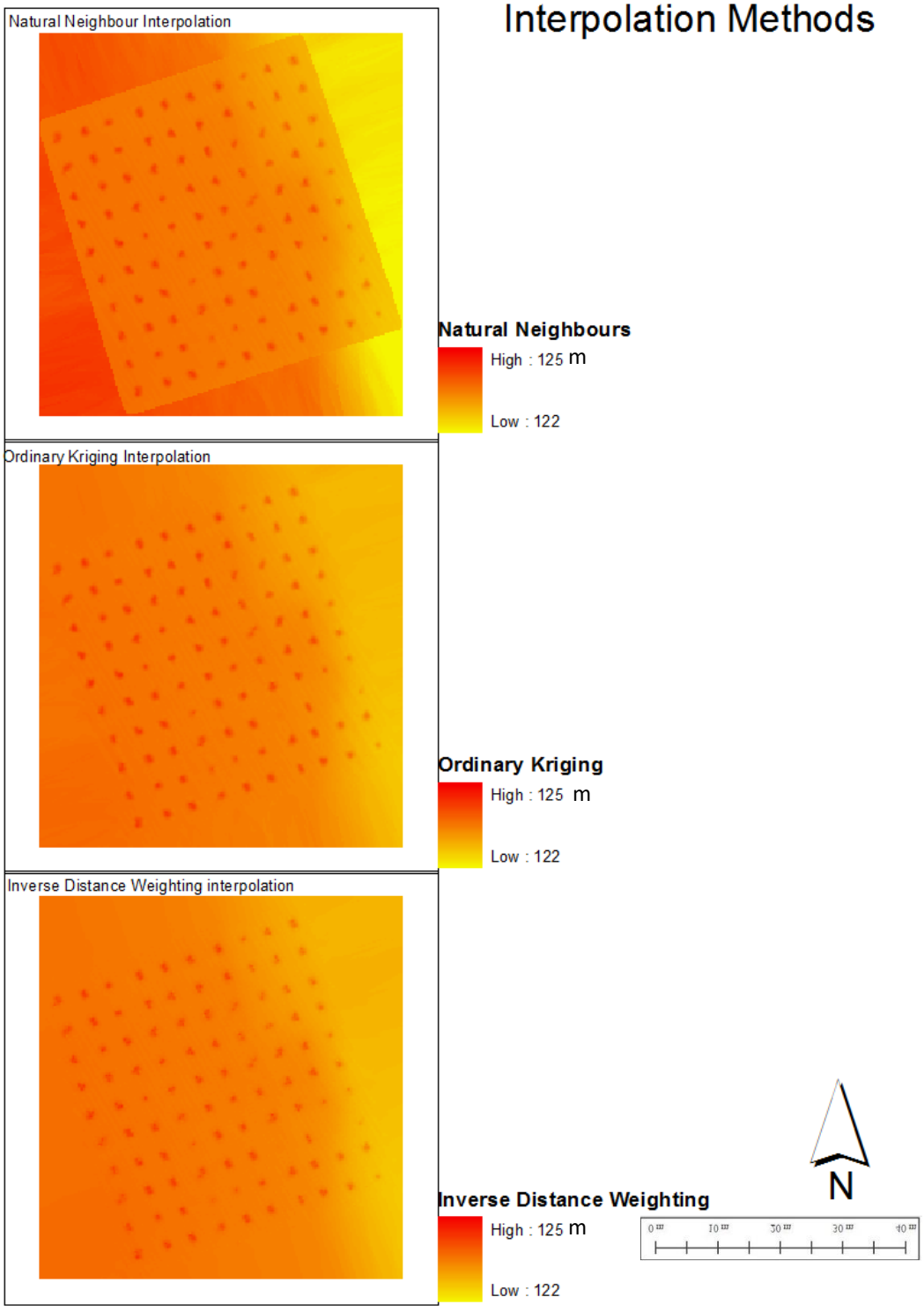

Figure 5-8 shows the interpolated surface for a) natural neighbour interpolation, b) Ordinary Kriging and c) Inverse distance weighting All heights are in metres.

In order to assess the difference in techniques a range map was produced, this can be seen in figure 5-9. The differences are measured in centimetres the largest differences are in the order of 0.1 m; this is below the accuracy of the scanner. As such small differences can be seen from the interpolation techniques, inverse distance weighting was chosen. Inverse distance weighting offers a computationally simple but effective technique for the surface creation.

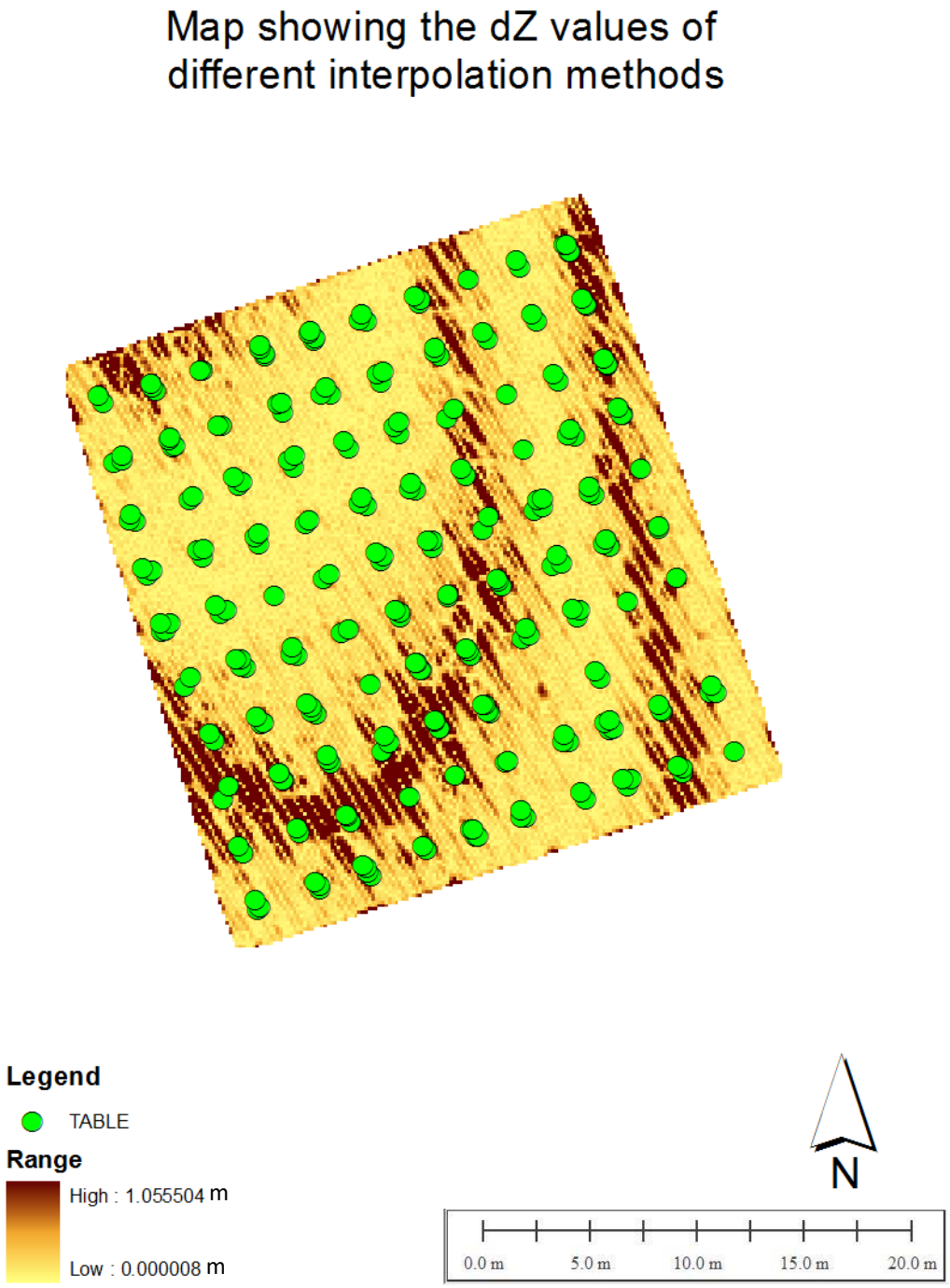

Figure 5-9 Map showing the range difference (dZ) between the interpolation methods, the units are cm, the difference between techniques is very small. The green points are LiDAR strikes on the tables.

The tables will be discussed in detail as individual configurations, further discussion will focus on the combined results before discussing trends and patterns.

5.2 Results for 2.5 m table separation experiment

This section describes the results for the first table configuration; these tables were spaced 2.5 m apart. The results flow in order of processing flow, as such, the point cloud is described prior to the derived surfaces and the resulting analysis is then described.

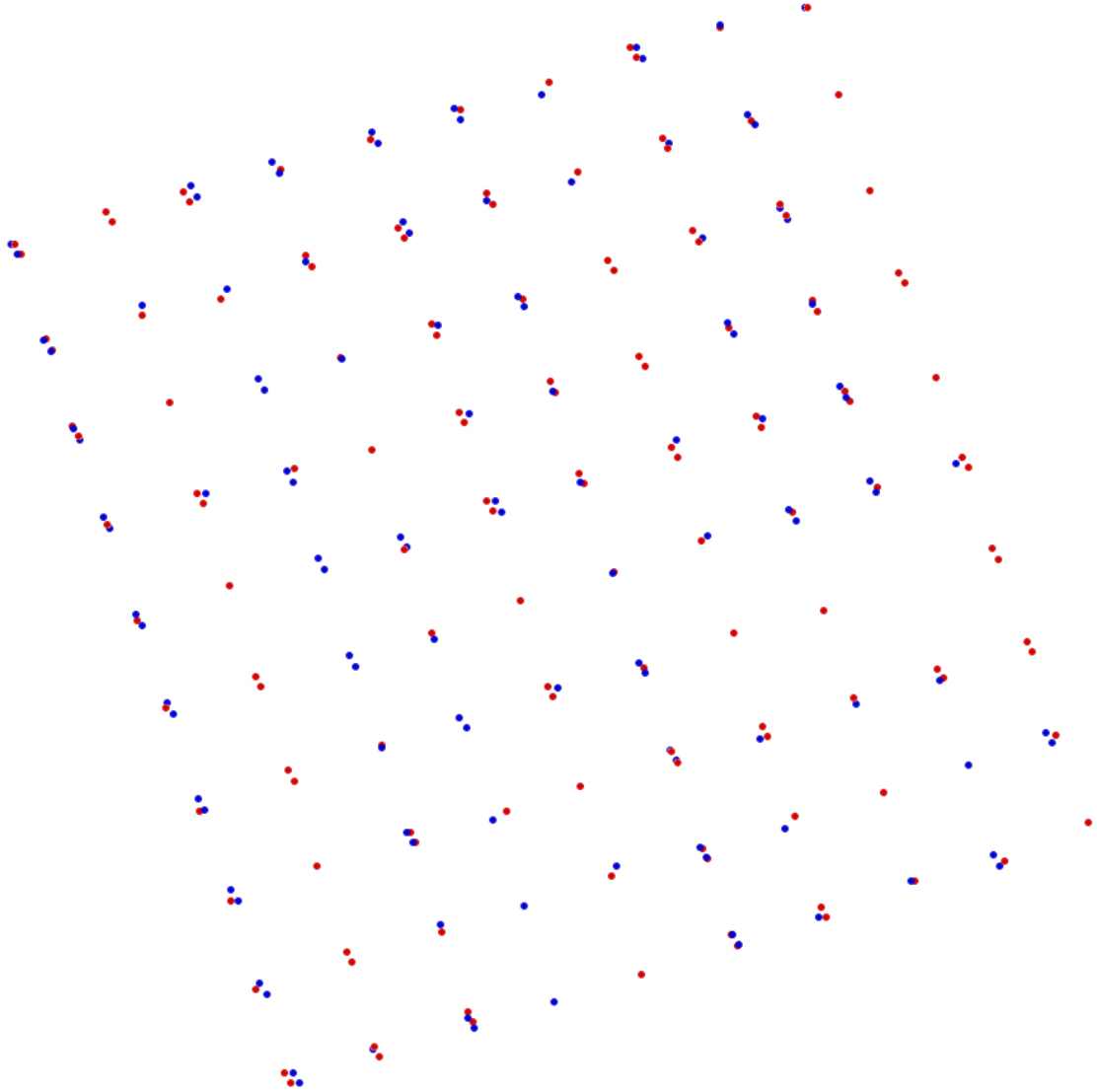

Figure 5-10 showing the tables detected for the 2.5-metre configuration. No other LiDAR returns are shown in this image. The LiDAR returns are coloured by flight line.

Figure 5-10 shows the two table data for the two over flights for the 2.5-metre table configuration. The data has many very important observations. When considering the two over flights together, one table was entirely unobserved. The remaining tables varied between one to four laser strikes. Figure 5-10 shows these variations, it is clear that the tables were inconsistently observed by the laser system. Figure 5-11 and figure 5-13 provide

a breakdown by flight. Figure 5-11 and figure 5-13 show 8% and 24% missing tables for flight 1 and 2 respectively. This threefold increase in unobserved tables is difficult to explain with the controls placed upon the experiment.

The results below build up the investigation into the table observations. Individual flights are described using surface models normalised against the ground surface. Both over fights are then combined to show the results of the doubled point density from the two over flights. Subtraction of the individual flight lines from each other is used to produce a difference model. The results are then analysed graphically using a series of bar charts and histogram to allow patterns to be observed.

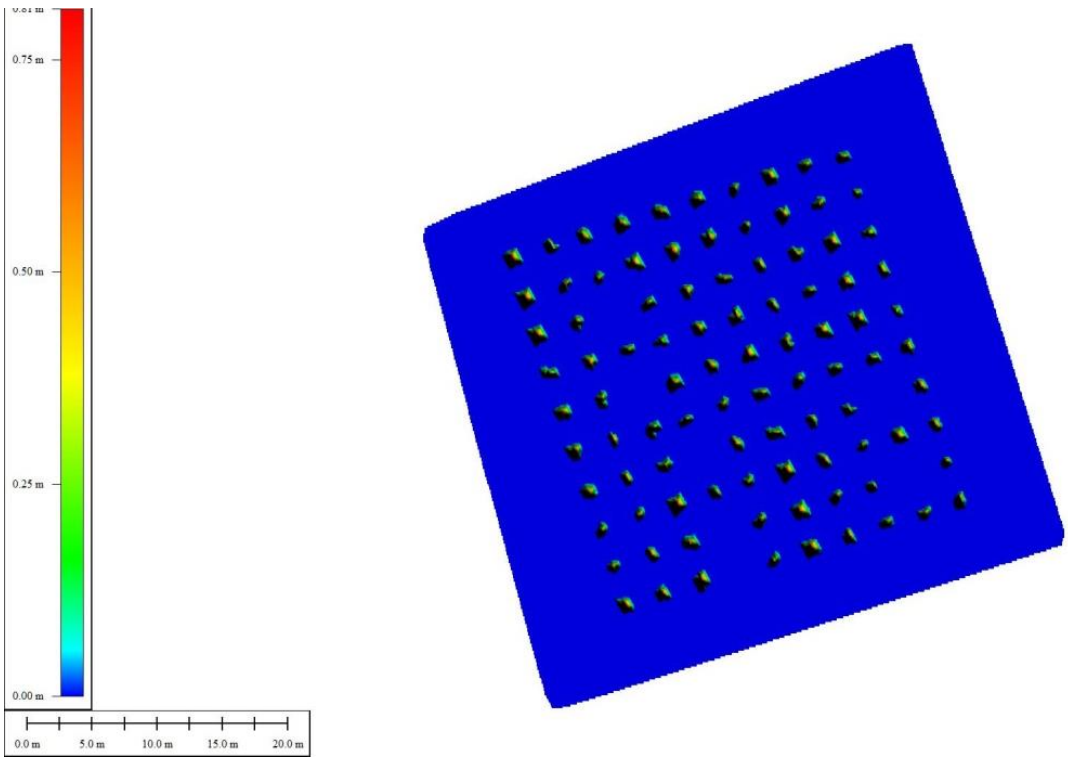

Figure 5-11 Surface model showing the normalised DSM for the flight 1 tables for the table 1 configuration. Table separation is 2.5 metres.

The surface model shown in figure 5-11 shows the table results as a surface model, the missing tables are clearly observable, a trend running broadly north the south can be observed with the tables missing at D1, 2 and 4 and the pattern continuing to C6 and C8 locations. Further missing tables can be observed at I2 and I4. The 3 dimensional perspective model shown in figure 5-12 demonstrates the observed versus omitted tables well.

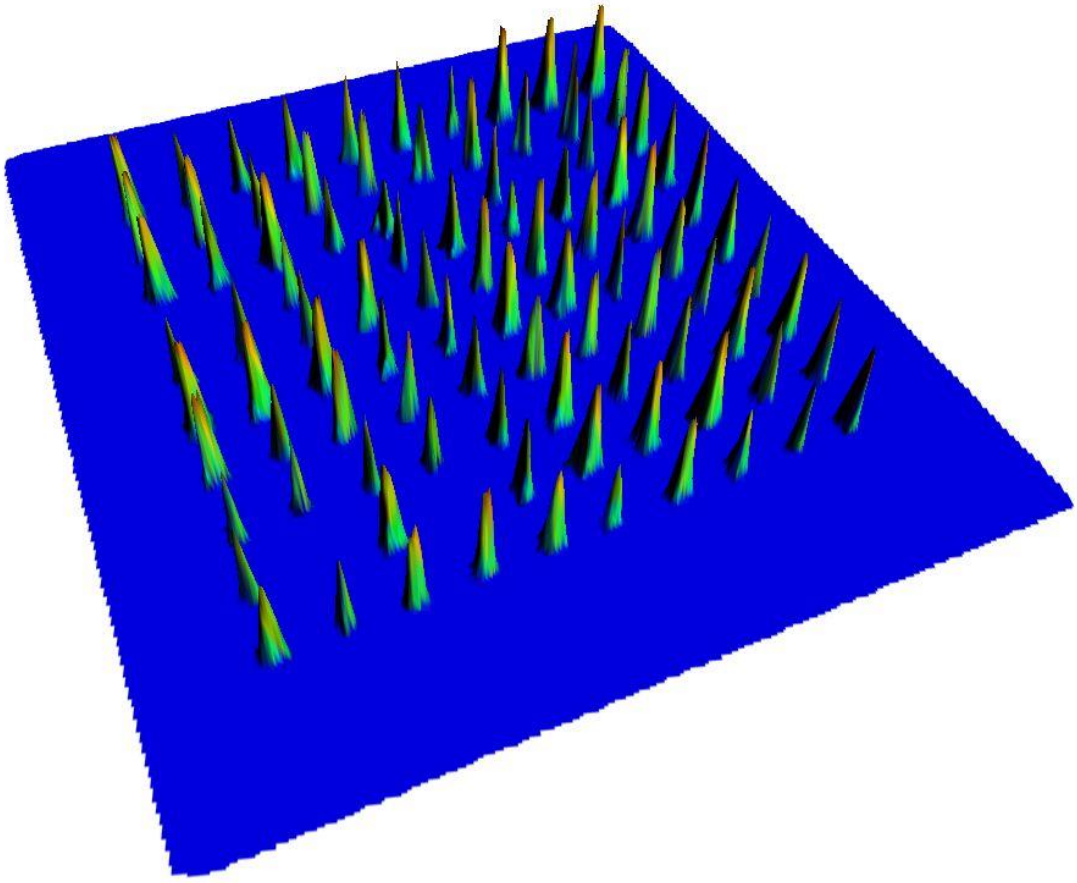

Figure 5-12 three-dimensional perspective of surface model for flight line 1 of table 1, table separation is 2.5 metres.

Figure 5-12 is orientated to display the topographic variations, the maxima and minima are clearly visible, the blue represents minima with red representing maxima.

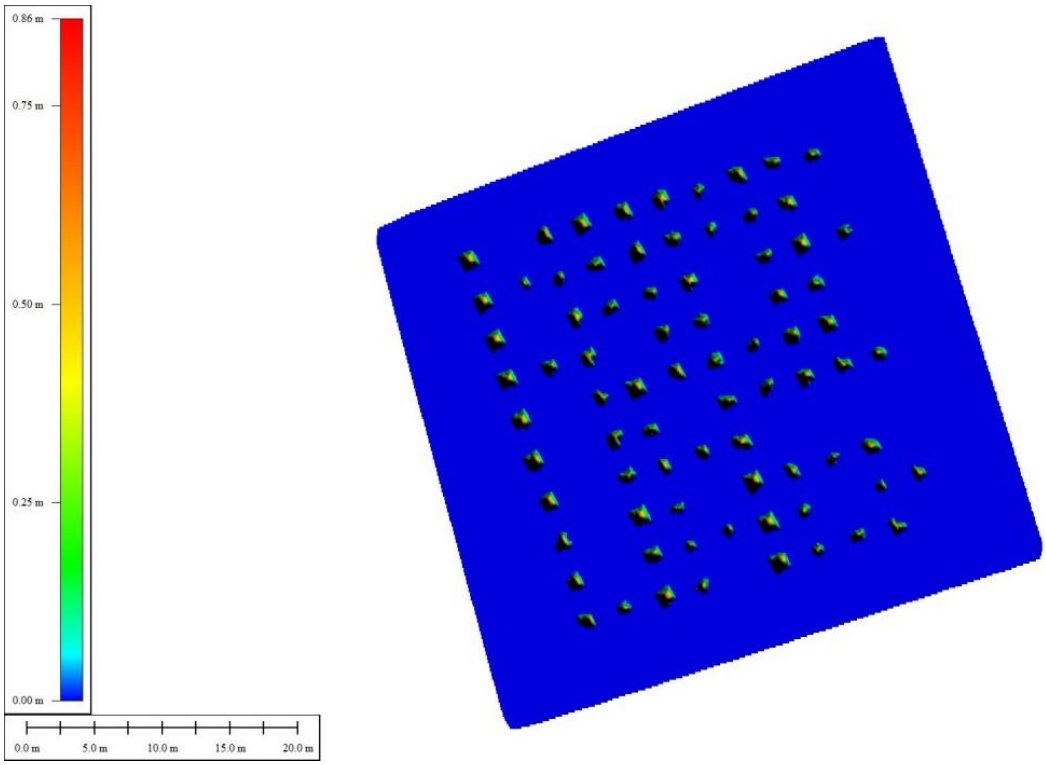

Figure 5-13 Surface model showing the normalised DSM for flight 2 of the table 1 configuration. Table separation is 2.5 metres.

Figure 5-13 shows the second over flight of the tables, this surface model has interesting patterns displayed, the tables found along the B column of the arrangement show 70% omission, row J shows 60% omission and similarly the row 4 tables show 50% omission. Whilst these patterns seem to exist, looking at the three dimensional view shown in figure 5-14 the omissions are very apparent. The recorded table heights are also clearly different between rows.

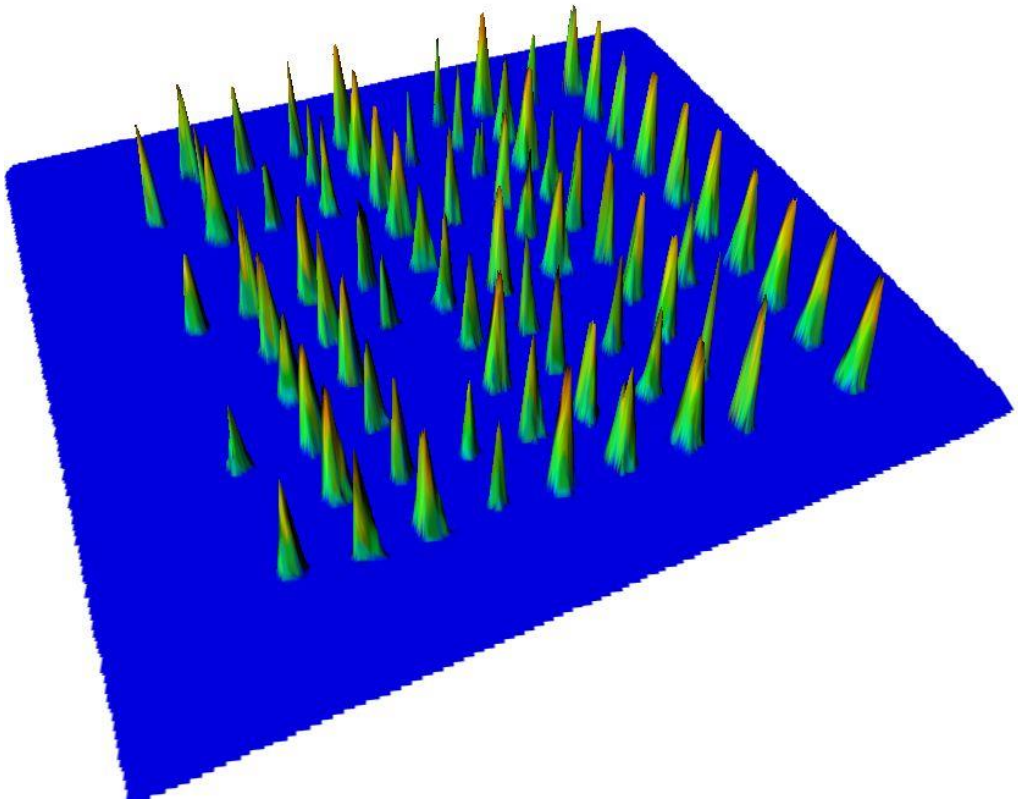

Figure 5-14 three-dimensional perspective of surface model for flight line 2 of table 1. Table separation is 2.5 metres.

Figure 5-14 is oriented to show the terrain variations clearly, along the left hand edge (row J in this orientation) the omitted tables are clear, the variations in height are also very apparent.

By combining both flight lines of the same table configuration the point density doubles and the number of table's unobserved decreases, the surface model showing this can be seen in Figure 5-15.

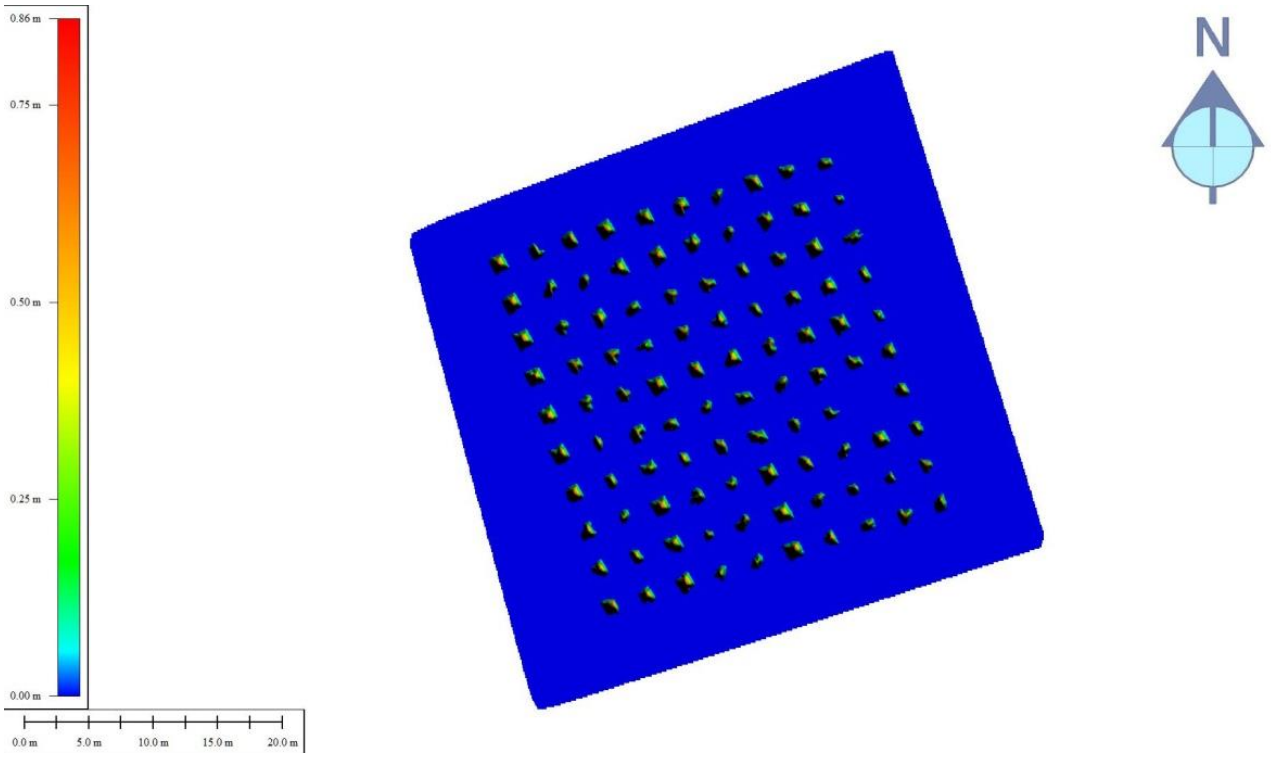

Figure 5-15 Shaded surface model showing the table surface produced by two over flights of the 2.5 metre configuration, ground level removed to express elevations above local ground height.

The tables are not all observed even with the doubled point density, the maxima exist at the northwest corner and the missing table to the southeast corner remains unobserved by both flights.

The three dimensional perspective in figure 5-16 shows the variations in height, and equally shows the increased detection rate from the combining of the flights.

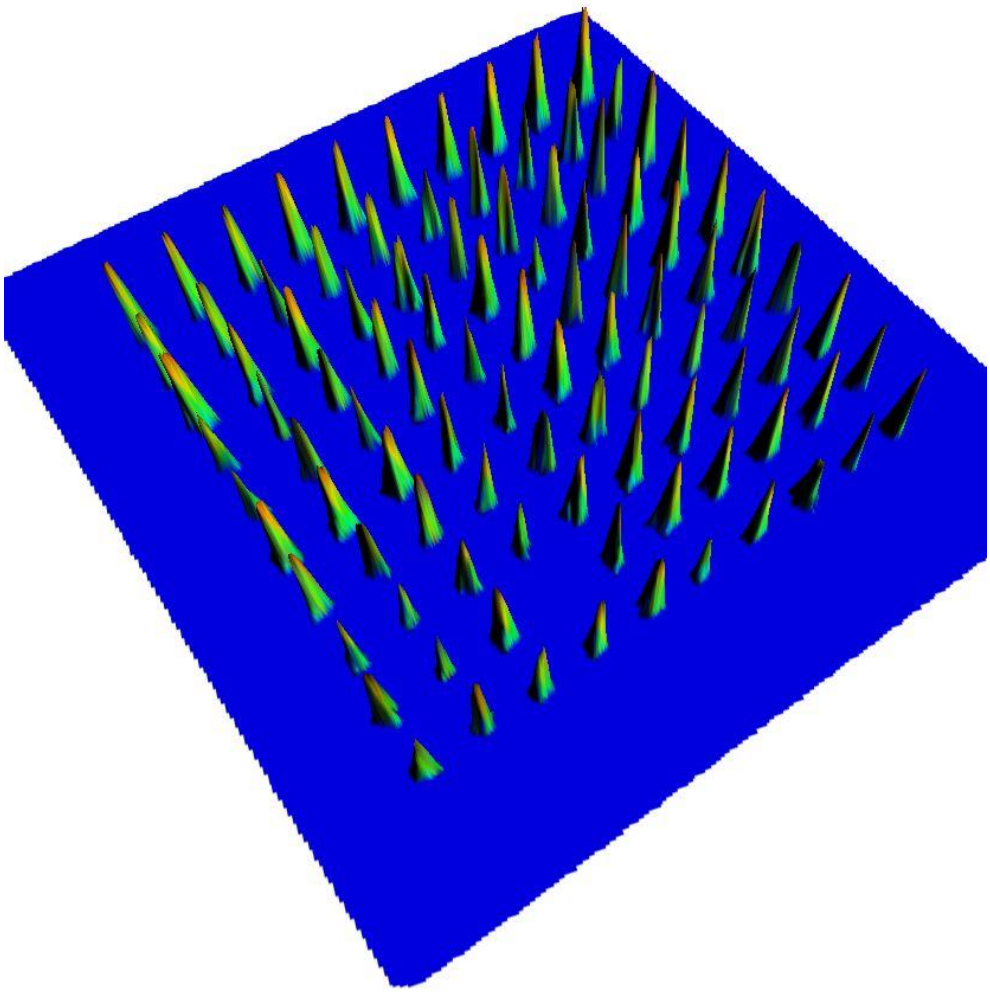

Figure 5-16 3-dimensional view of figure 5-15 showing the peaks and troughs. Table separation is 2.5 metres.

In order to view the difference between the two flight lines and to try to find an emerging pattern for the detection or omission of the tables, a DEM of Difference (DoD) was created, this subtracts flight 1 heights from flight 2 heights to show areas of difference. Areas where the surfaces are congruent will show as 0 m (white) in the DoD. Figure 5-17 shows the resulting surface model.

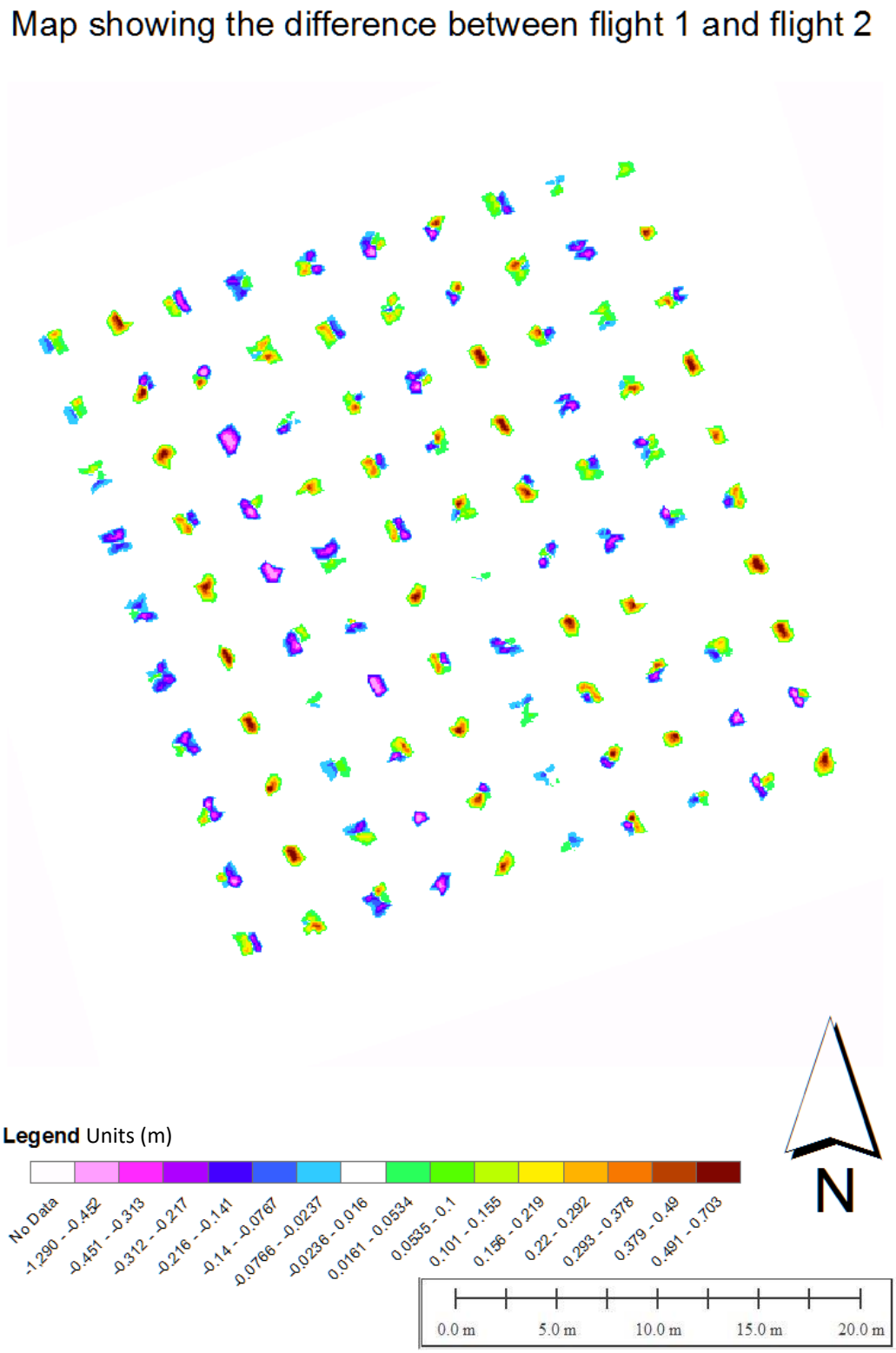

Figure 5-17: showing the difference model between two flights with the same parameters over the 2.0m table arrangement.

Whilst the patterns described above can be seen in the DoD the overall arrangement appears to be random, the centre of the tables showing a stronger agreement between the flights than the outer edges of the configuration.

In order to investigate this further, the number of strikes per table has been extracted from the point cloud data, the bar charts in the following figures are used to display the percentage of tables receiving the respective number of strikes. The results from the 100 tables are expressed as a percentage, given the number of tables in the study; this also describes the absolute number of tables.

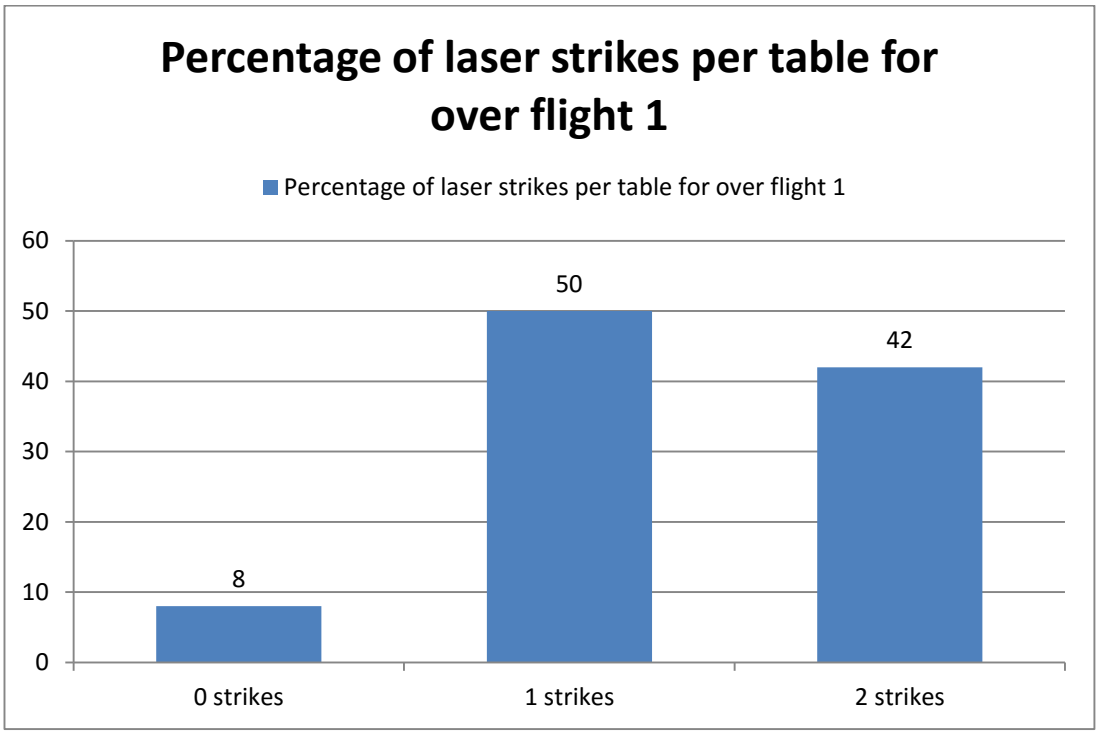

Figure 5-18 bar chart showing the percentage of laser strikes per table for flight 1

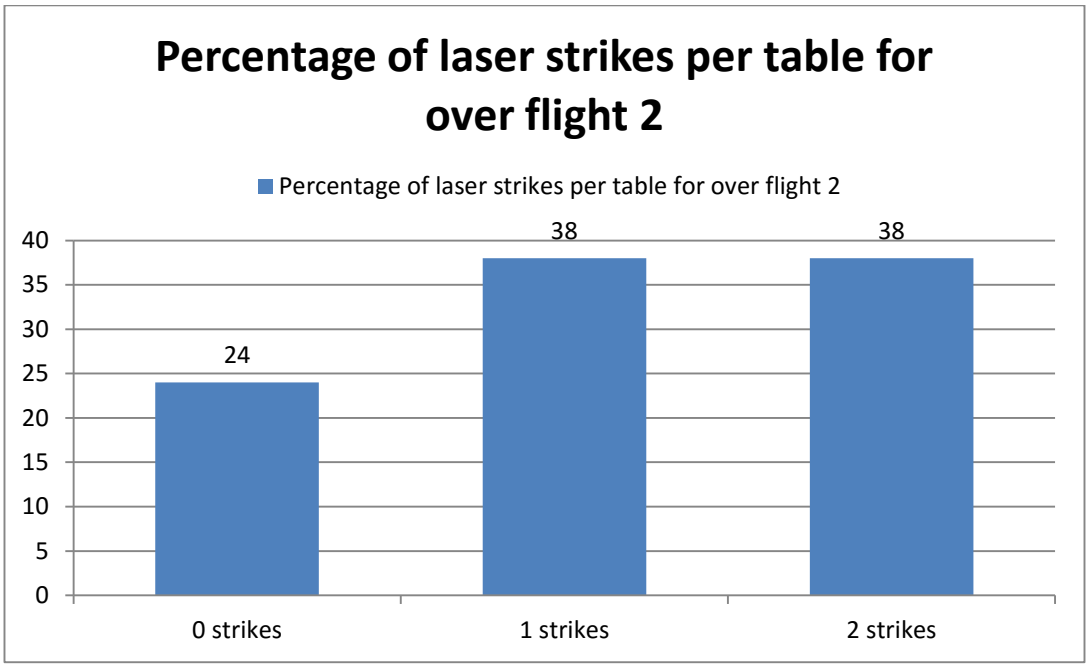

Figure 5-19 bar chart showing the percentage of laser strikes per table for over flight 2

Figure 5-18 and figure 5-19 show the results for flight line 1 and 2 respectively, Flight line 1 has detected 92% of the tables with flight line 2 only detecting 76%, and this is a stark contrast given both flights have identical survey parameters. Whilst flight 1 detected more tables overall, of the tables detected, a smaller proportion received two strikes the overall detection rate remains higher in flight 1.

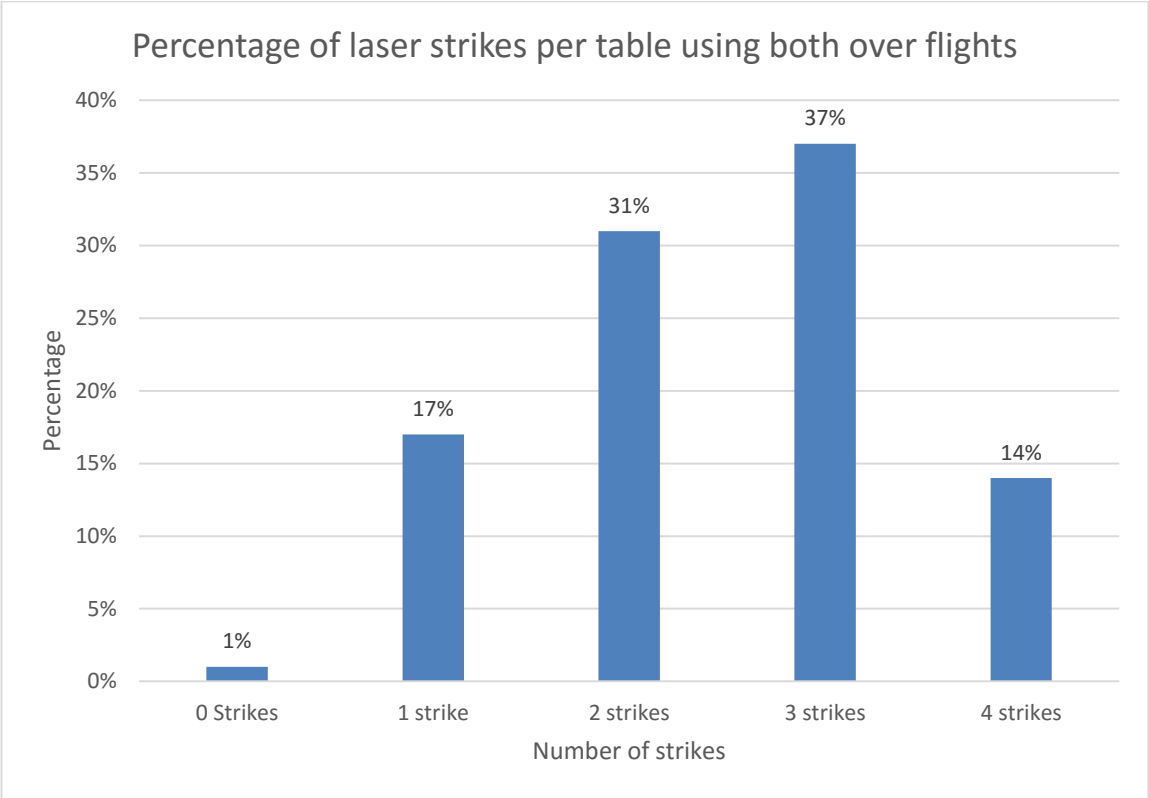

Figure 5-20 Bar Chart showing the breakdown of laser strikes per table for 2.5 metre table configuration by percentage

Merging both flights together, the analysis is shown in figure 5-20. One table is undetected and the remaining tables receive between one and four strikes. The expectation is that all tables should receive four strikes using the point density calculation. 14% of tables were observed with two returns from each flight, leaving 86% to be under observed from expectation.

In order to assess the relative performance of one flight over another, the deviation from the average number of strikes for the table has been calculated. Figure 5-21 shows the results. The blue line shows the difference between flight 1 and 2and associated frequency at each bin. The red line shows the deviation of flight 2 from the mean number of strikes and green

the same for flight 1. The central tendency of both flights is to pick up the same number of strikes as the other flight, with the move from zero difference showing greater discrepancies.

The flight 1 – flight 2 graph line shows the tendency of flight 1 to observe fewer strikes and is shown in the skew of the curve.

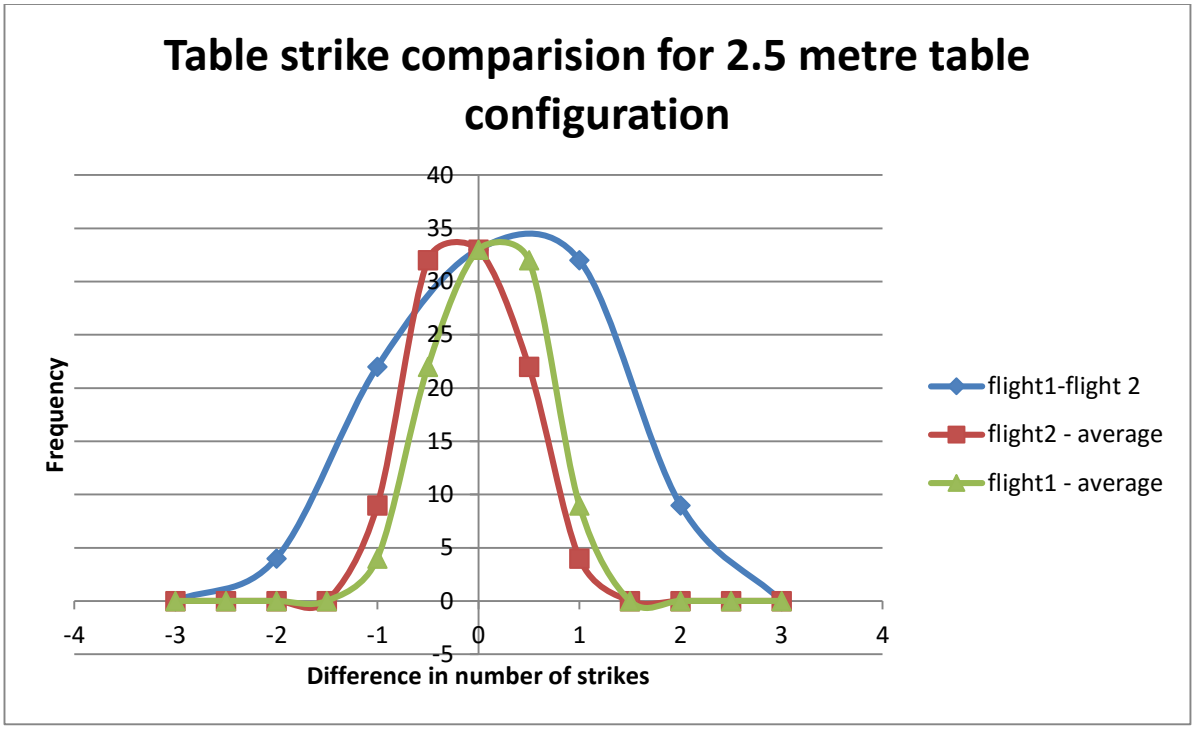

Figure 5-21 Graph showing the variance in table strikes for the 2.5 metre separation tables. Results are for the same table configuration and flight parameters

The data for this table configuration make it clear that LiDAR has not picked up the tables in a verifiable manner. The tables are inconsistently identified between the two flights.

5.3 Results for 1.5 m table separation experiment

The table two results will follow the same sequence as those of table1, the individual flight line surfaces will be described before combining the two flights, then differencing of the flight lines will be used to check for variation between the flight lines. Graphical analysis will be used to investigate the table detection characteristics.

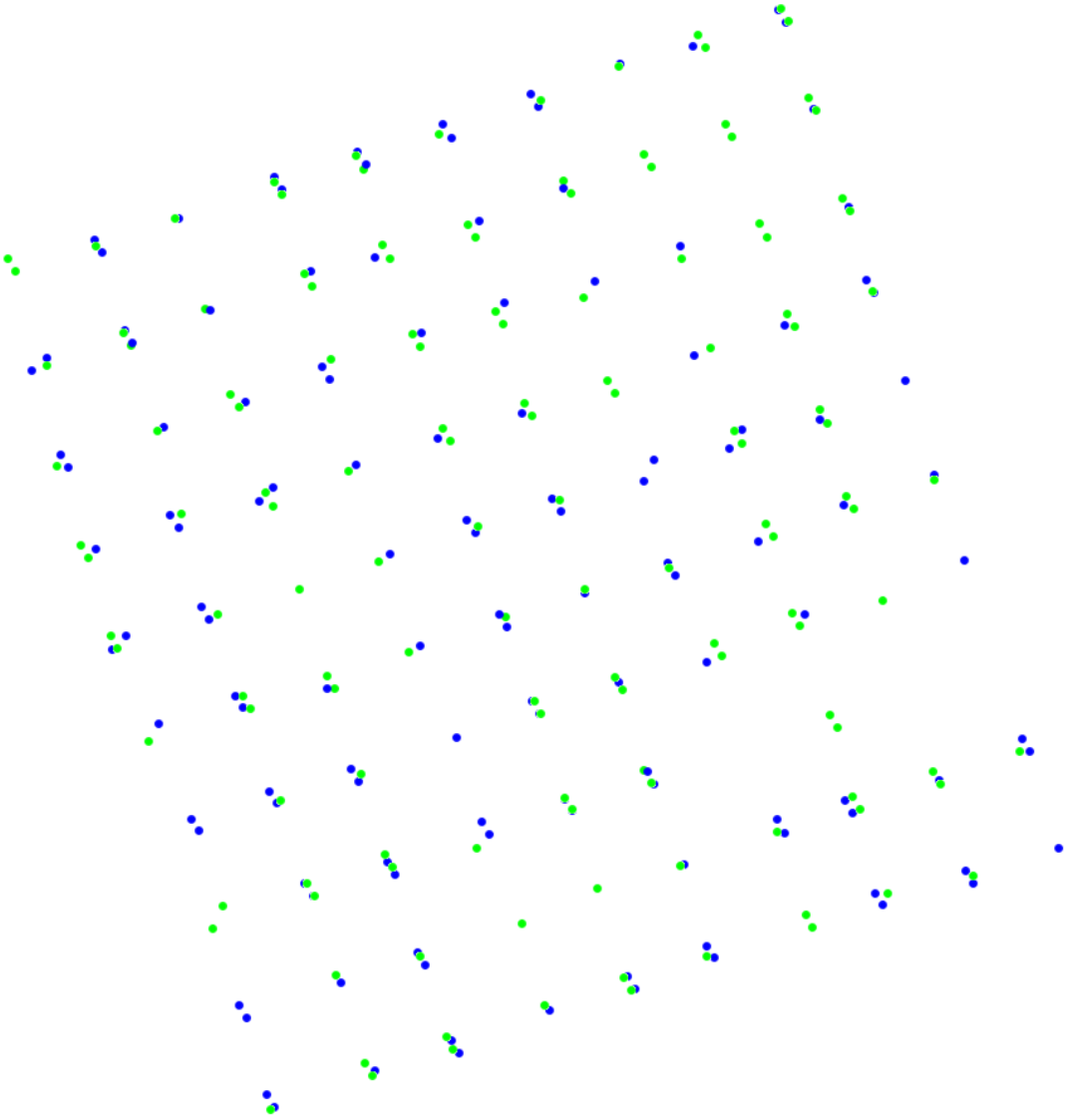

Figure 5-22 showing the two flight lines from the 1.5 metre table configuration. Points coloured by flight line

Figure 5-22 shows the table configuration for the second table configuration. The missing tables in the southeast quadrant can be seen clearly, as can the difference in density of strikes on the tables.

The individual flight lines have been analysed to look for table detection and omission patterns. Figure 5-23 shows the surface model for the table strikes for flight line 5. This figure shows a number of tables undetected and a range of elevations from the surface. Again, the centre of the table areas shows greater homogeneity with the outer edges clearly showing a number of tables undetected. Six tables have been undetected by this flight line.

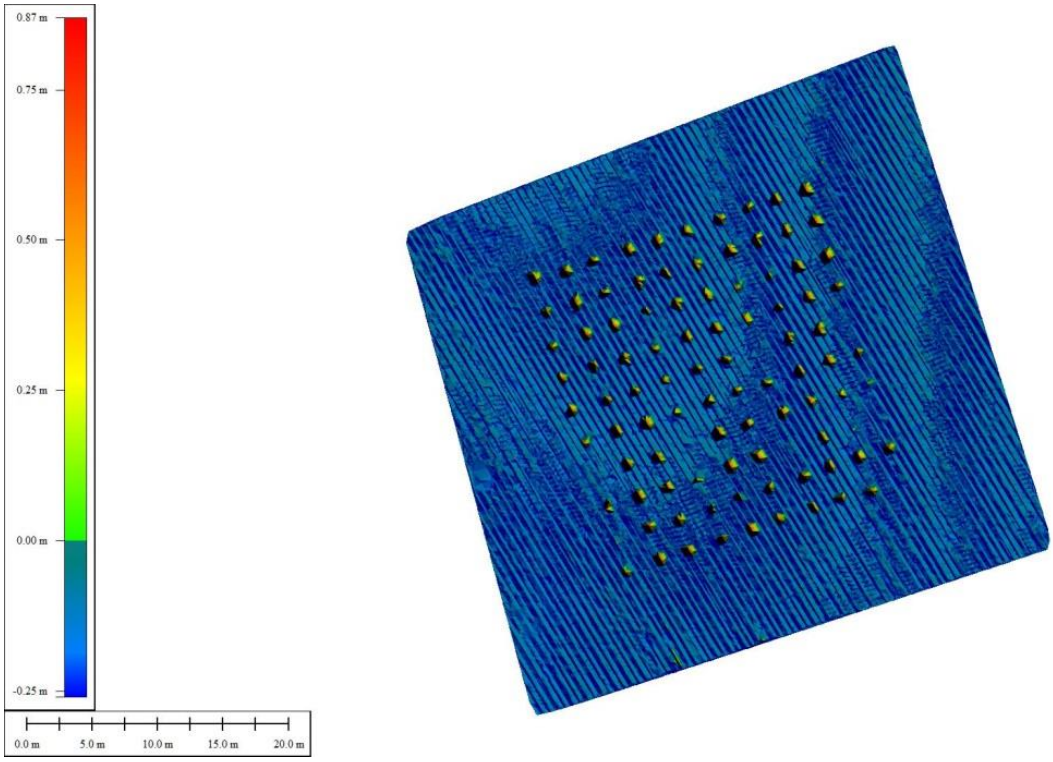

Figure 5-23 shows the normalised DSM for flight 5. Table separation is 1.5 metres.

The omitted tables and topographic expressions can be clearly seen in figure 5-23. The red areas are higher elevations with the blue areas showing minima.

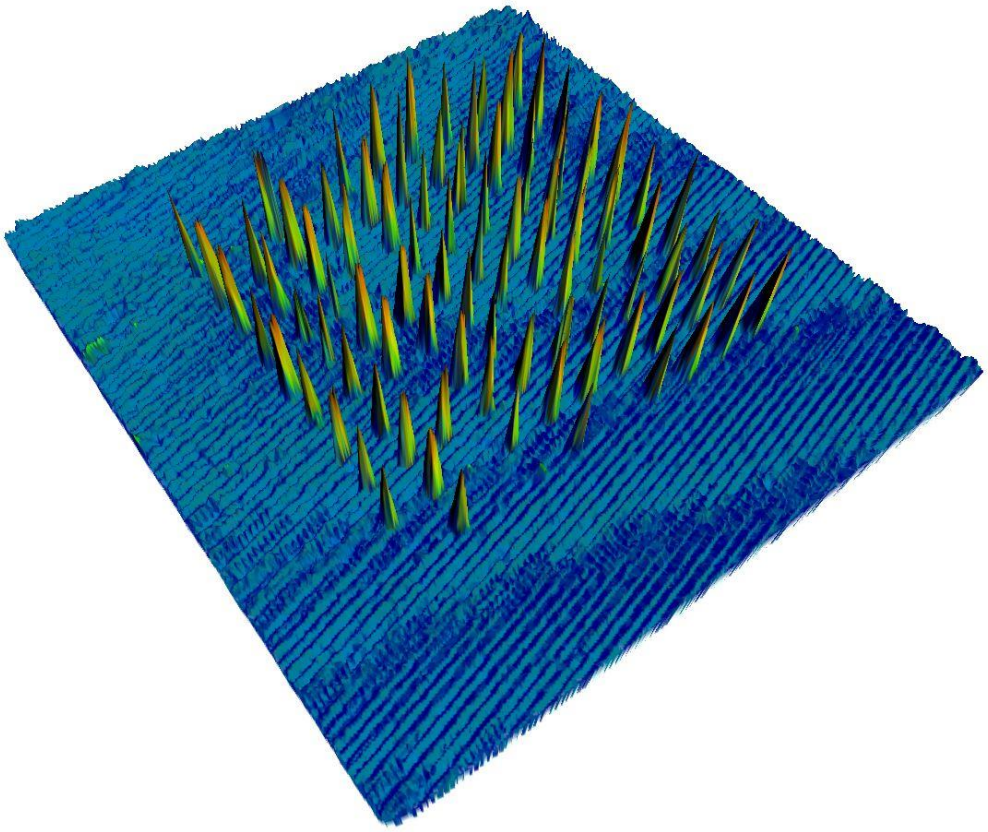

Figure 5-24 shows a 3 dimensional view of flight line 5's normalised DSM, this highlights the difference between the observations. Table separation is 1.5 metres.

A similar pattern can be seen in figure 5-24 the main deviation in height comes to the outer edges of the table area. The southeastern corner has a very clear minima (blue) there is also a number of tables omitted at the northern edge.

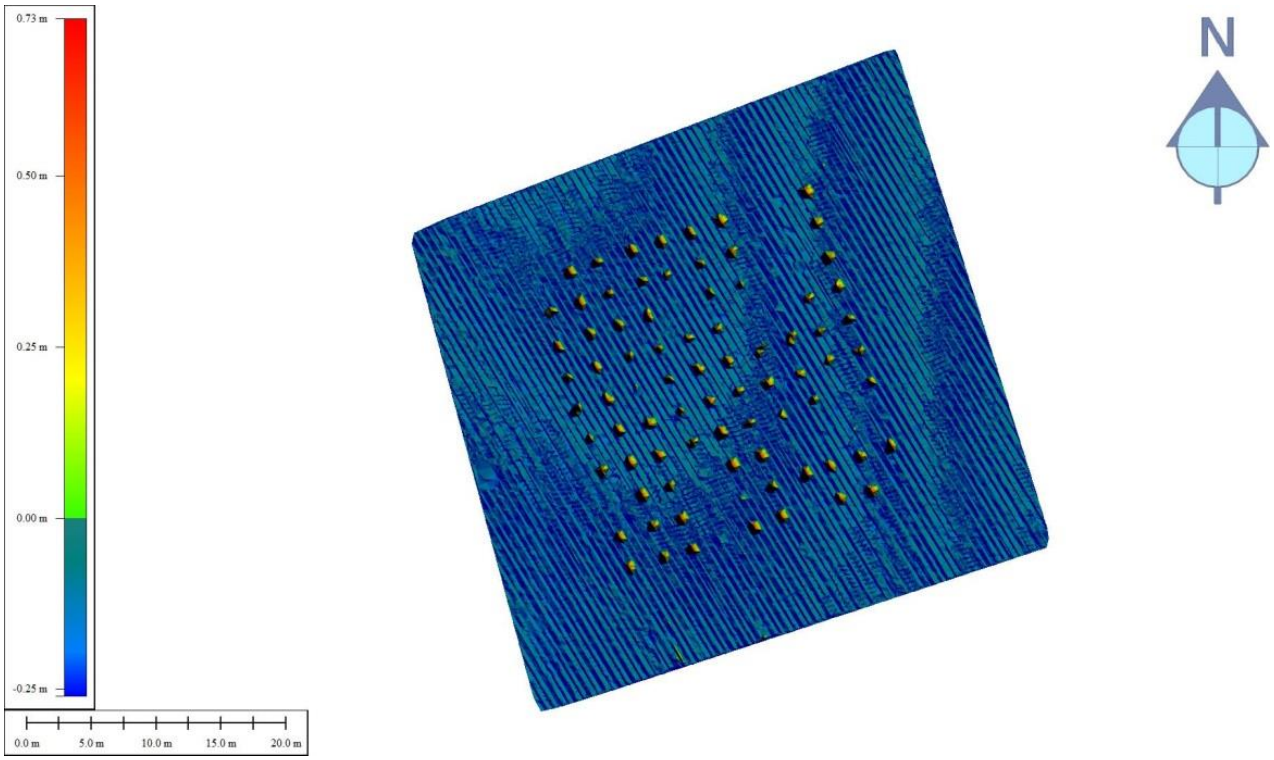

Figure 5-25 flight 7 normalised DSM. Table separation is 1.5 metres.

The three dimensional representation of the flight 7 normalised DSM is shown in figure 5-26 shows the omitted and detected tables in detail.

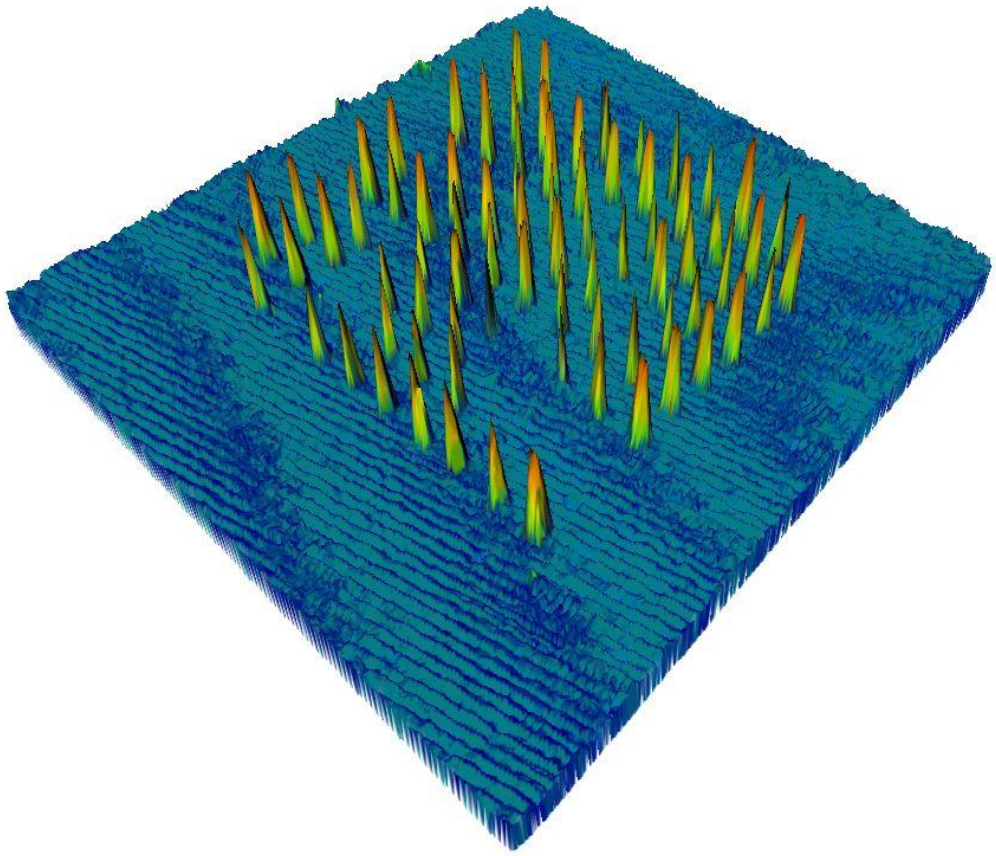

Figure 5-26 3D view of flight 7 normalised DSM. Table separation is 1.5 metres.

Merging both flight lines together to double the point density gives much better table detection. Figure 5-29 shows much better table detection with only three tables omitted. Interestingly the three tables all form part of the end of a row, with the third table form the edge detected but the other three omitted.

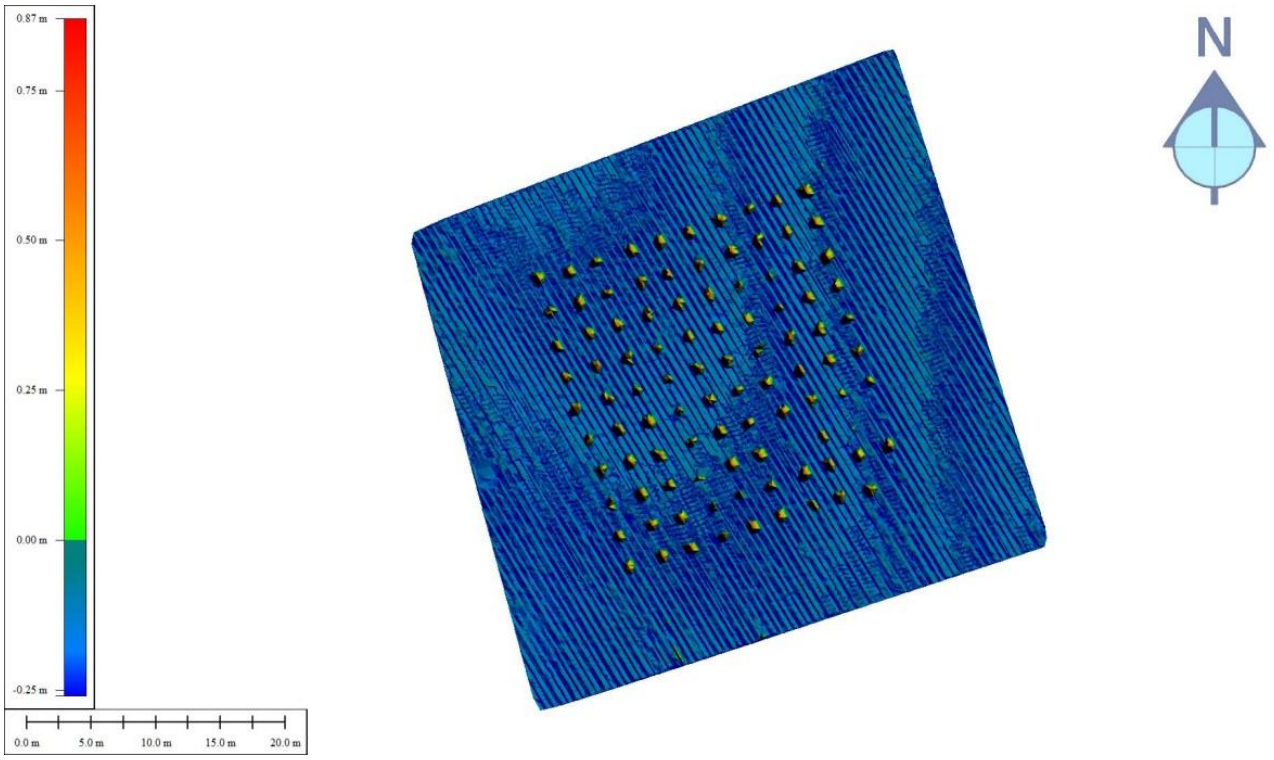

Figure 5-27 both flights shown as a normalised DSM. Table separation is 1.5 metres.

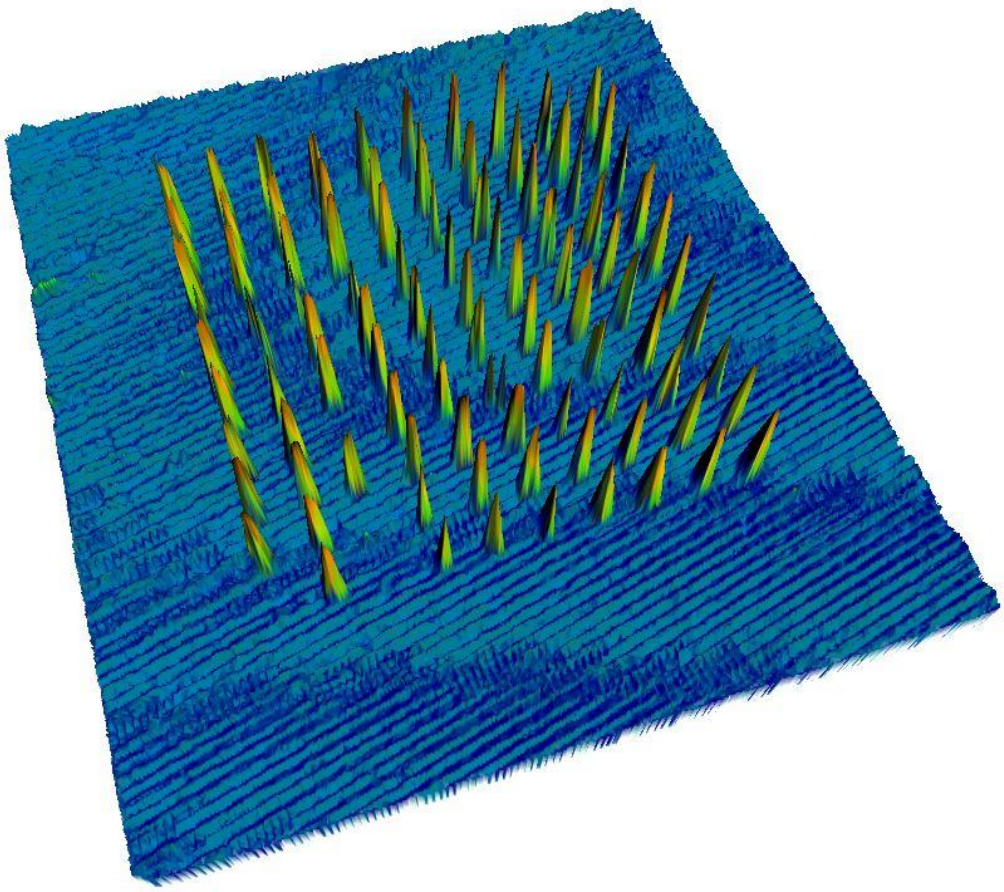

Figure 5-28 both flights merged shown in a three-dimensional view. Table separation is 1.5 metres.

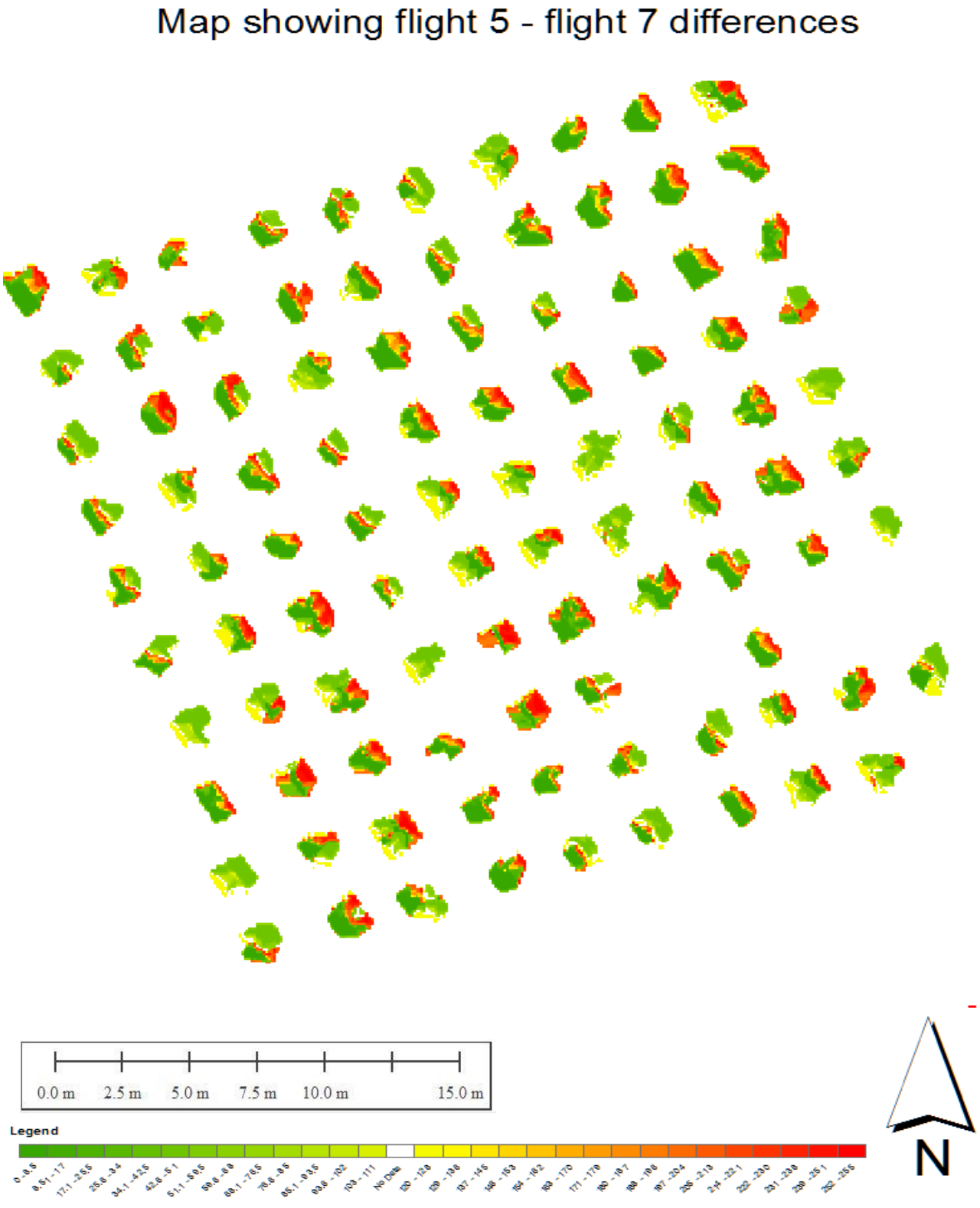

Figure 5-29 Different model showing flight 5 - flight 7 heights. Table separation is 1.5 metres.

The results are displayed graphically below in figure 5-30, figure 5-31 and figure 5-32 the individual flight lines are analysed then the combined flight lines are analysed.

Flight 5 shows 10 missing tables with 53% of tables receiving less than the expected number of hits.

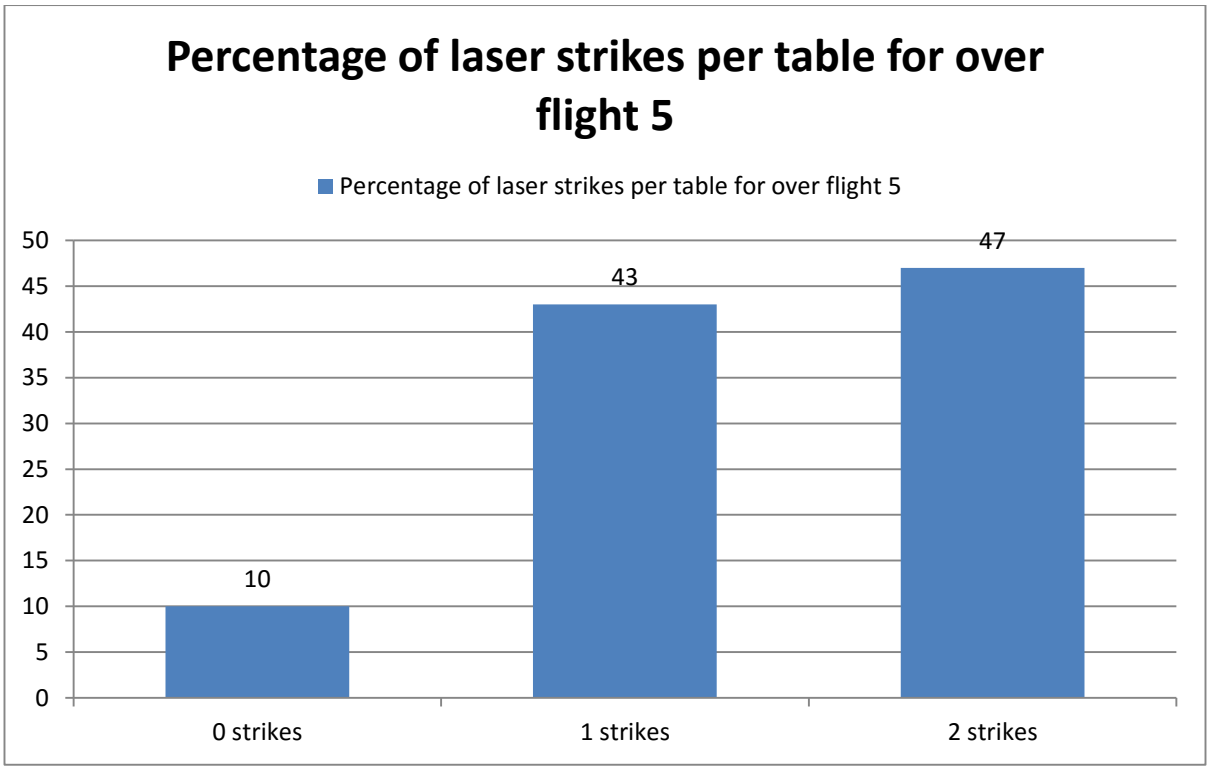

Figure 5-30 Bar chart showing the percentage of tables receiving 0, 1 or 2 strikes for over flight 5

This compares to flight seven having 15 missing tables and a 58% rate of under detecting the tables (less than two strikes). As such, flight 5 can be seen to be more successful win its

detection of tables. This flight orientation proved to be more successful for the table 1 configuration as well.

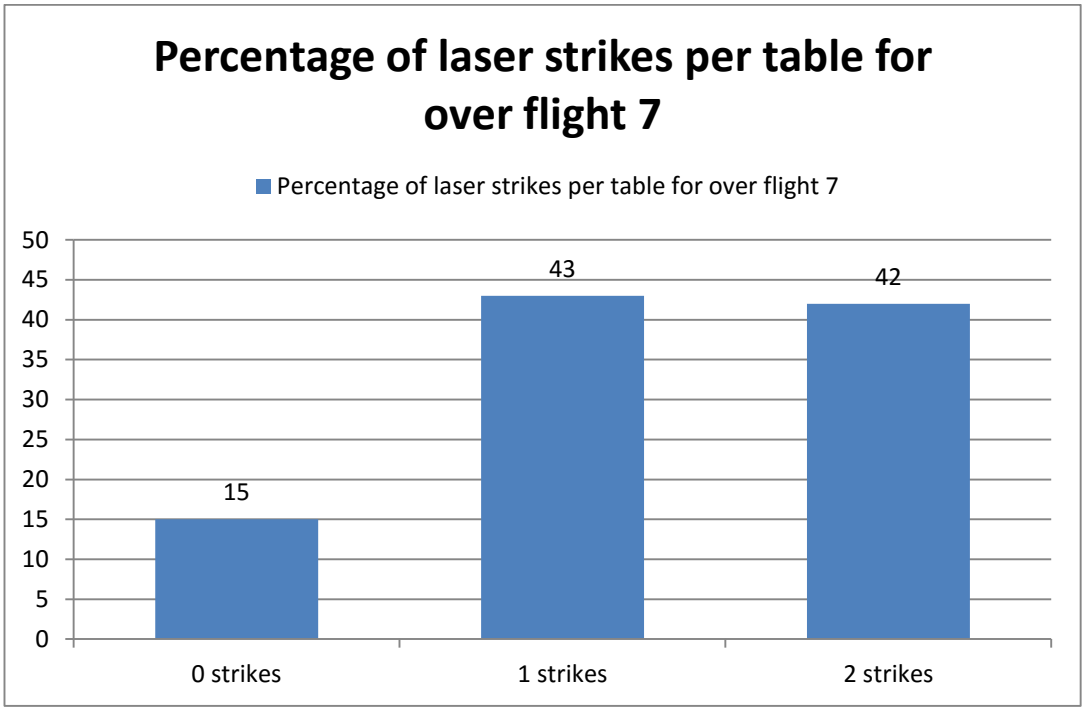

Figure 5-31 Bar chart showing the percentage of tables receiving 0, 1 or 2 strikes for over flight 7

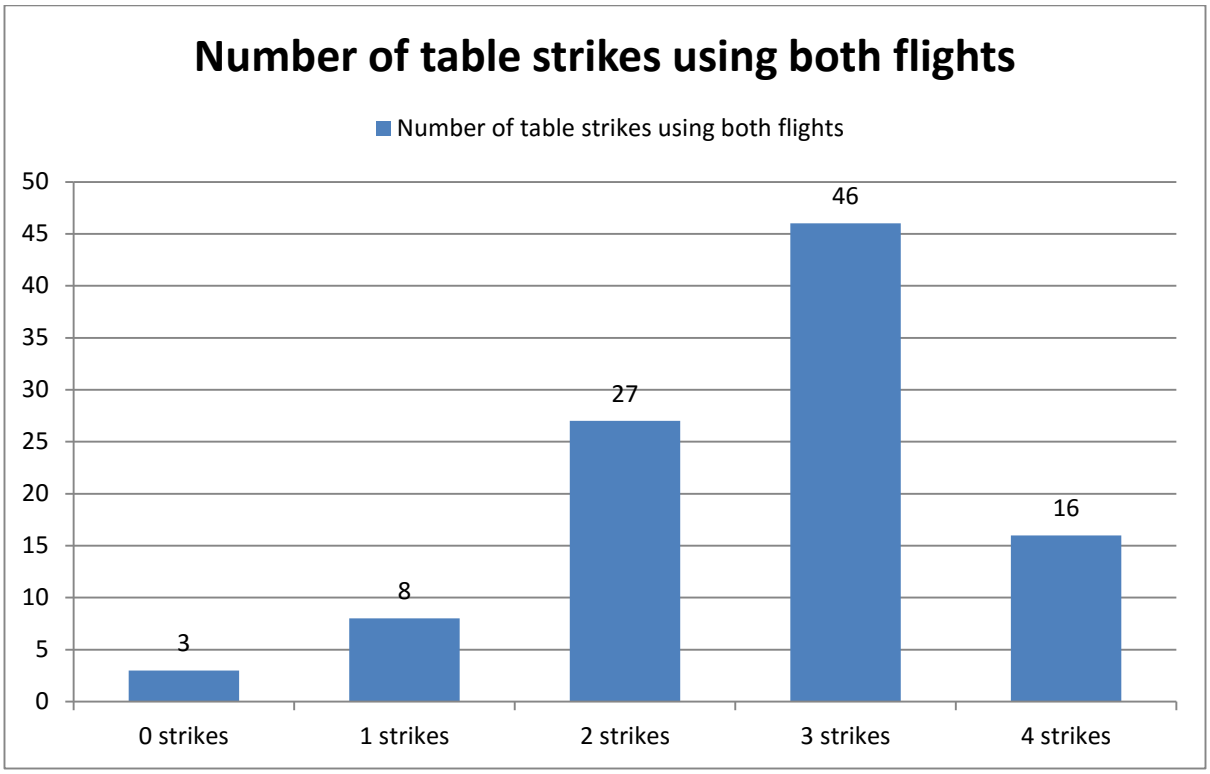

Figure 5-32 Bar chart showing the number of laser strikes per table for the two overpasses at the 1.5 metre table configuration

Putting the flights together reduces the undetected rate to 3%, with 46% receiving the expected four returns.

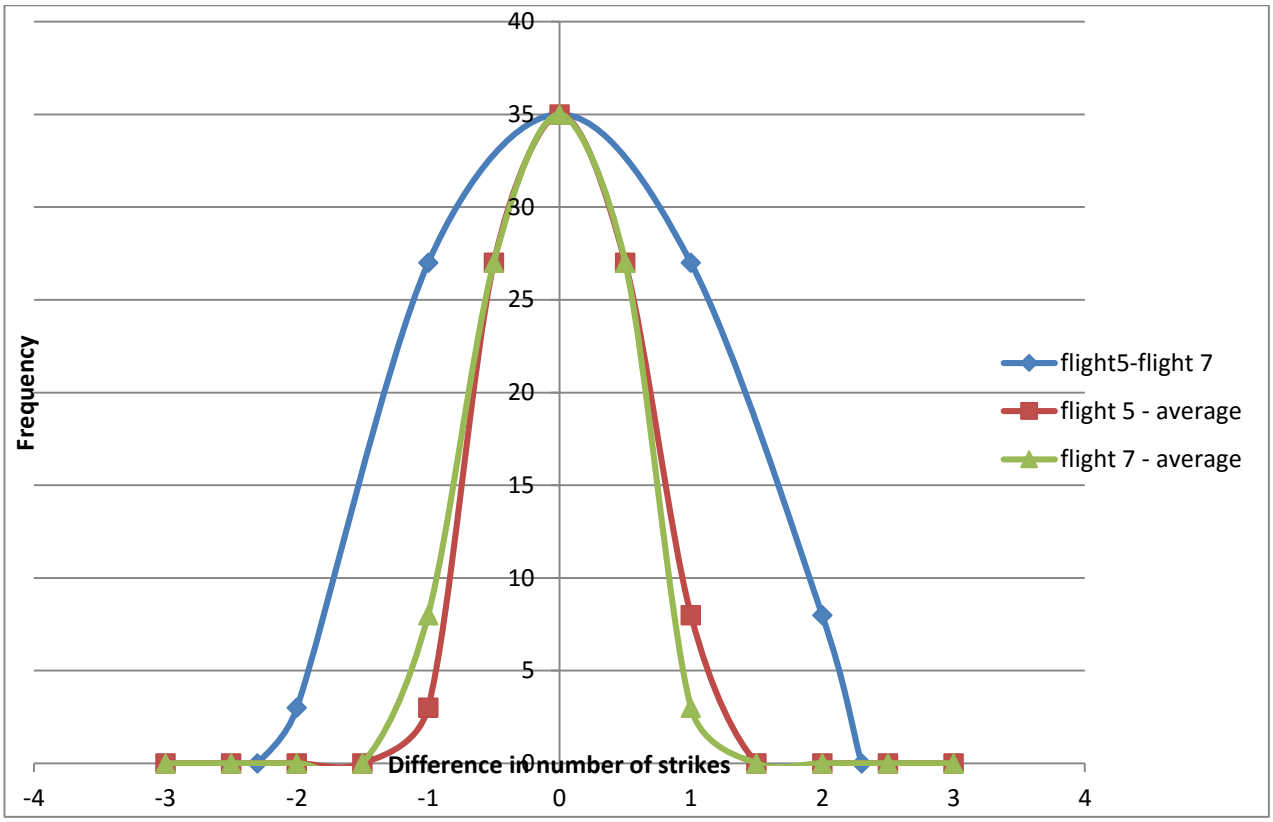

Figure 5-33 graph showing the differences between flight 5 and flight 7 and the deviation of each flight from the average for that table.

Figure 5-33 provides a histogram of the flights. The blue line shows the difference in observations for a table, the red and green flights show the flight value minus the mean number of table strikes respectively. All lines show a central tendency towards the mean and the same number of observations per table.

5.4 Results for 1.0m table separation experiment

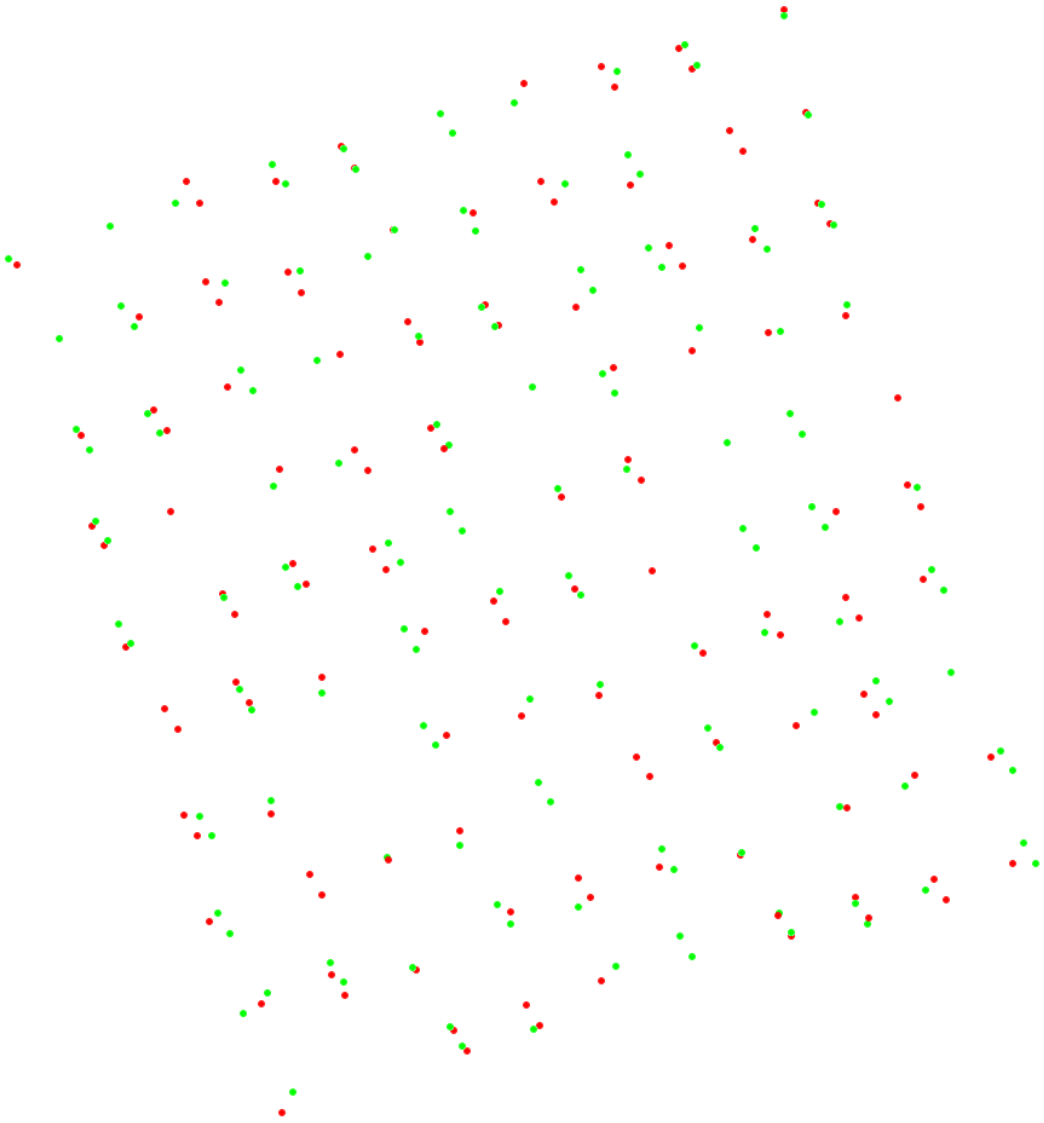

Figure 5-34 showing the tables observed by over fights 9 and 11. Points coloured by flight line. Table separation is 1.0 metres.

This table configuration was flown using flights 9 and 11, they are shown in figure 5-34 and this shows a number of missing tables, notably to the southern portion of the tables. A number of tables have received strikes from only one flight line.

The surface model below in Figure 5-35 and Figure 5-36 show flight 9's normalised surface model, the roughness from the areas of undetected tables can be seen with elevations ranging from 0.52 metres to 0.90 metres.

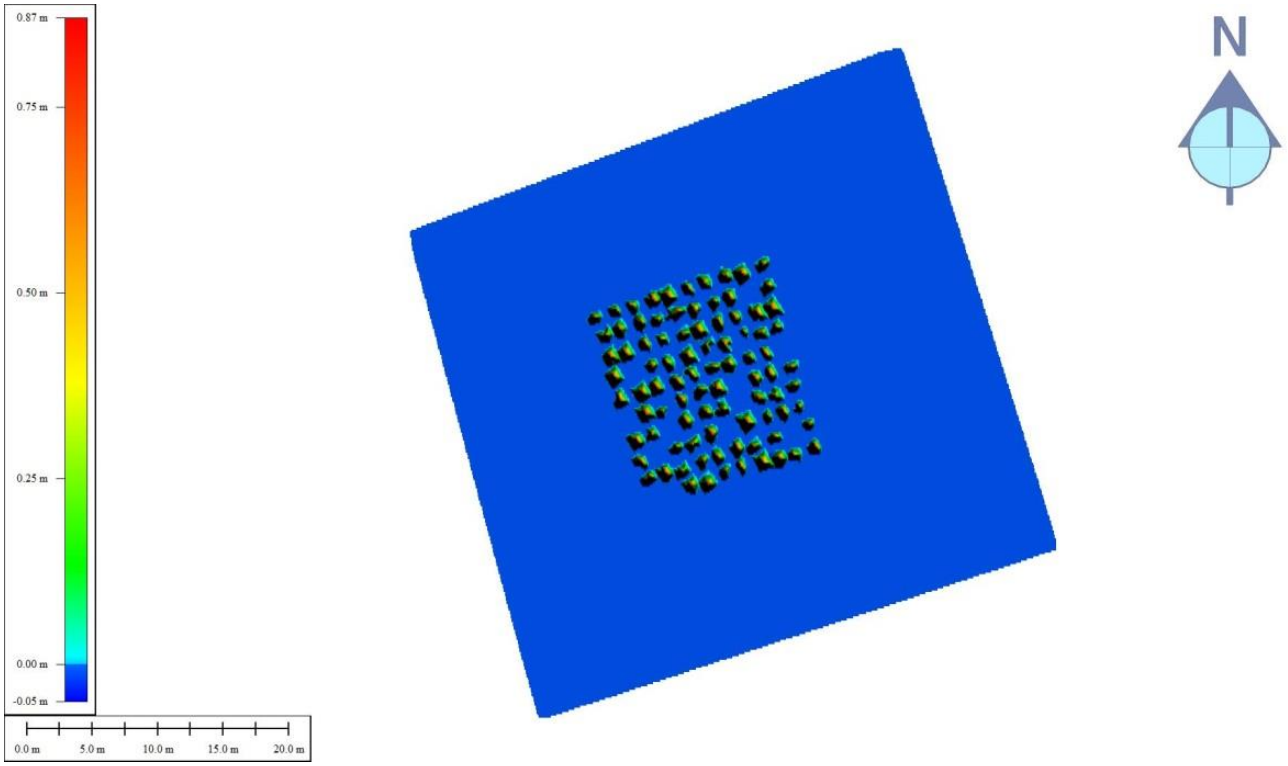

Figure 5-35 surface model for flight 9 normalised DSM. Table separation is 1.0 metres

.

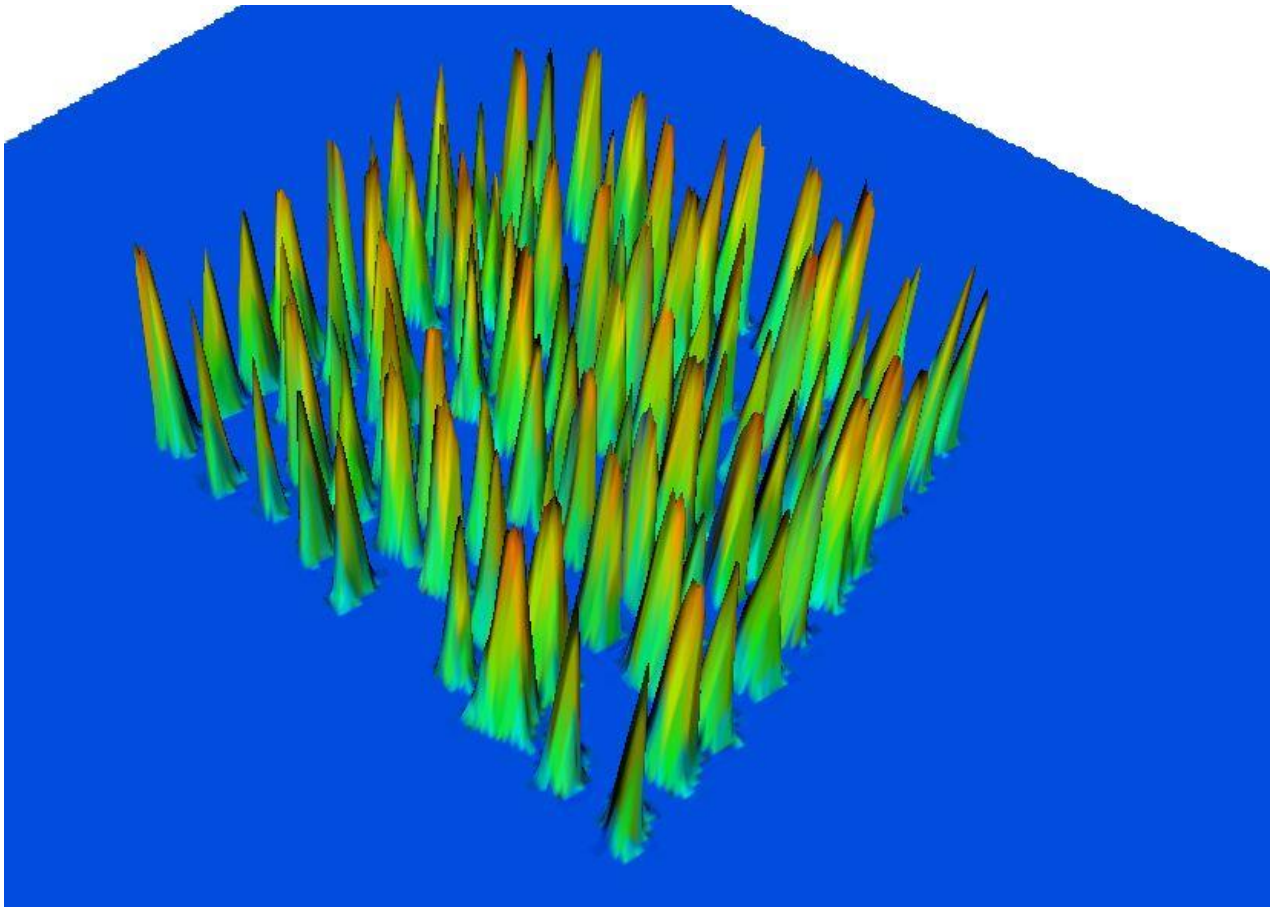

Figure 5-36 3D view of surface model for flight 9 normalised DSM. Table separation is 1.0 metres.

Error! Reference source not found. shows a three-dimensional representation of figure 5-35, this gives perspective to the surface smoothness, the notable dip in blue to the centre of the table arrangement is a missing table.

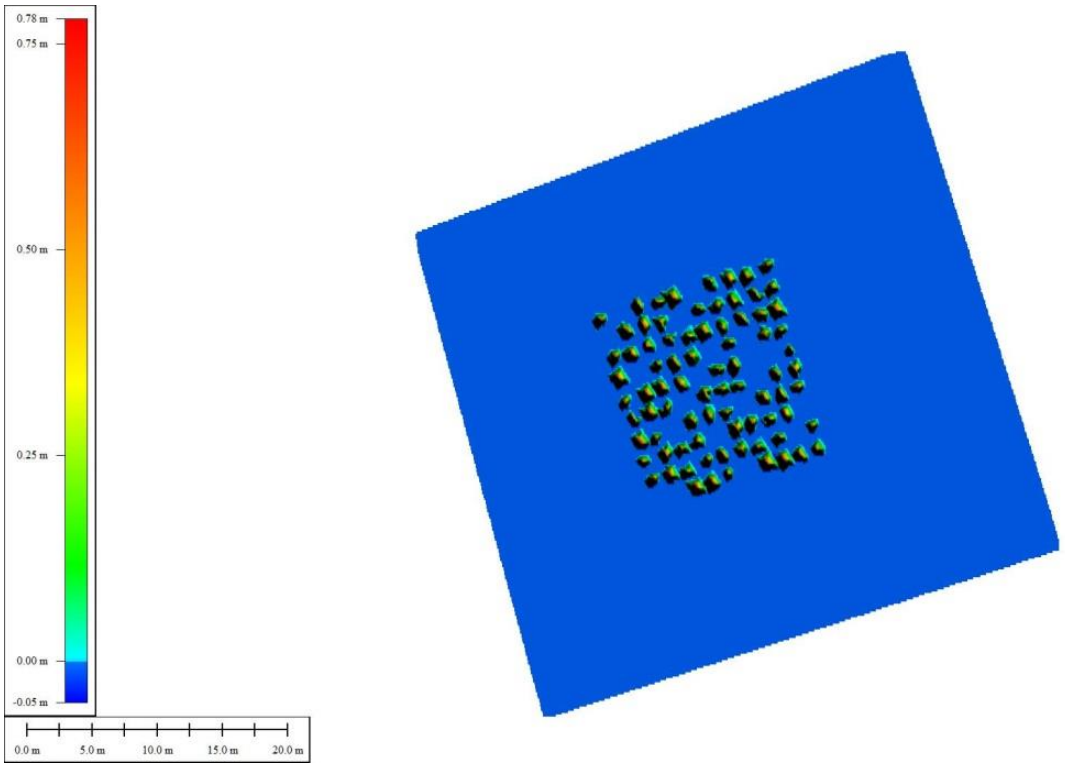

Figure 5-37 surface model for flight line 11 normalised DSM. Table separation is 1.0 metres.

.

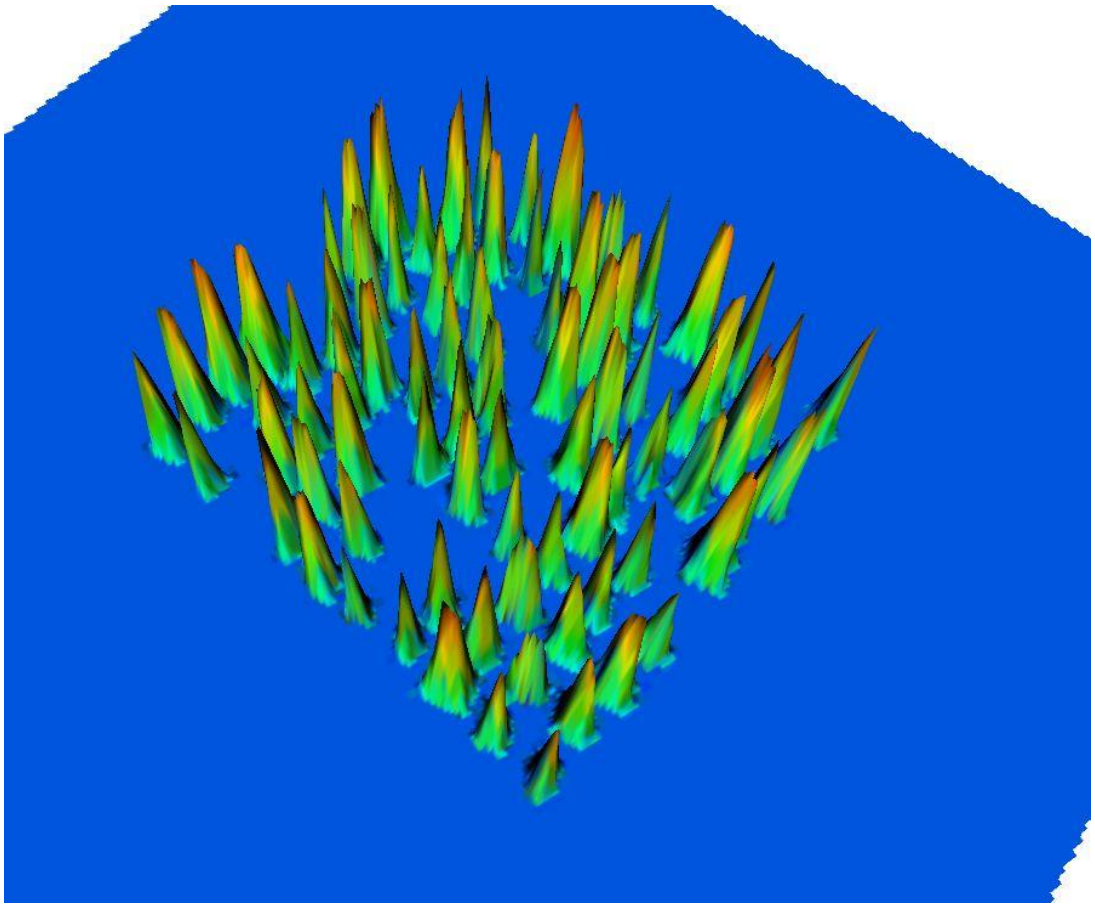

Figure 5-38 showing a 3 dimensional view of the flight 11 normalised DSM. Table separation is 1.0 metres.

By combining both flight lines to produce a higher resolution model, the effective point-density doubles. As such, the number of unobserved tables decreases to 2%. Figure 5-39. Whilst the number of tables observed has increased the surface model shows many linear artefacts. These artefacts are shown in the 3 dimensional view shown figure 5-40.

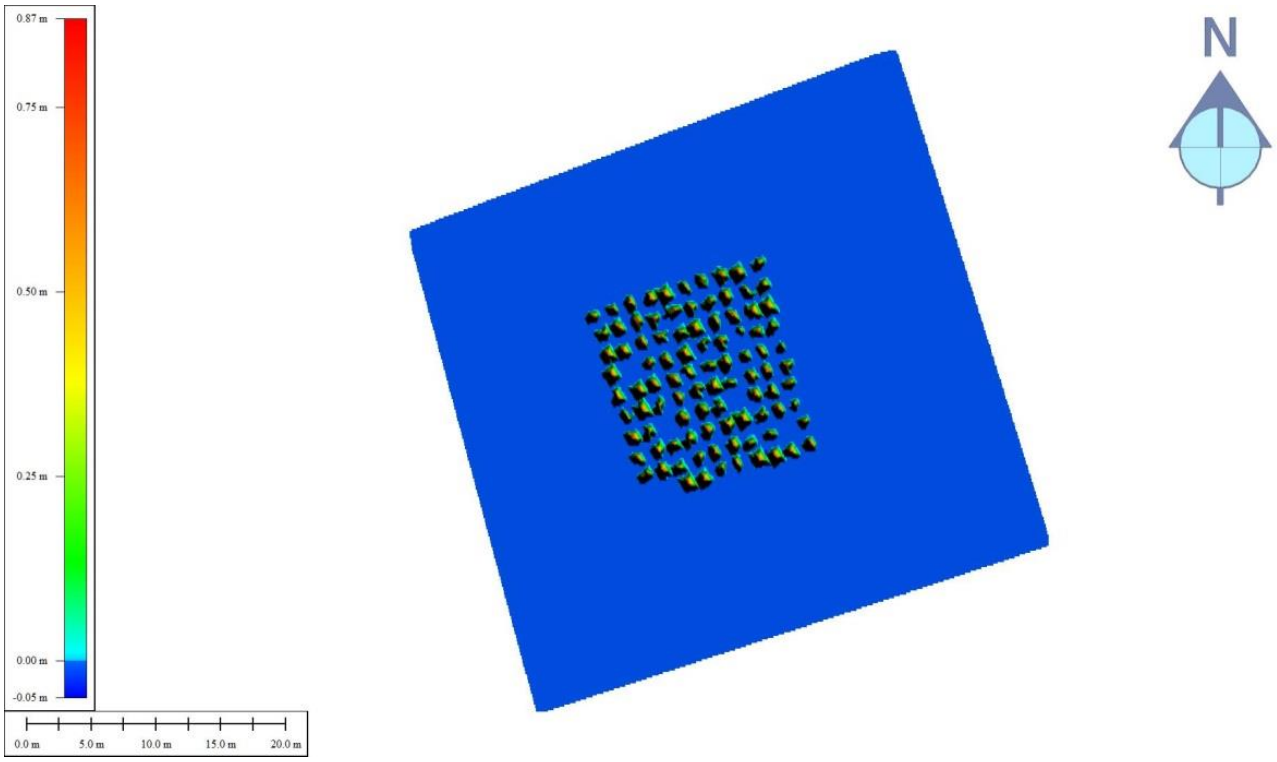

Figure 5-39 showing the surface model derived from overlapping two flight lines. Table separation is 1.0 metres.

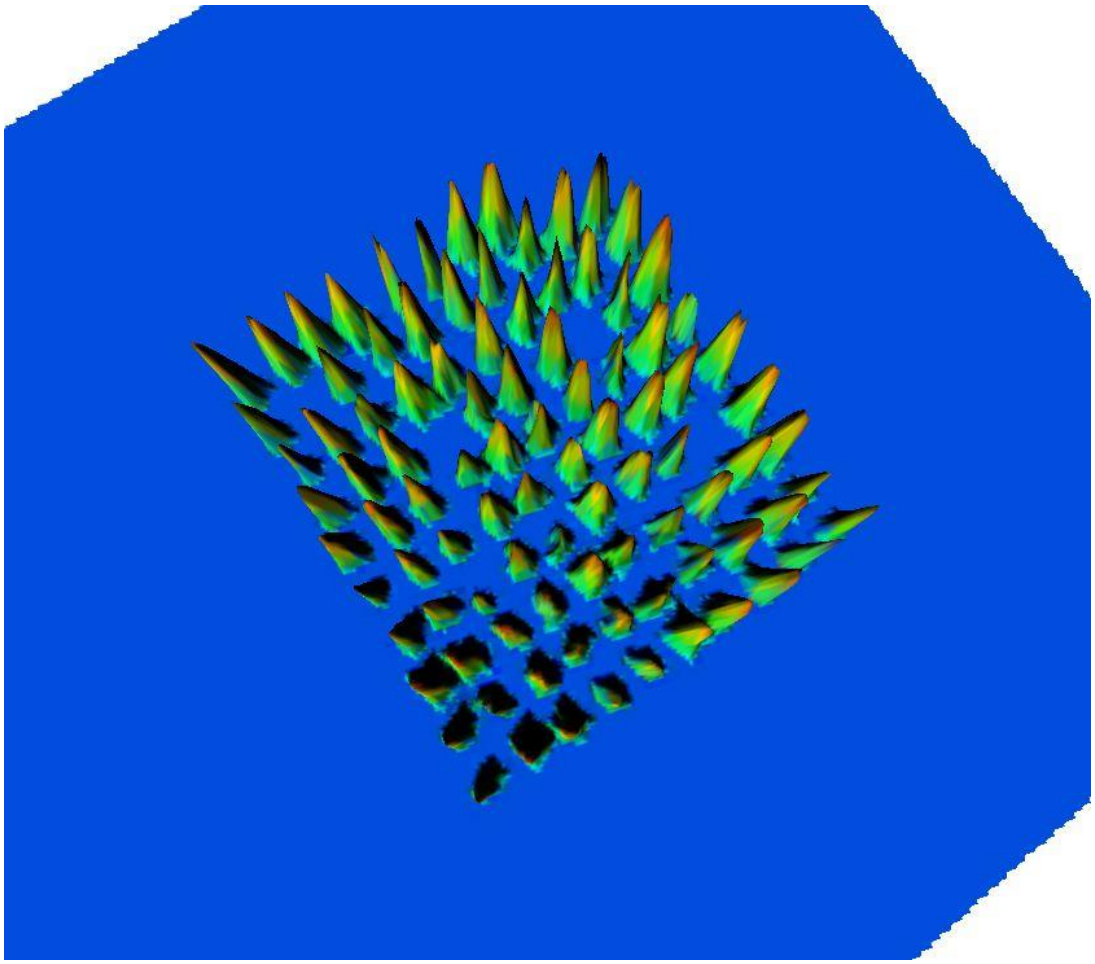

Figure 5-40 3D view of both over flights surface model. Table separation is 1.0 metres.

Comparing the two flights by differencing the elevation values shows interesting results, figure 5-41 is a subtraction of flight 9 from flight 11. It is clear that the same tables are not the ones being unobserved.

The central tables show a stronger degree of agreement in terms of table height, the number of strikes is not being assessed in figure (DoD), just the detection or omission of the table by the laser scan.

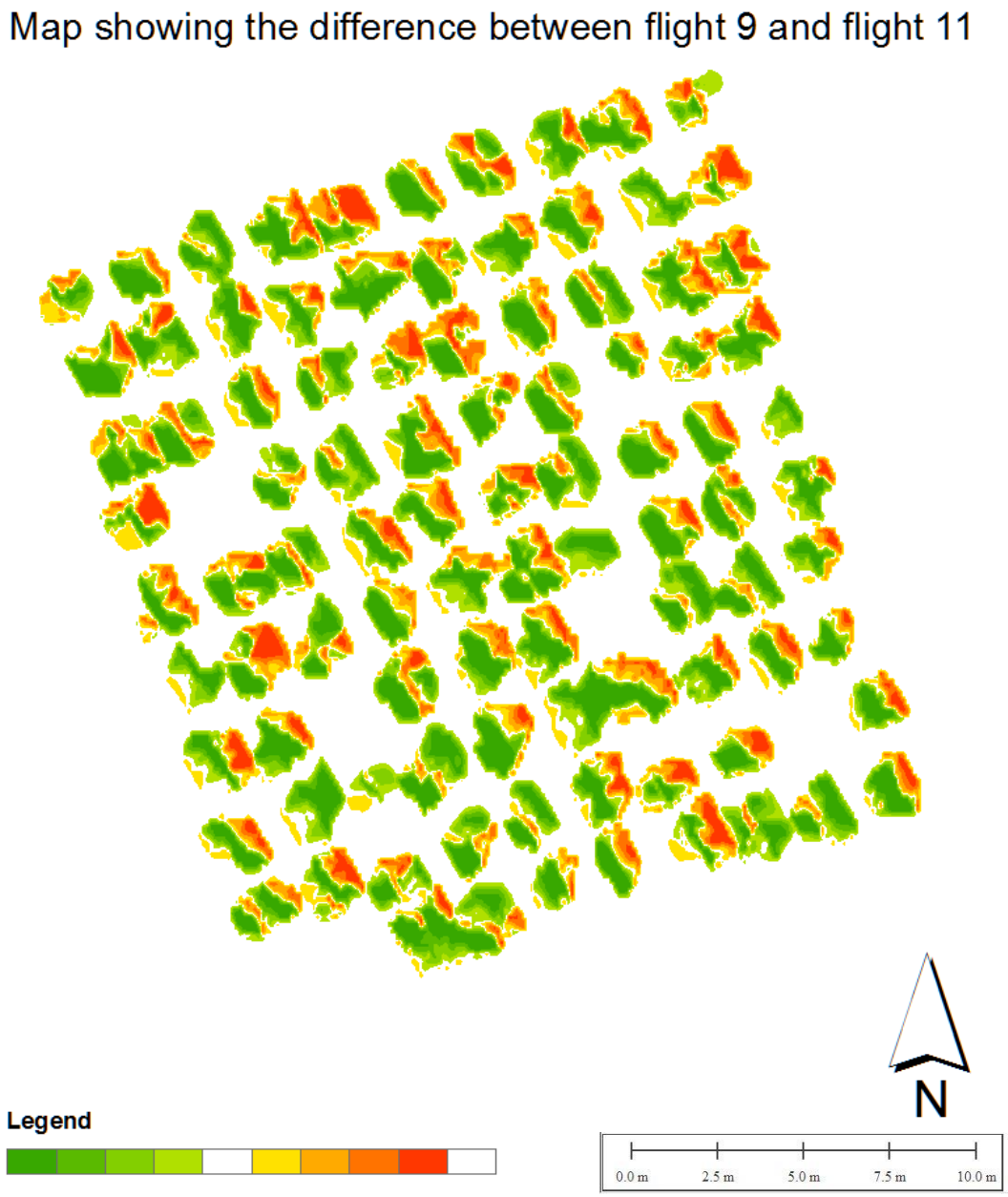

Figure 5-41 surface model showing a DEM of difference between flight 9 and flight 11

The table observations are broken down graphically below, figure 5-42 shows the results of the table observations with both over flights combined. Two percent of flights were unobserved; this figure is similar to the 1% figure seen for the other table configurations. For this table configuration, 83% of tables were under observed compared to expectation.

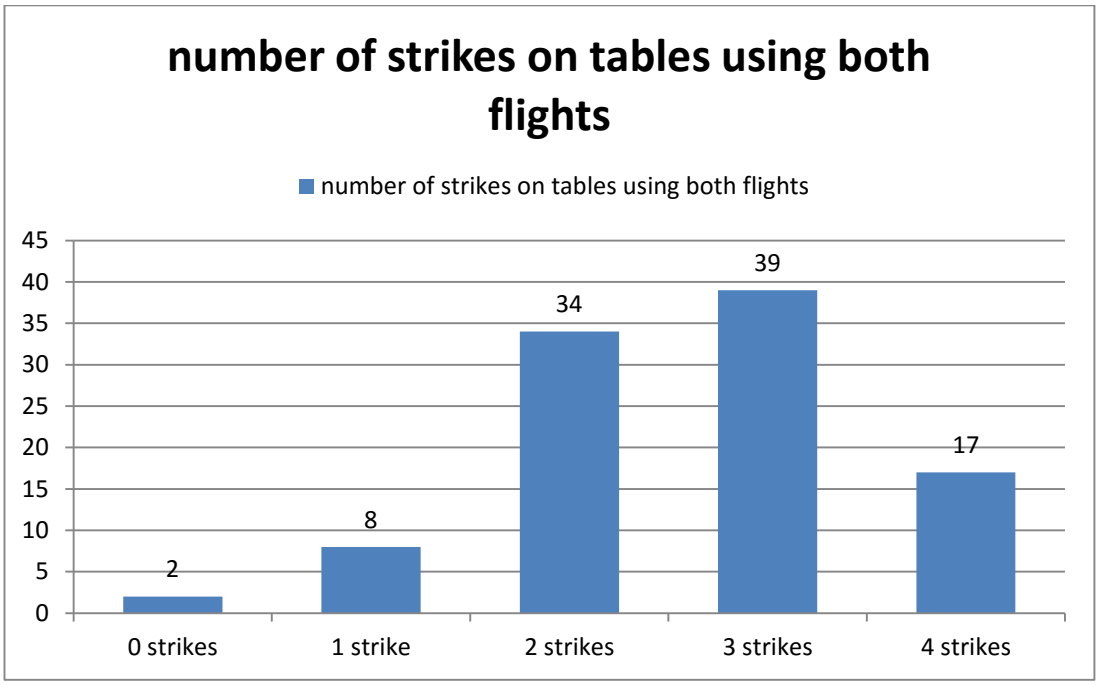

Figure 5-42 Bar chart showing the number of strikes on the table 3 configuration using both overflights.

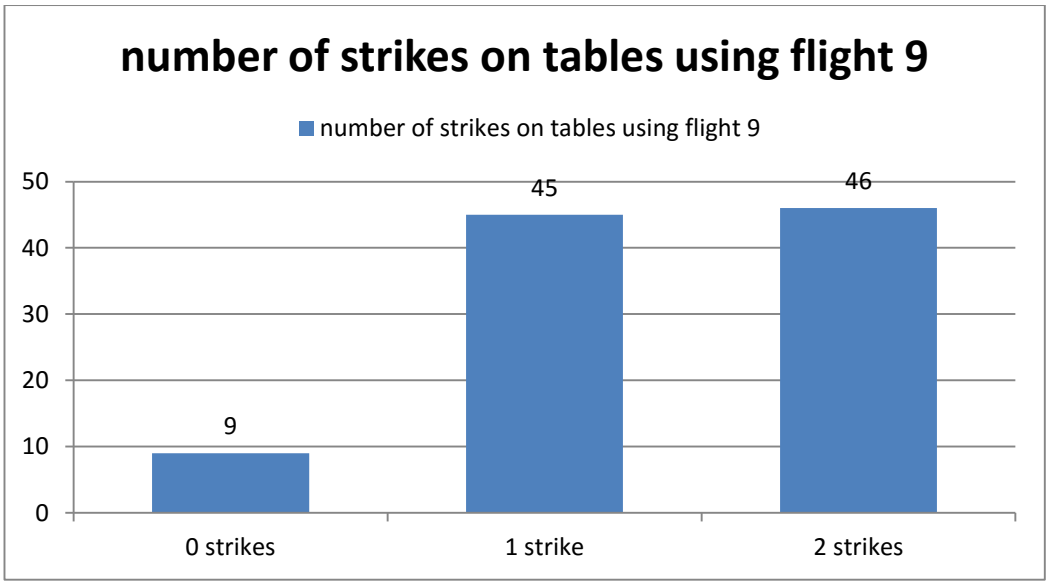

Figure 5-43 Bar chart showing the number of strikes on the table 3 configuration just using flight line 9

The single flight line shows 54% of the tables to be under detected. Nine per cent of the tables were undetected, this is a similar value to the previous flights of the same orientation.

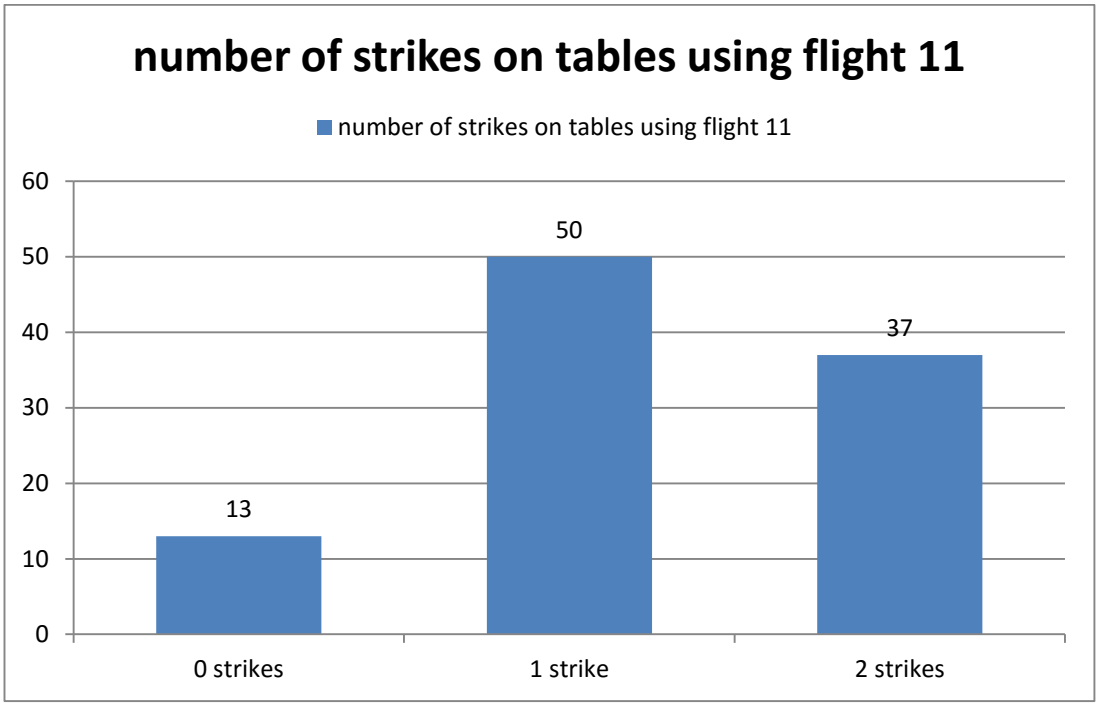

Figure 5-44 Bar chart showing the number of strikes on the table 3 configuration just using flight line 11

Figure 5-44 shows the number of tables detected with each number of pulses, 13% of tables were unobserved, with only 37% observed as expected.

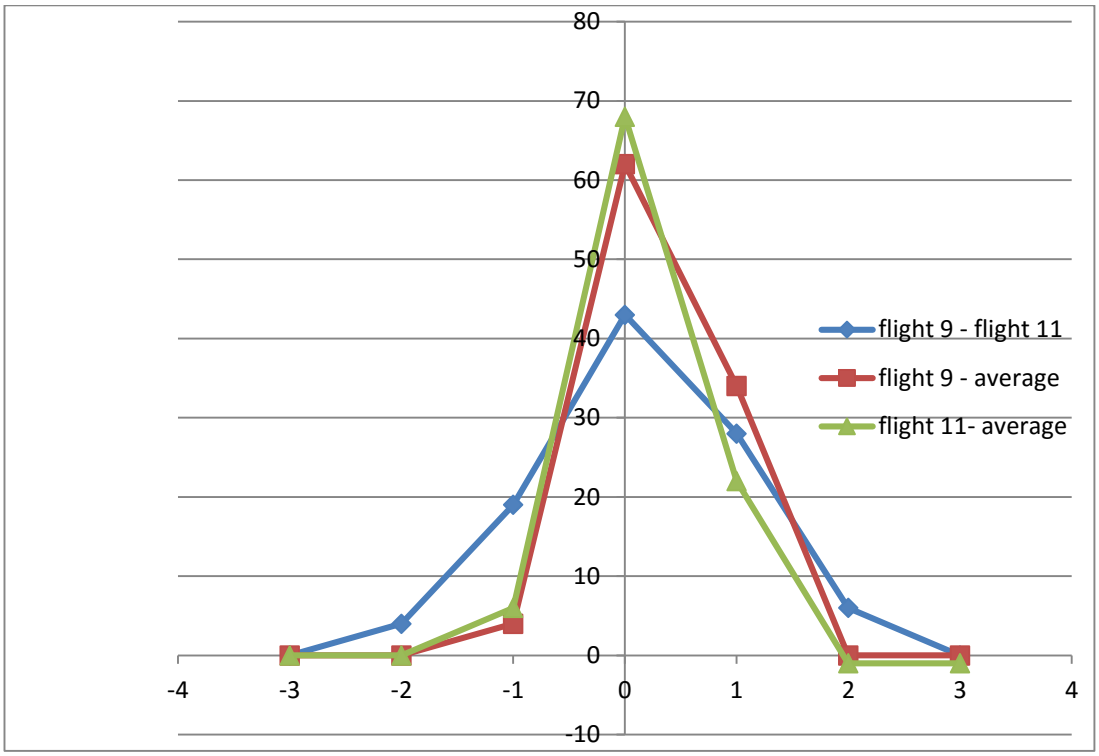

Figure 5-45 graph showing the differences between flight 9 and flight 11 and the deviation of each flight from the average for that table.

5.5 Results for 0.5 m table separation experiment

The results for the final table separation scenario are outlined. The tables are spaced 0.5 metres apart; this is smaller than the table size of 0.6 metres along its shortest axis. The results are more difficult to distinguish as separating tables out individually is more difficult.

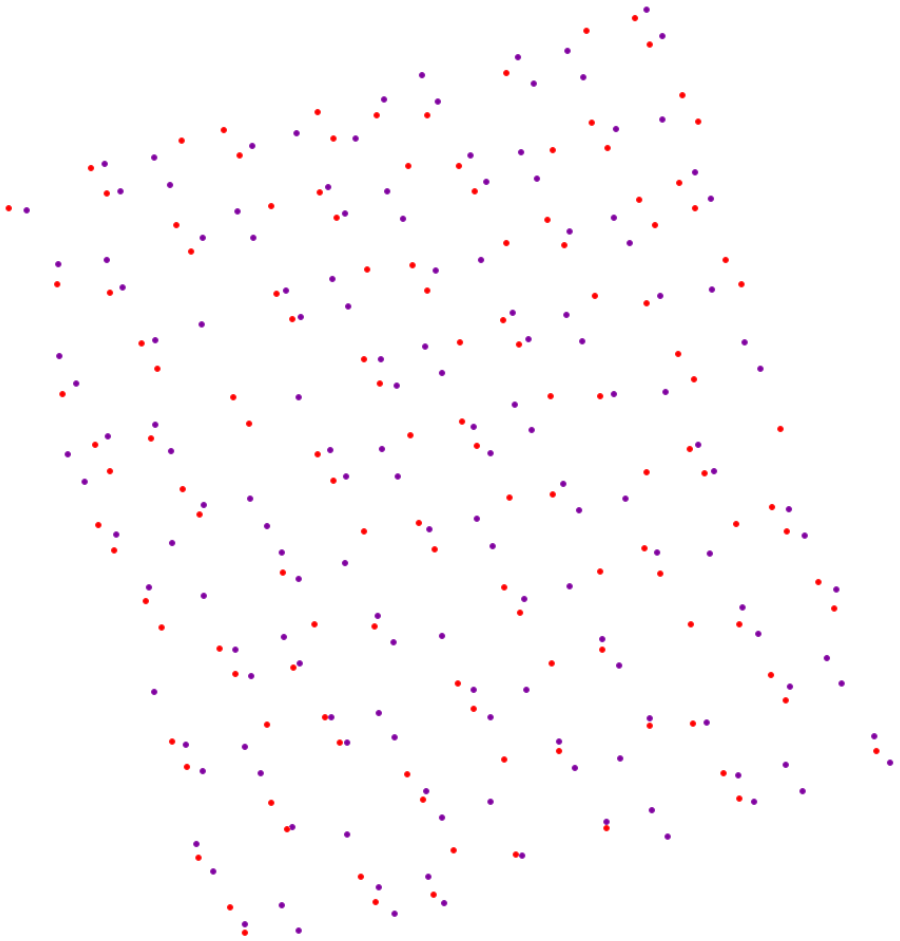

Figure 5-46 Showing the LiDAR table strikes for the table 4 configuration. Points coloured by flight line. Table separation is 0.5 metres.

The figure 5-46 shows the LiDAR strikes for the flight lines over this table configuration, the two flight lines (13 and 15) are coloured red and blue respectively. The clustering of points can be seen as with the previous table configurations, however the boundaries are more difficult to distinguish, *a priori* details regarding spacing and the nature of the object allow for intelligent reasoning to separate the tables apart, the linear patterns seen in previous configurations is present but weaker.

Figure 5-47 shows the table detection for the single flight line 13. The smoothness of previous table configurations has been replaced with a hummocky terrain; it is difficult to determine where individual tables are placed. A missing table can be identified in the southwestern corner of the configuration.

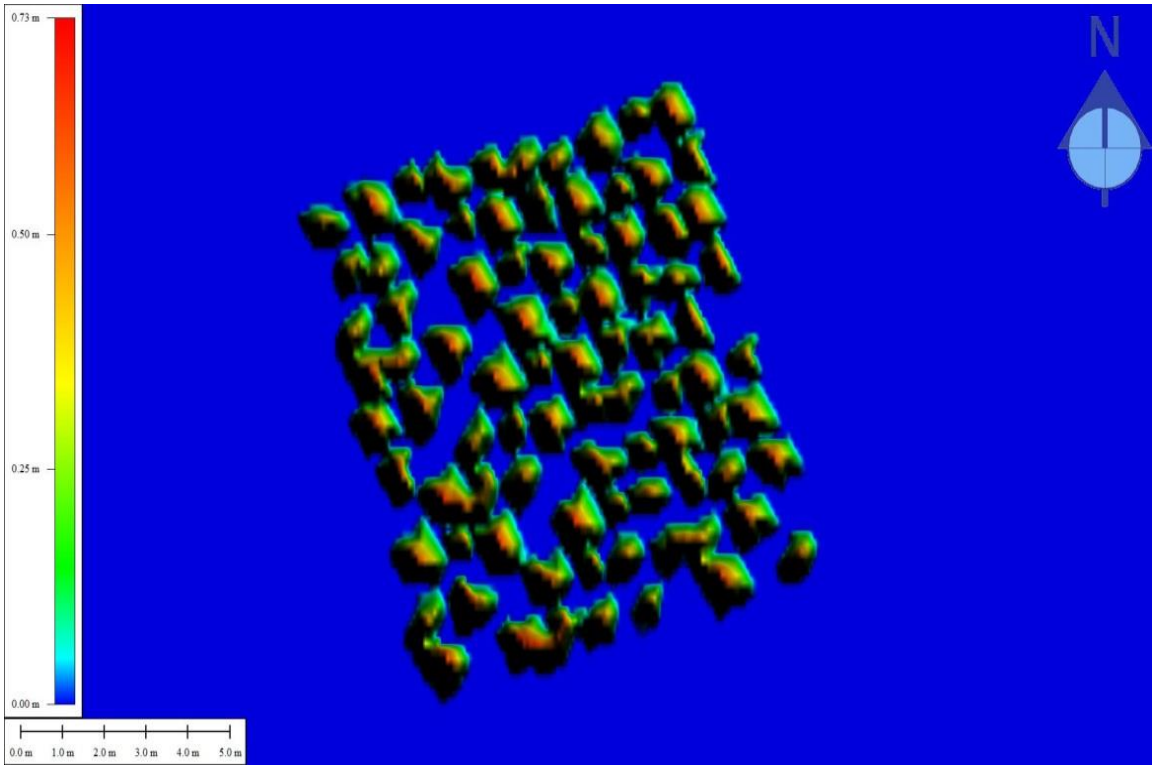

Figure 5-47 Flight 13 normalised DSM Table separation is 0.5 metres.

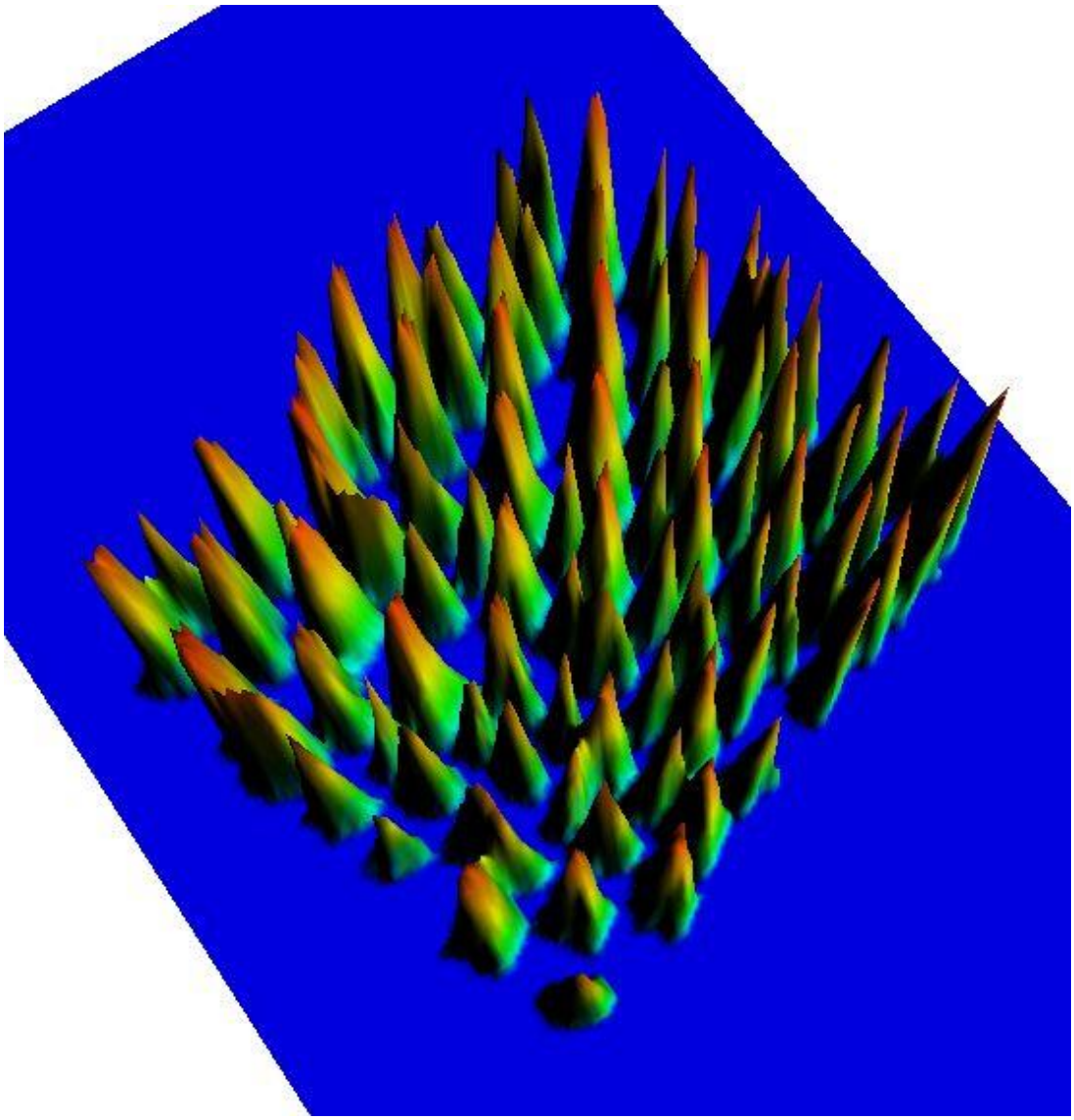

Figure 5-48 3d view of flight 13 ndsm Table separation is 0.5 metres.

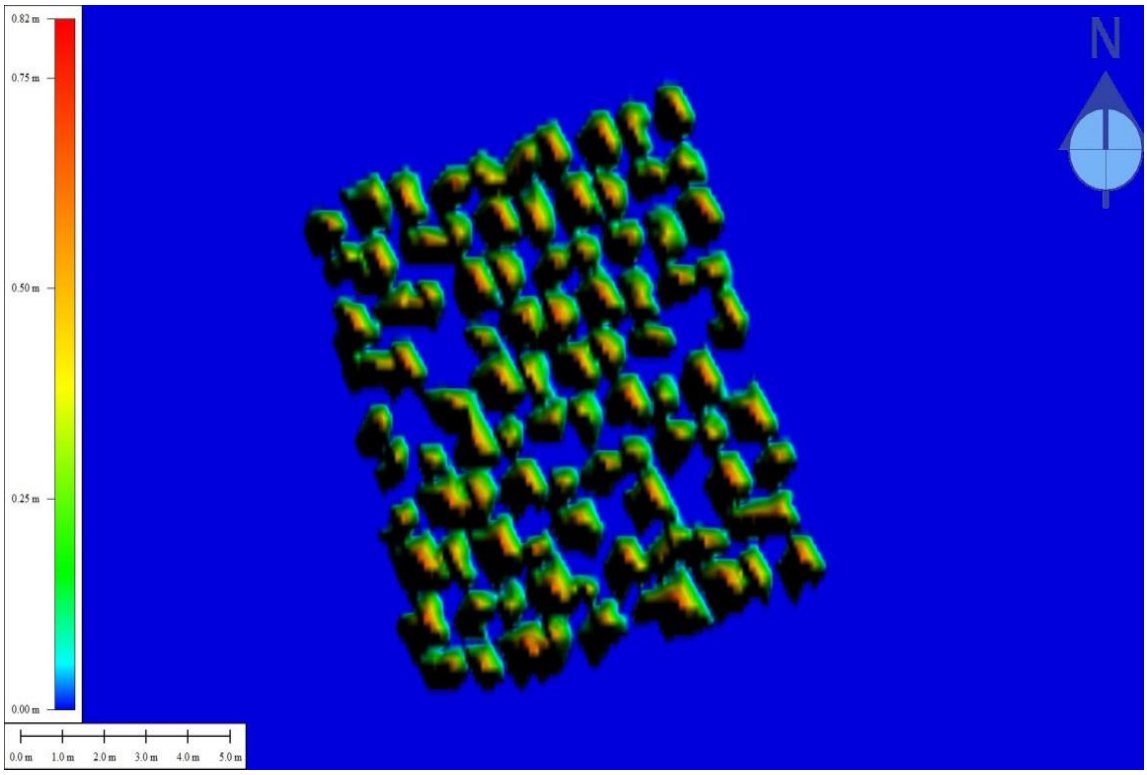

Figure 5-49 flight 15 ndsm Table separation is 0.5 metres.

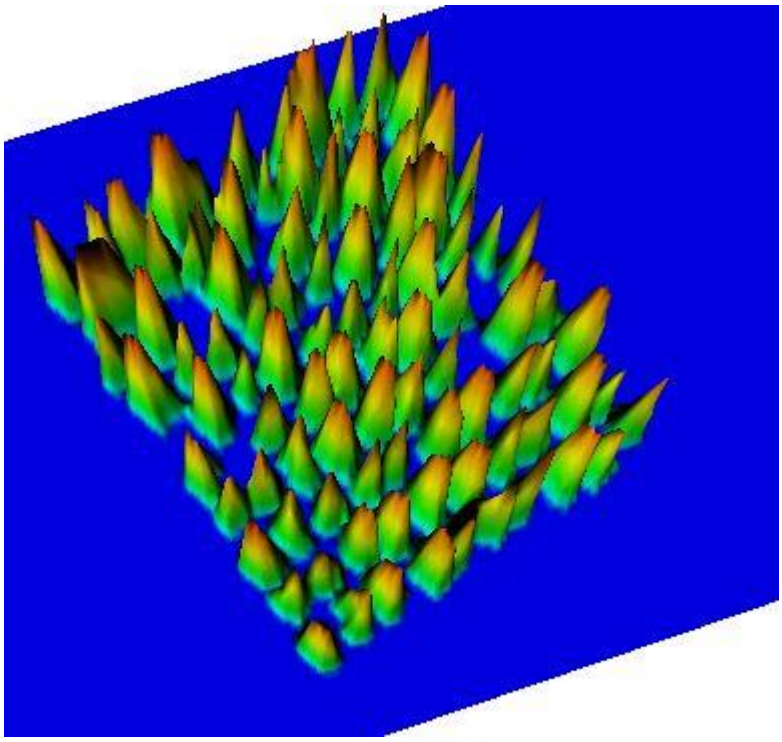

Figure 5-50 shows the 3 dimensional perspective view of the surface. Table separation is 0.5 metres.

Flight 15 is the alternative flight line over the table 4 configuration. This shows a number of minima (in green) these are numerous and although are shown all over the surface there is a cluster towards the northeast quadrant. The results show 13 missing tables; these can be identified in the surface.

Using both flights to characterise the tables is shown in figure 5-51 this has only one missing table. The surface is varied with many maxima and minima within the table area; no clear delineation of tables is possible at this separation.

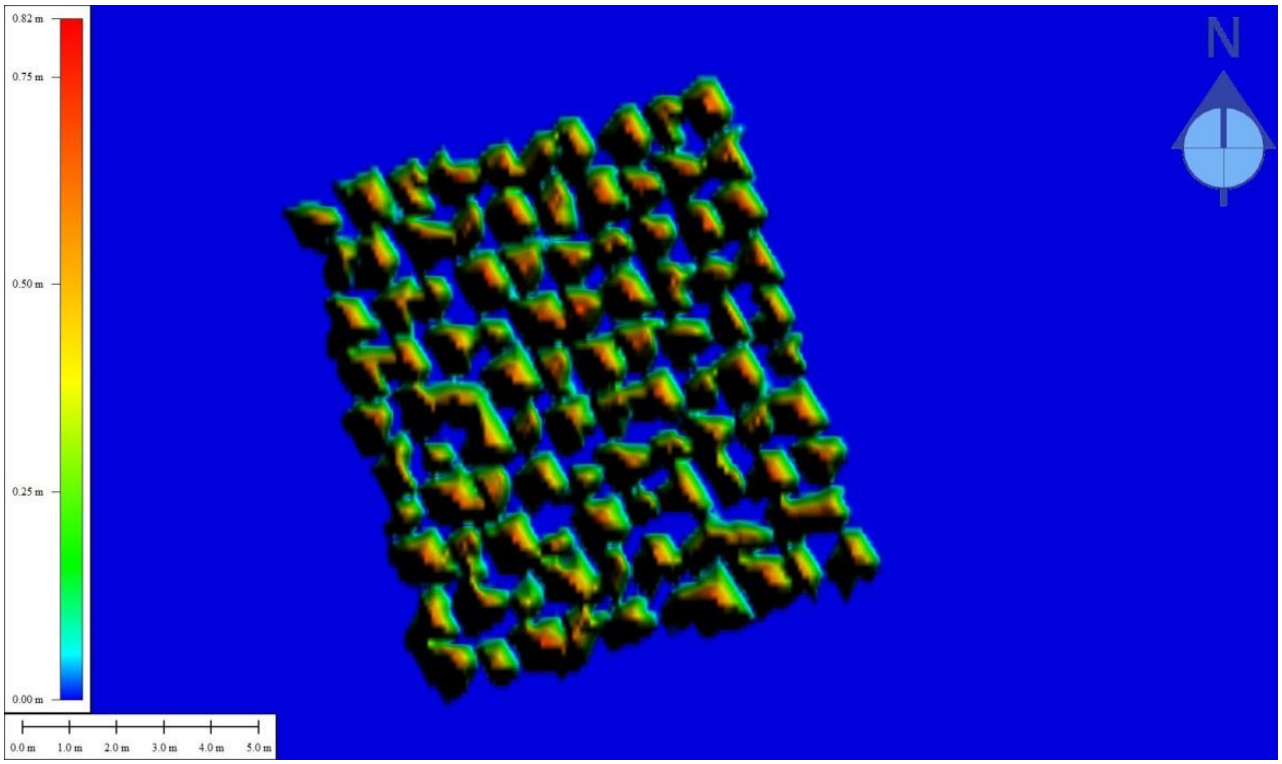

Figure 5-51 both flights normalised Digital Surface Model. Table separation is 0.5 metres.

The three dimensional view shows a varied surface with many maxima and minima, it is clear that this is not a good representation of the table surface.

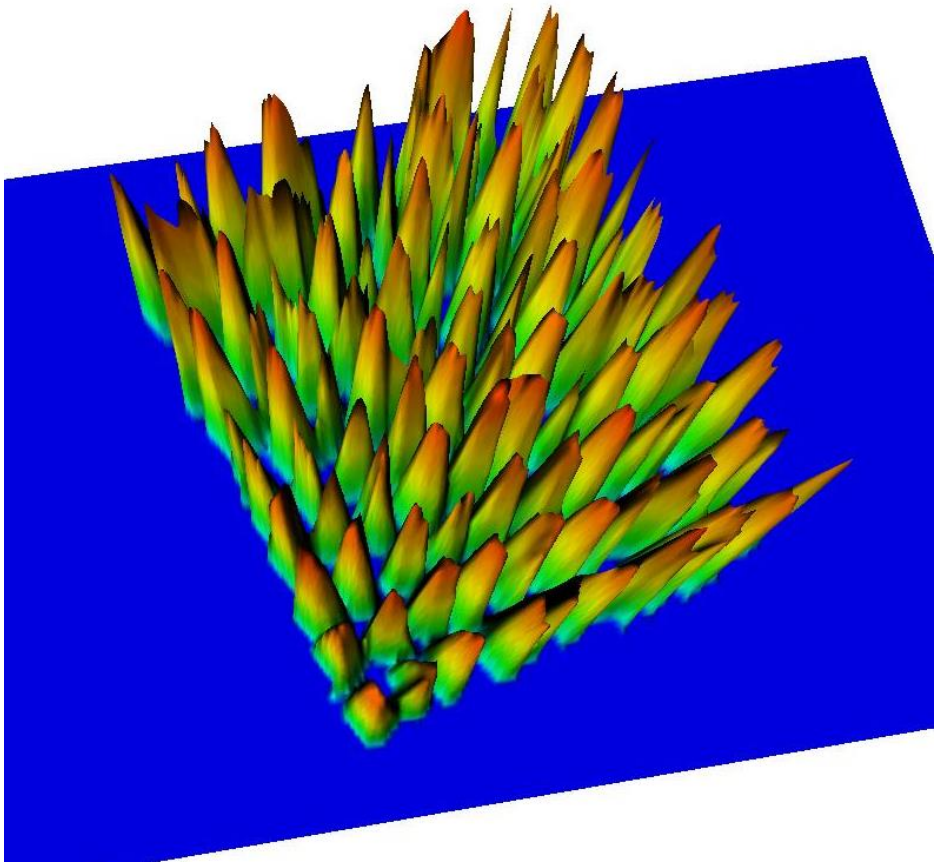

Figure 5-52 both flights nDSM 3d table separation is 0.5 metres.

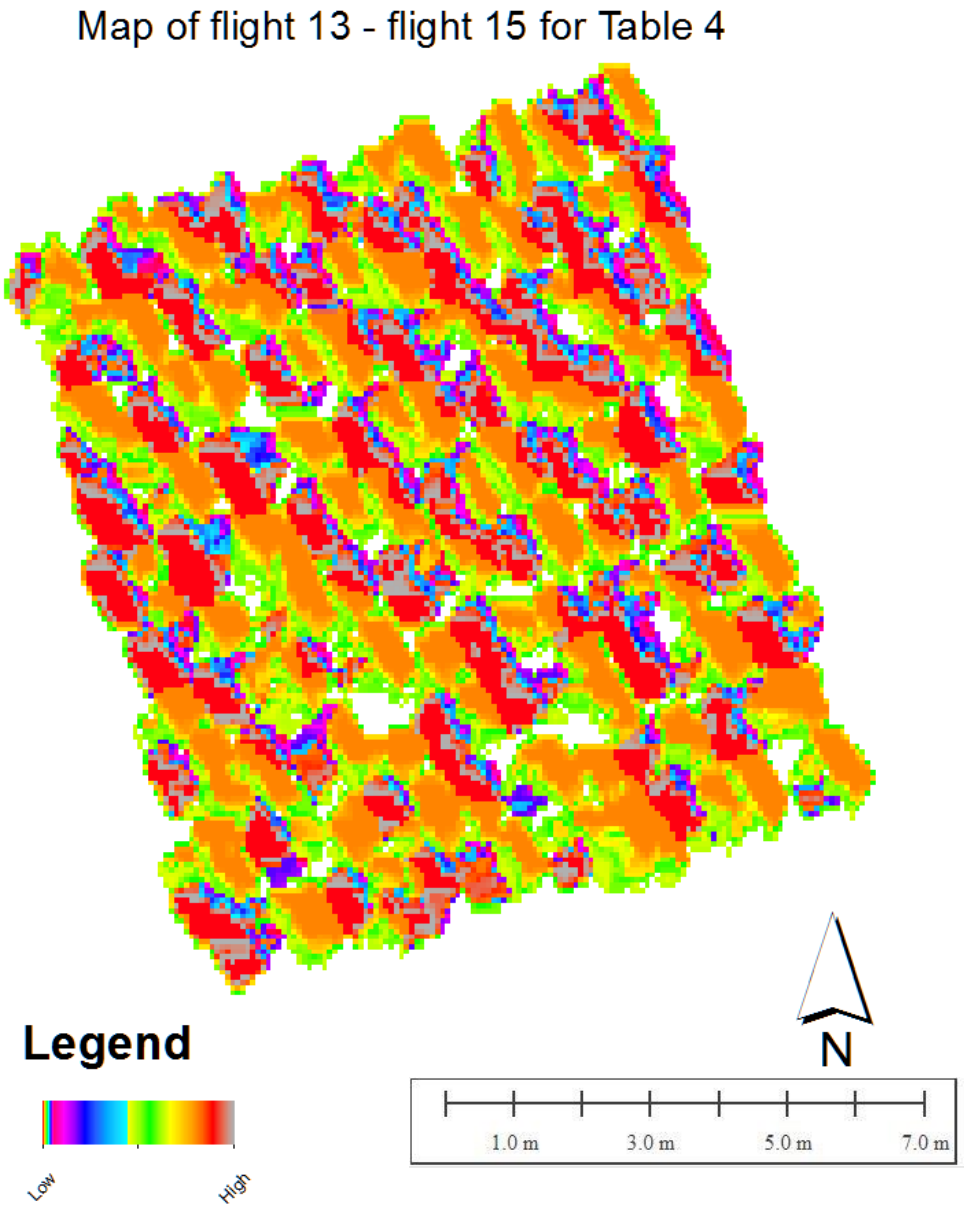

Figure 5-53 difference between 13 and 15 nDSM table separation is 0.5 metres.

Comparing the differences between the two flight lines using a DEM of difference the 13 missing tables from flight 13 and 3 missing tables from flight 15 are evident. A number of

deviations between the surfaces can be seen as spikes; these include a large cluster to the southwest corner.

Figure 5-54 shows the 3 dimensional perspective view of the DEM of Difference, the stark elevation changes are clear. These appear to be randomly distributed across the table surface.

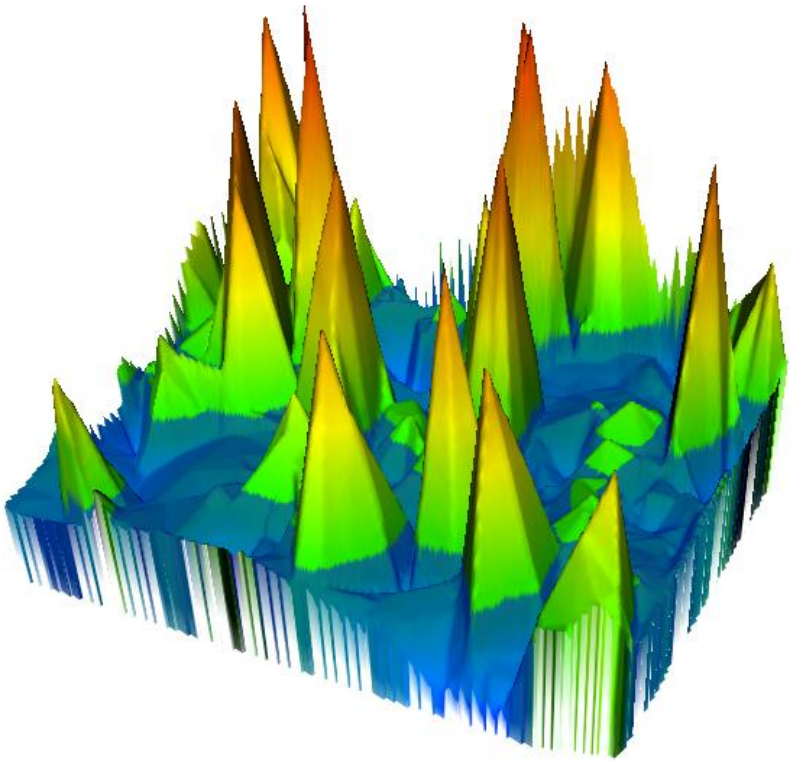

Figure 5-54 3d view of difference between flight 13 and 15 table separation is 0.5 metres.

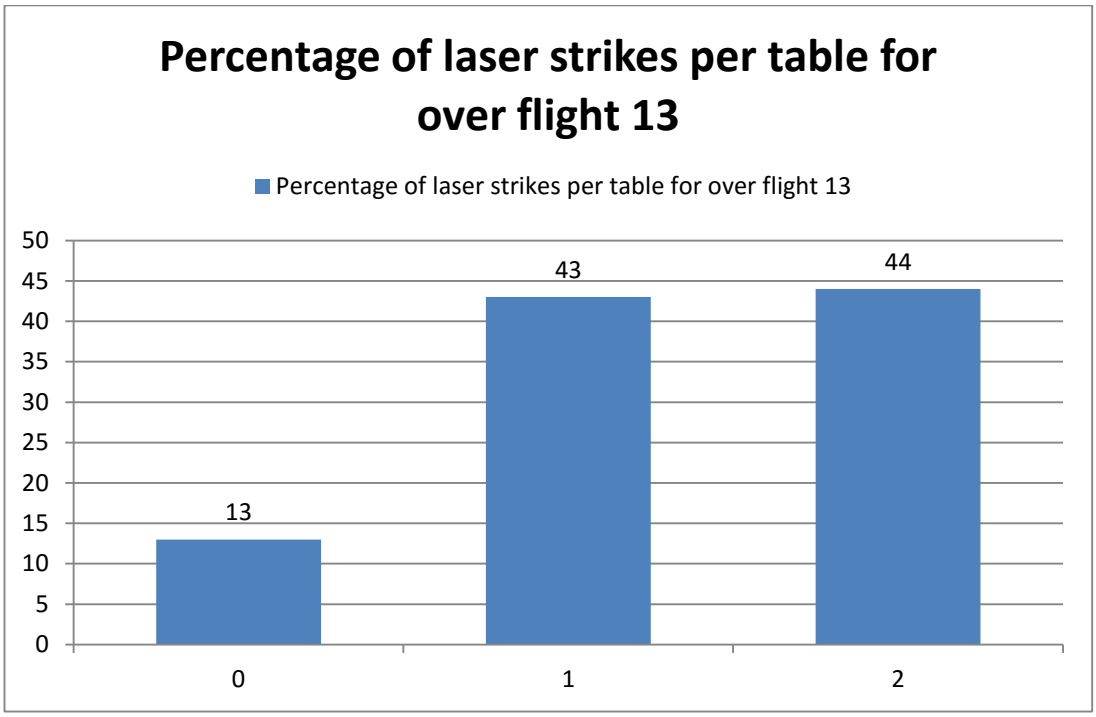

Figure 5-55 bar chart showing the number of strikes per table for flight line 13

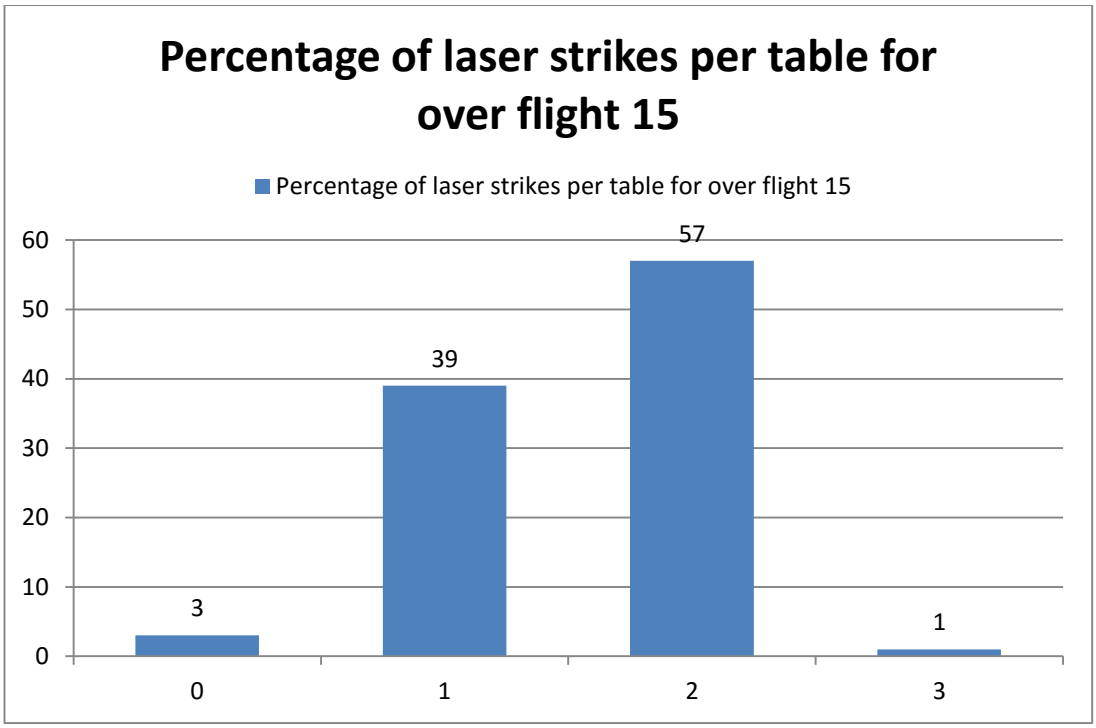

Figure 5-56 Bar chart showing the number of strikes per table for flight line 15

Comparing figure 5-55 and figure 5-56 it is clear that a large disparity exists between the two flights, flight line 15 is the first and only flight to have recorded in excess of the expected number of strikes per table with one table receiving three strikes. Flight 13 showed thirteen omitted tables, this is the most of any of the flight lines.

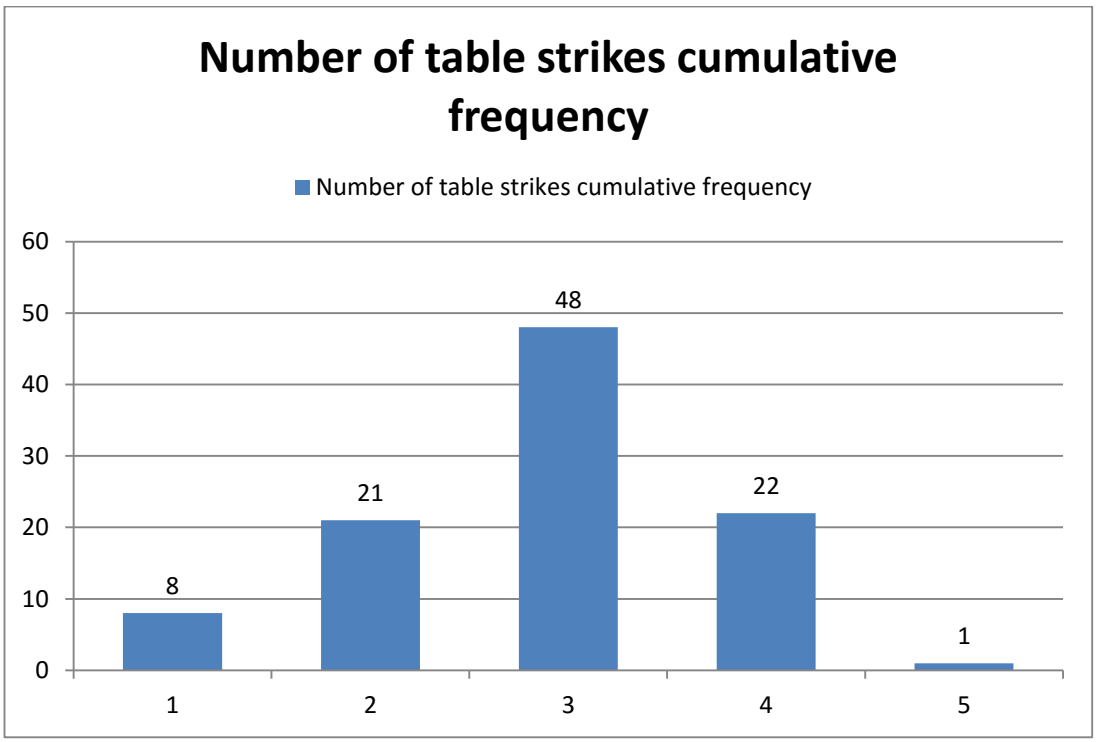

Figure 5-57 Bar chart showing the number of strikes per table for table 4 configuration using both overlapping flights

Using both overlapping flights all the tables are detected with one table receiving five strikes. This is the best detection ration with 23% receiving the expected number of strikes or greater and 71% receiving greater than three strikes.

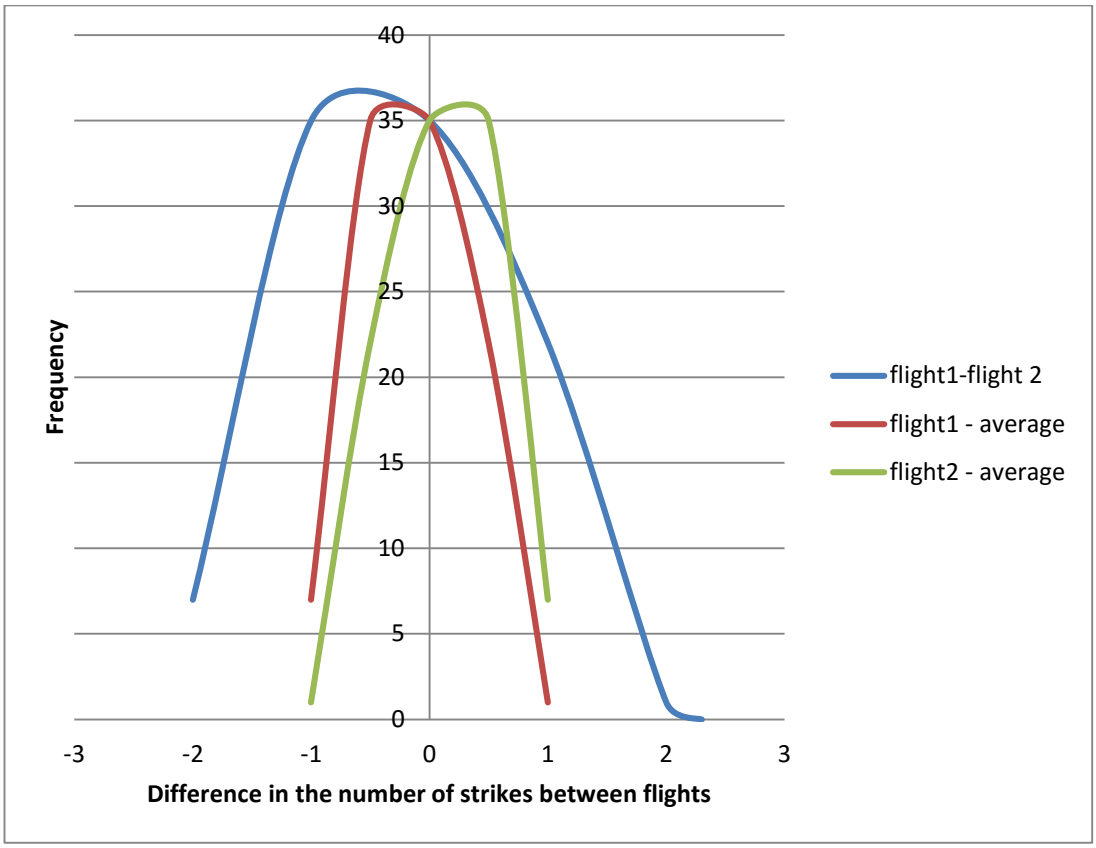

Figure 5-58 Graph showing the number of strikes per table and the deviation from the average strikes per table

The graph shown in figure 5-58 shows the deviation of a flight from the average strikes for the table and the change in the number of hits from one flight line to the other.

5.6 Comparison of tables

Comparing the number of strikes per table, for each table arrangement will identify any trends in object detection and object horizontal separation. By separating the results by flight line, the verifiability of the results can be investigated. Both flights had opposing but parallel tracks.

Table 5-2 shows the number of hits from the flight one flights for all the table configurations. This is coloured red for low values, yellow for middling values and green for high values. It is clear to see that the number of hits is randomly distributed across the tables. This can be compared to the hits from the second set of flight lines shown in table 5-3.

Comparing the two flights by subtraction as shown in table 5-5 shows very little agreement between the first and second over flights. This suggests that surface reflectivity is not a significant factor in this experiment. Table 5-4 shows the number of strikes received for each table in total, this again shows a disparity across the table range but no clear pattern emerges.

J	6	6	5	7	7	5	4	5	6	6
I	5	6	5	6	8	7	6	7	5	6
H	6	6	4	5	6	7	6	7	8	7
G	7	4	6	3	8	6	8	4	6	6
F	7	5	3	6	6	6	4	6	8	1
E	4	6	4	5	5	5	3	6	7	5
D	3	6	4	3	5	6	5	6	3	6
C	7	4	7	3	7	5	5	5	5	5
B	4	7	3	5	4	6	4	5	5	4
A	6	4	8	4	5	6	6	6	3	4
	1	2	3	4	5	6	7	8	9	10

Table 5-2 Showing the number of strikes each table received for the first flight lines in total for all table configurations

	1	2	3	4	5	6	7	8	9	10
J	4	4	7	6	7	6	6	7	6	6
I	5	6	5	6	6	5	6	4	5	3
H	7	4	5	6	6	6	3	5	4	5
G	8	6	5	4	6	4	3	6	5	4
F	6	6	6	7	6	6	7	4	4	4
E	6	5	6	4	5	5	6	4	6	4
D	7	5	5	6	5	5	3	4	3	4
C	5	6	7	6	4	7	4	2	5	1
B	7	4	5	4	4	6	6	4	4	7
A	6	4	8	6	4	5	5	7	8	4

Table 5-3 Showing the number of strikes each table received for the second flight lines in total for all table configurations

	1	2	3	4	5	6	7	8	9	10
J	10	10	12	13	14	11	10	12	12	12
I	10	12	10	12	14	12	12	11	10	9
H	13	10	9	11	12	13	9	12	12	12
G	15	10	11	7	14	10	11	10	11	10
F	13	11	9	13	12	12	11	10	12	5
E	10	11	10	9	10	10	9	10	13	9
D	10	11	9	9	10	11	8	10	6	10
C	12	10	14	9	11	12	9	7	10	6
B	11	11	8	9	8	12	10	9	9	11
A	12	8	16	10	9	11	11	13	11	8

Table 5-4 Showing the number of strikes each table received for the all flight lines in total for all table configurations

J	2	2	-2	1	0	-1	-2	-2	0	0
I	0	0	0	0	2	2	0	3	0	3
H	-1	2	-1	-1	0	1	3	2	4	2
G	-1	-2	1	-1	2	2	5	-2	1	2
F	1	-1	-3	-1	0	0	-3	2	4	-3
E	-2	1	-2	1	0	0	-3	2	1	1
D	-4	1	-1	-3	0	1	2	2	0	2
C	2	-2	0	-3	3	-2	1	3	0	4
B	-3	3	-2	1	0	0	-2	1	1	-3
A	0	0	0	-2	1	1	1	-1	-5	0
	1	2	3	4	5	6	7	8	9	10

Table 5-5 showing the sum of first flight table strikes minus the sum of the second flights table strikes

j	0.707	0.886	0.535	0.518	0.463	0.744	0.463	0.535	0.535	0.535
i	0.707	0.535	0.463	0.535	0.463	0.535	0.535	0.744	0.886	0.641
h	0.518	0.707	0.835	0.518	0.535	0.518	0.641	0.535	0.756	0.756
g	0.641	0.707	0.744	0.641	0.463	0.707	0.916	0.463	0.518	0.707
f	0.518	0.744	0.991	0.518	0.756	0.535	0.744	0.707	0.756	0.744
e	0.707	0.916	0.707	0.354	0.707	0.463	0.641	0.707	0.518	0.641
d	0.886	0.744	0.835	0.835	0.707	0.518	0.535	0.707	0.707	0.886
c	0.756	0.886	0.463	0.641	0.916	0.756	0.835	0.641	0.886	0.886
b	0.744	0.744	0.535	0.835	0.535	0.535	0.463	0.641	0.641	0.744
a	0.535	0.926	0.000	0.707	0.641	0.744	0.916	0.518	0.744	0.756
	1	2	3	4	5	6	7	8	9	10

Table 5-6 showing the standard deviation from each overfligth over each table arrangement

Table 5-6 shows the standard deviations between the flights and table configurations, the table at location A3 received two strikes for each table configuration and flight all others received varying amounts with an average deviation of 0.66 strikes.

For the first flight over each table set heads in a south westerly direction. The second flights for each table head in the opposing north easterly direction. They both intersect with the tables at a similar incident angle figure 5-59 shows the position of the aircraft relative to the tables.

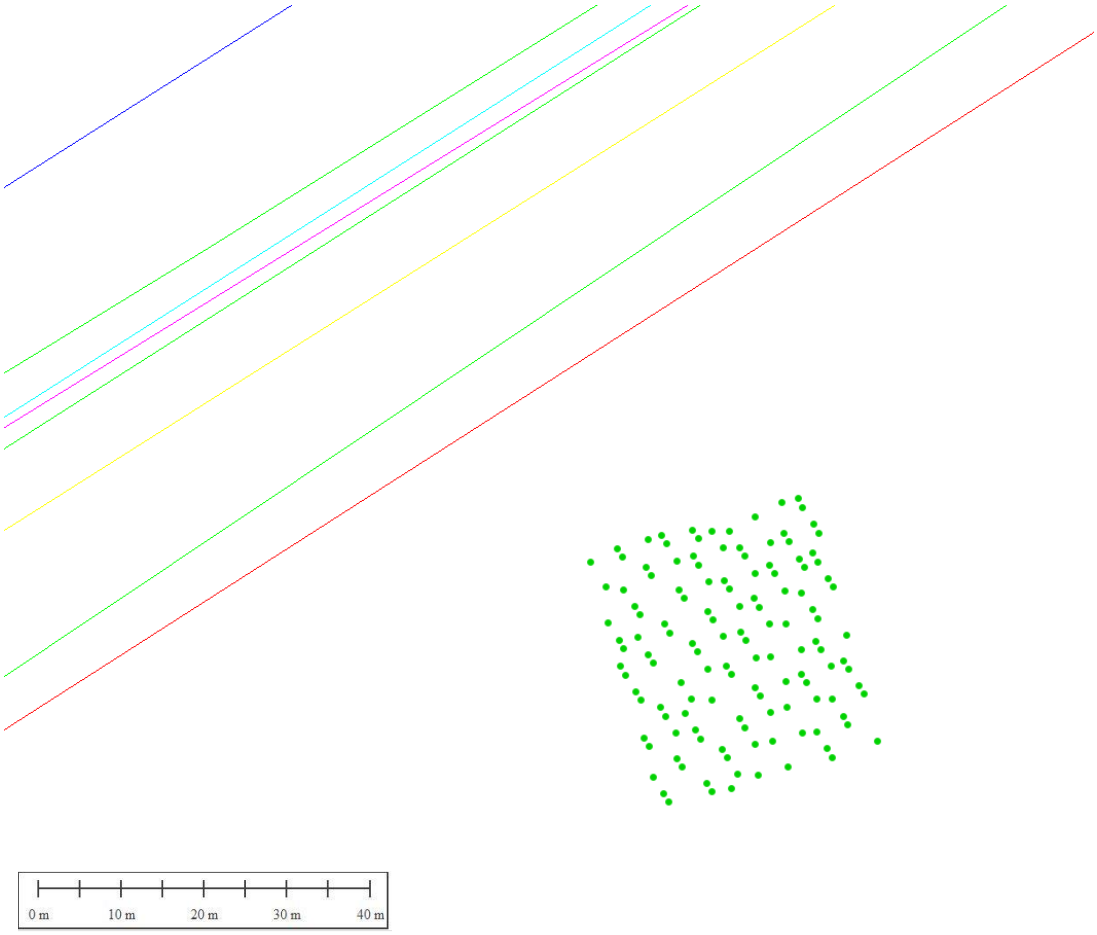

Figure 5-59 showing the relation of the tables (green points) to the aircraft trajectory (coloured lines). N.B. lines are for flight lines running in both directions

Looking at the flights heading in a south-westerly direction these results were graphed for each table configuration. Figure 5-60 shows the results, the blue bars represent the number of omitted tables, the red flights those receiving a single strike and green those receiving two strikes. The number of tables omitted increases as the tables move closer together this relationship can be observed with an R^2 value of 0.70. The values for one and two strikes show no relationship.

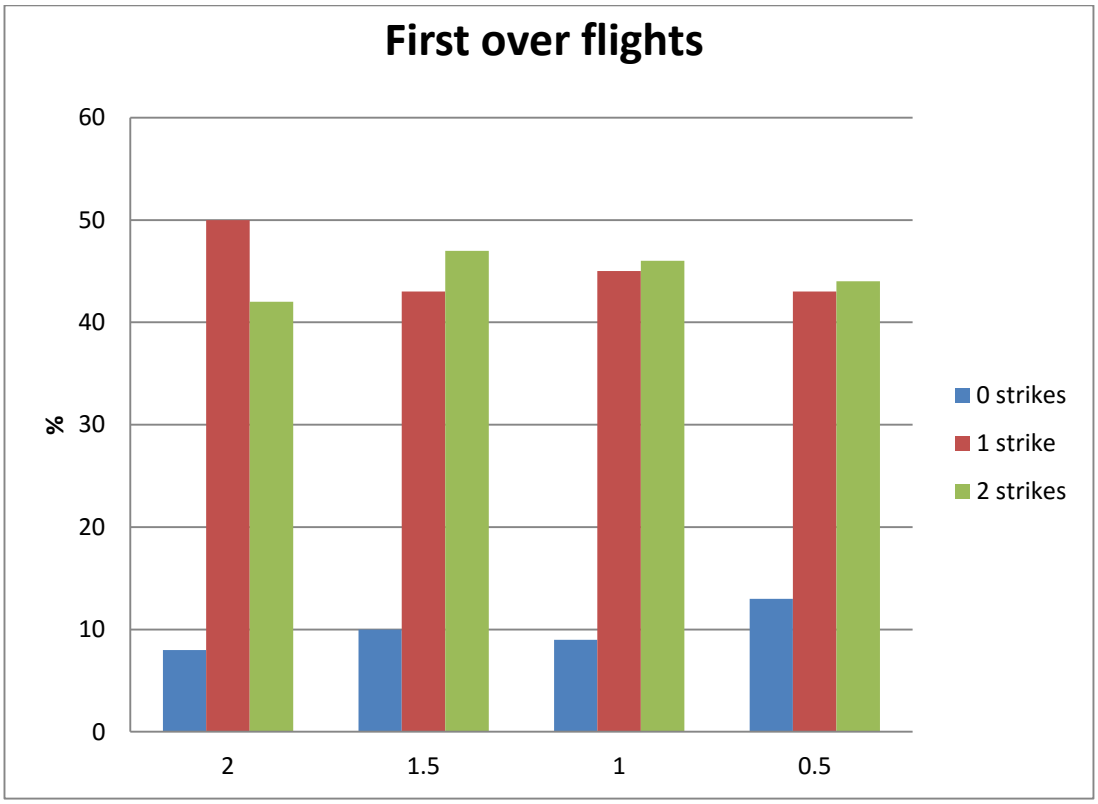

Figure 5-60 Bar chart showing the number of tables receiving 0 (blue), 1(red) or 2(green) number of strikes for the first flights over the tables

Repeating this study for the flights in the opposing direction shows interesting results. Figure 5-61 shows the results. The results for table omissions shows a very strong negative correlation with an agreement of $R^2 = 0.95$, the tables receiving one, two or three strikes show no correlation.

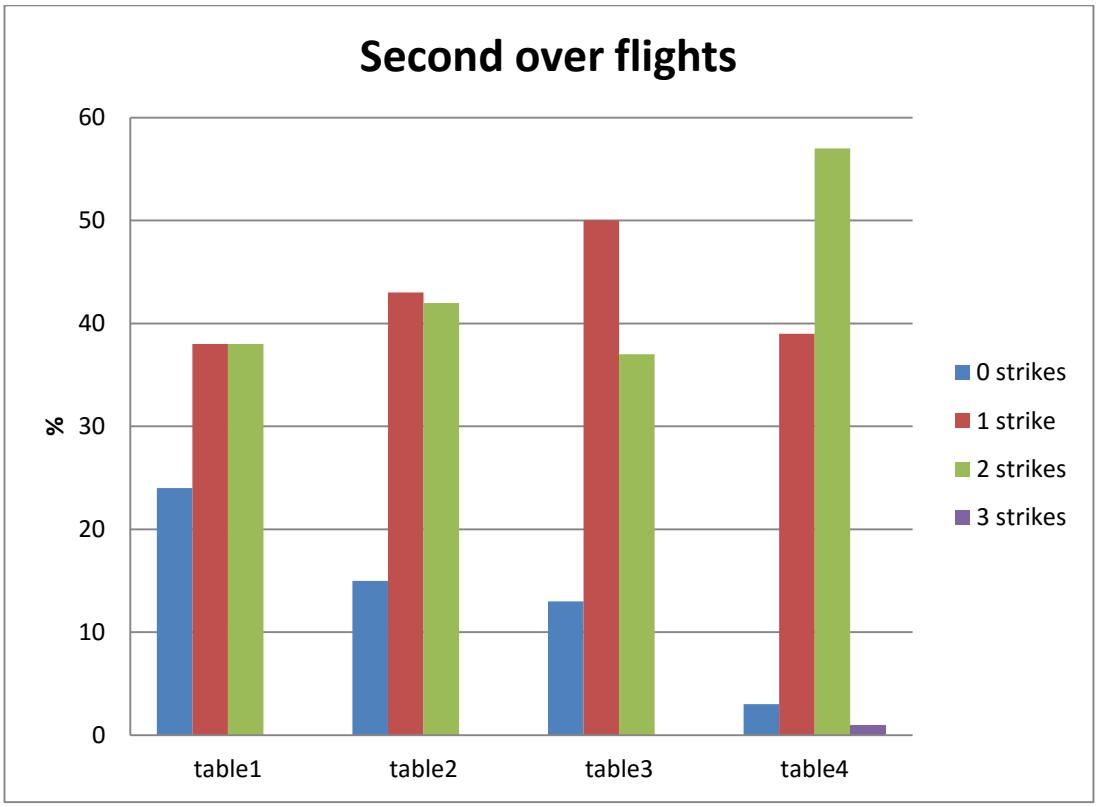

Figure 5-61 Bar chart showing the number of tables receiving 0 (blue), 1(red) or 2(green) number of strikes for the second flights over the tables

When looking at the results for both flight lines merged, the chaotic interactions can be clearly seen. No strikes form a consistent relationship between the table spacing.

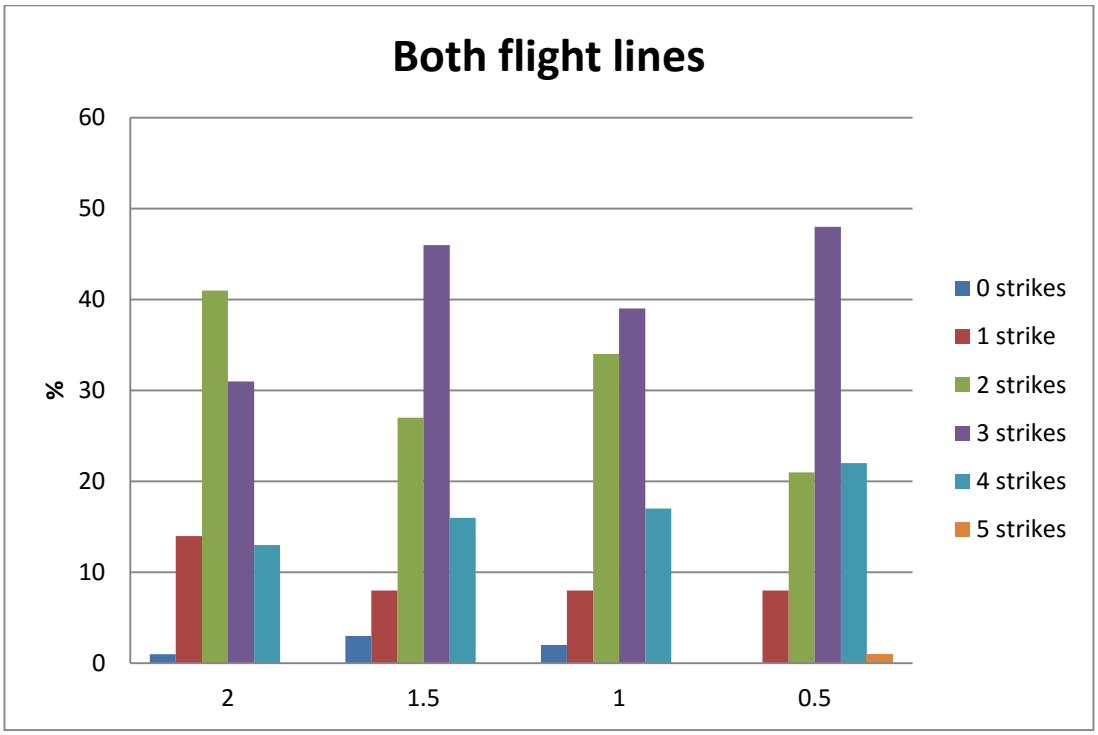

Figure 5-62 Bar chart showing the number of tables receiving 0 (blue), 1(red) or 2(green) number of strikes for both flights over the tables

Comparing the number of omitted tables for each table arrangement the negative relationship for the first flight lines and the positive relationship for the second flight lines is clearly visible. This information is shown in figure 5-63 where the blue positive trending line represents the number of omissions from the first over flights, the red from the second over flights and the green the combined flights.

The opposing relationships between the two flight directions suggest using a simple linear trend that the south westerly (first) flight direction would have no omissions when the tables reach 0.4 metres apart, given the measurement cannot be negative (distance is a ratio value) this becomes an implausible suggestion. The north easterly (second flight) direction would show no omissions at 4.6-metre separations. Given the contradictory evidence presented by

the first flight line it suggests the relationship is either non-existent or is undetectable from the data gathered.

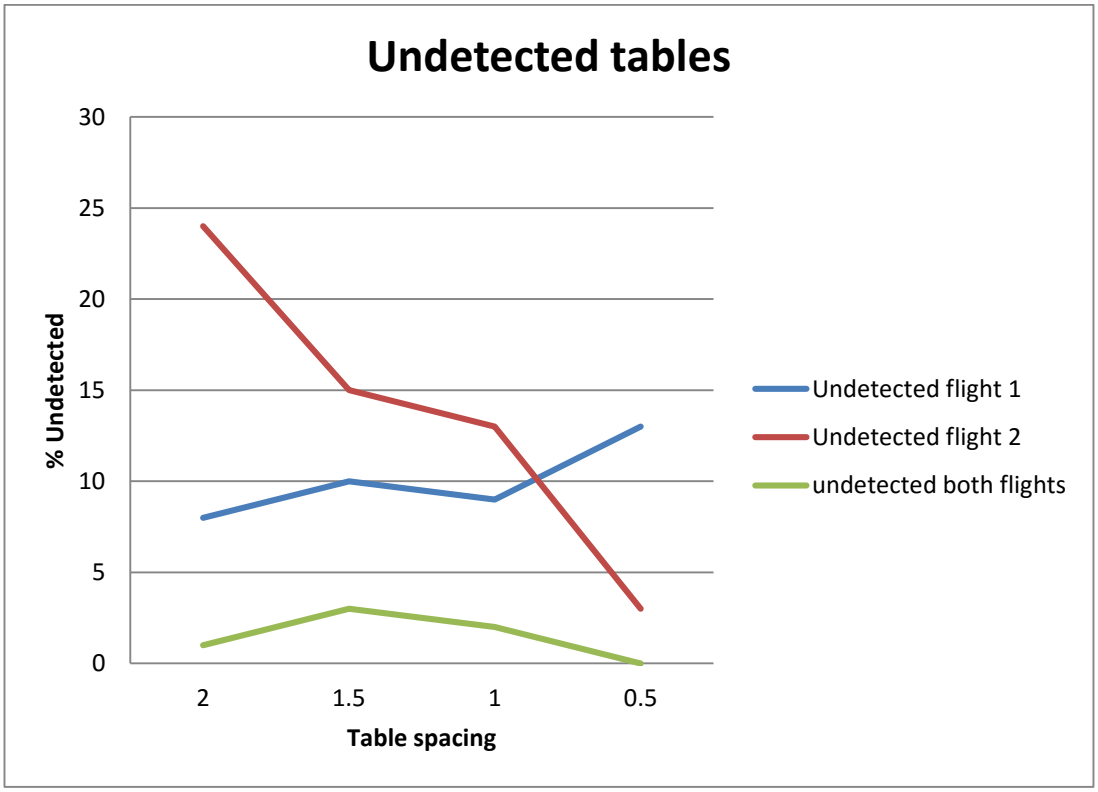

Figure 5-63 Graph showing the number of undetected tables per flight and table arrangement

Results presented regarding the comparison of tables at different separations suggests that within the conditions of this experiment that there is no correlation between object separation and detection likelihood. The results strongly suggest that features that would normally be expected to be present in the data using an approach such as Barber (2007) is not suitable for real world applications. The

5.7 Point Spacing and Separation

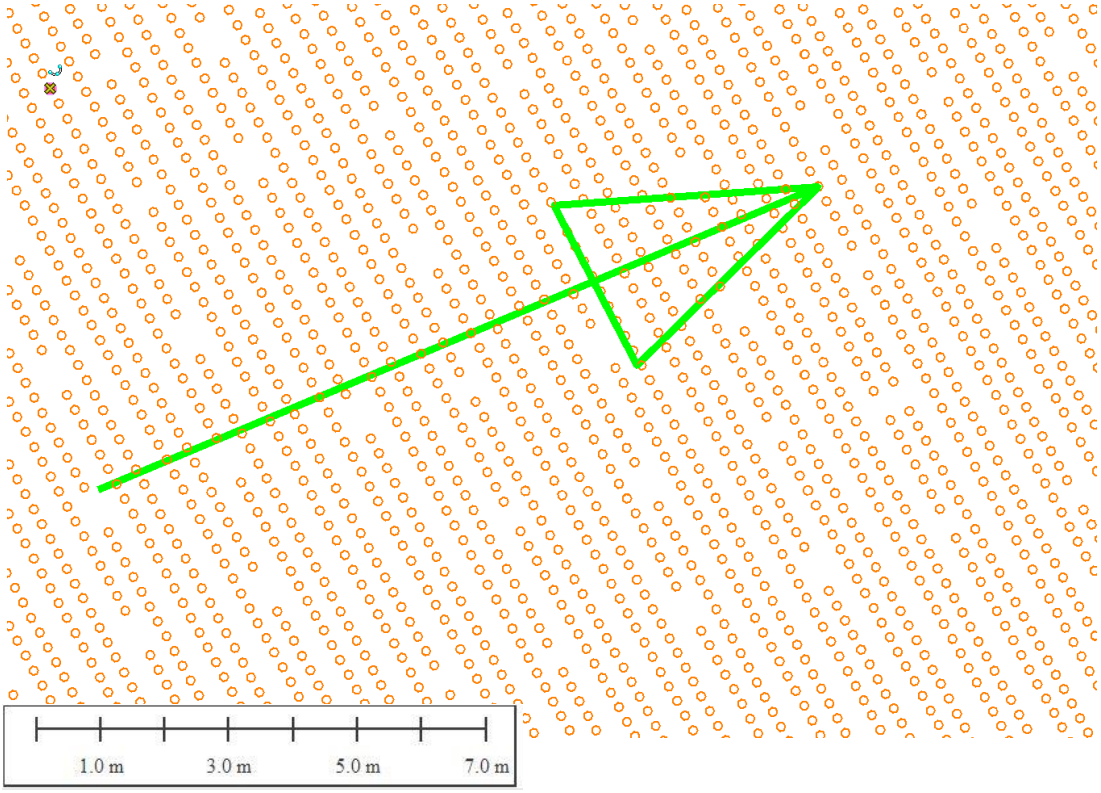

Figure 5-64 Showing point spacing for a single flight line. Points are displayed as 0.1 m circles, flight direction indicated by arrow. The figure shows the irregular spacing of the point cloud.

Figure 5-64 shows the distribution of points for the Leica ALS 50 on a single pass over flat ground. The omission of strikes periodically across track is interesting. The ground surface is flat as shown in figure 5-64 these dropouts appear to be randomly caused. These dropouts can clearly have an effect on the ability to observe features.

The point spacing along track was measured at nadir, it is expected that the points will be equally spaced at this point under the assumption of a constant flying speed. Given the nature of a laser scanner with very high frequency across track scanning (50 Hz) and slow aircraft ground speeds, this assumption should be fine over a short number of oscillations. This can

be backed up looking at the aircraft trajectory and calculating speed. Figure 5-67 and figure 5-68 shows the accelerations (the graph gradient) for flight 6 and flight 7 respectively, as can be seen very little acceleration occurs except for over three periods, these periods seem to correlate to the changing from one full second to the next. All times are recorded as GPS times in seconds from the start of the GPS week.

Figure 5-65 shows the variation in point spacing over successive scan oscillations. A cyclical pattern exists in the data but it is difficult to establish a trend, extending the measures any further would risk introducing a significant change of speed into the measurement and affect the accuracy. The values for scan distances vary between 0.50 m and 0.63 m. This is a considerable distance and has an impact on the table detection. A table is 0.60 m by 0.7 m, so at 0.63 m it is feasible that a table would be completely omitted.

This study was repeated for another flight line over flat terrain, the results appear more regular and can be seen in figure 5-66, the oscillations appear more regular but have a maximum of 0.71 m, minimum of 0.46 m, mean of 0.60 m and standard deviation of 0.08 m. These contrasts to flight line 6 with a maximum of 0.63 m, minimum of 0.50 m, mean of 0.56 m and standard deviation of 0.03 m; the cause of these differences is unclear.

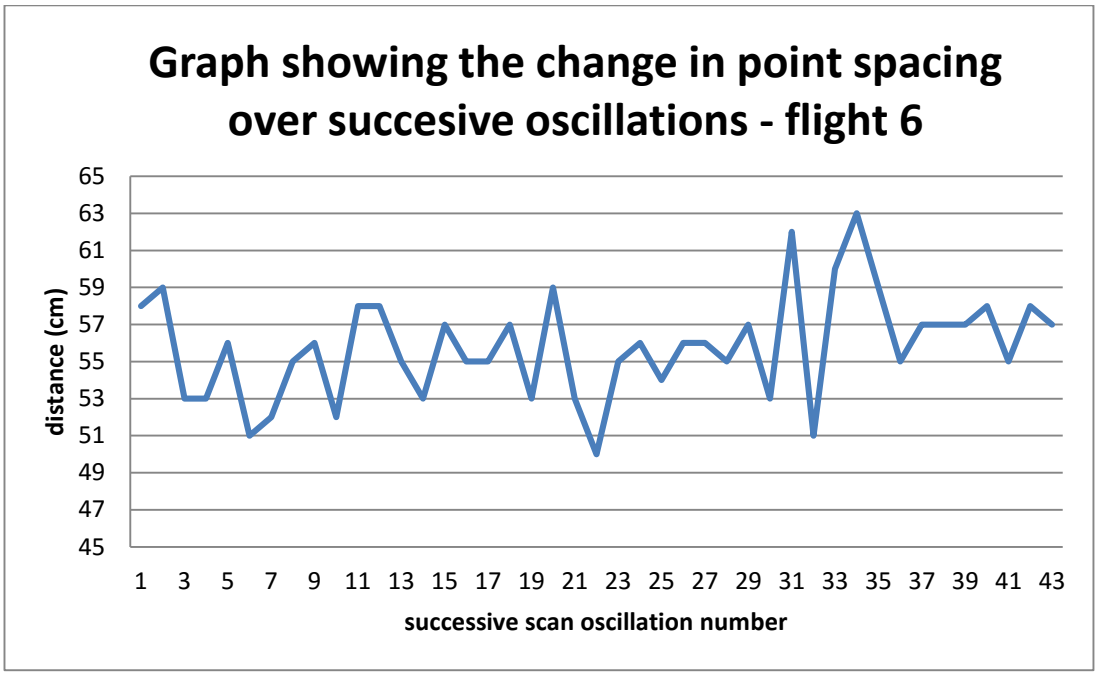

Figure 5-65 showing the change in scan pattern over each oscillation for a short time period

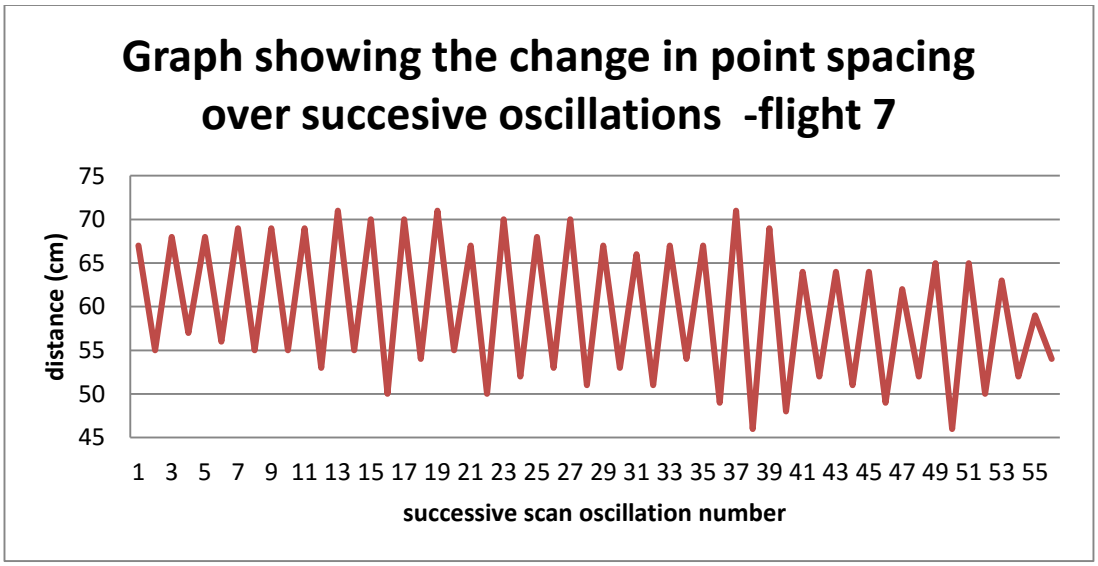

Figure 5-66 showing the change in scan pattern over each oscillation for a short time period

The figure 5.68 below support the hypothesis that over a short period the speed remains sufficiently constant to take consistent measurements. Figure 5.68 shows abnormal spikes in acceleration as the time approaches a whole second. Exports from the software show that

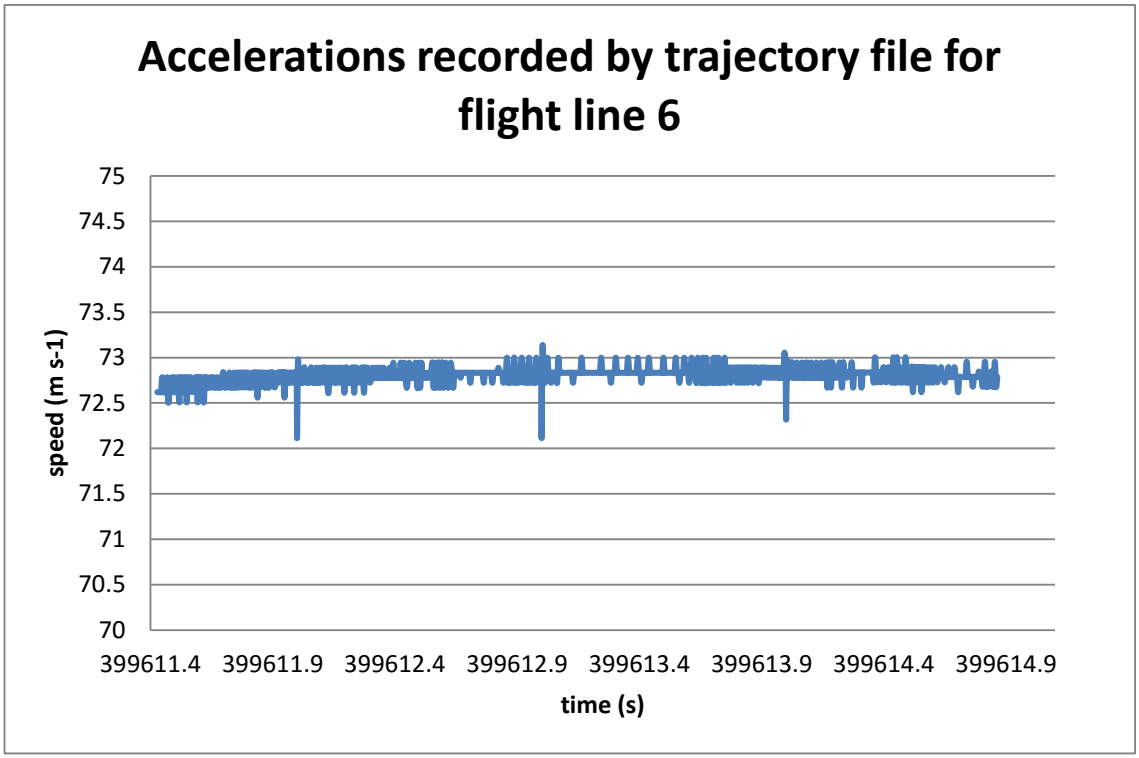

Figure 5-67 graph showing speed over time (acceleration) for flight 6. The spikes in acceleration shown at the whole second are an artefact of the trajectory software rather than true acceleration

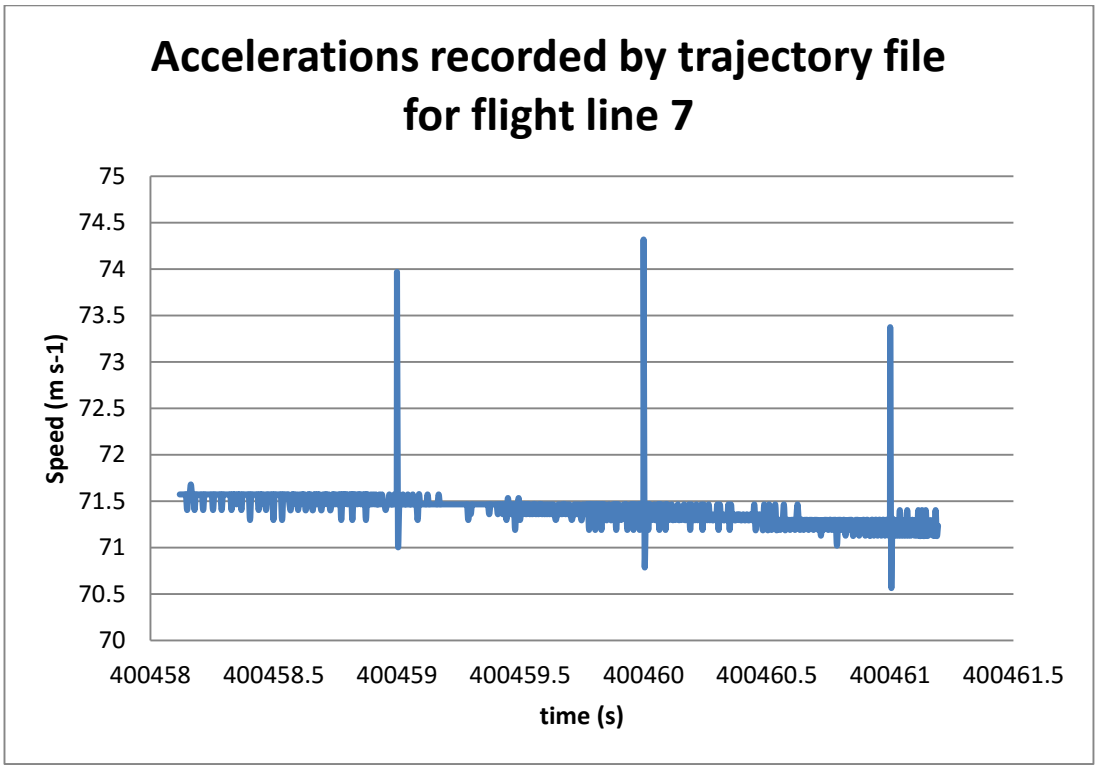

Figure 5-68 graph showing speed over time (acceleration) for flight 7

These anomalous accelerations were investigated further, in order to determine if the cause. In order to investigate this, the file produced in Applanix Pos MMS™ software containing the trajectory information was interpreted using the Applanix API. This ensures that the content of the file is written, as it is stored in the proprietary binary format. The results show that at the turn of each whole second the number is represented as an integer whereas, all other times are represented and stored as double precision float values. This occurs despite the time value being stored as a double precision float. Table 5-7 shows an example from the extracted time series.

GPS seconds
400459.9891
400459.9941
400459.9991
400460
400460.0041
400460.0091
400460.0141
400460.0191
Deleted for brevity
400460.9891
400460.9941
400460.9991
400461
400461.0041
400461.0091

Table 5-7Showing GPS times extracted from trajectory file. Note many values have been deleted to show the integer values (red) more clearly

The rounding of integer values is clearly inconsistent and the error appears as a sudden and substantial increase or decrease in acceleration.

The results presented in this chapter show the outcomes of the table study. This study has raised a number of questions regarding the ability of LiDAR to pick up and detect objects these will be discussed in the next chapter.

5.8 Repeatability Experiment Results

The repeatability experiments looked at three main landscapes, a flat hockey pitch, a suburban area and a forest plot. The flat hockey pitch tests the scans under ideal conditions of a flat hard surface. Then an urban environment creates a complex environment with well-

defined objects and hard surfaces. The forest links to the aims of the study and provides the most complex of the environments.

Initially, over the hockey pitch area, the change in elevation over the hockey pitch is seen in relation to the hockey field. Subsequently the elevation scatter plot for the area is shown before looking at the clustering of flights and the repeatability of each flight line. Figure 5-69 shows the entire point cloud for the hockey pitch area. The points are coloured by elevation showing a mild gradient from the northeast to the south west of the area.

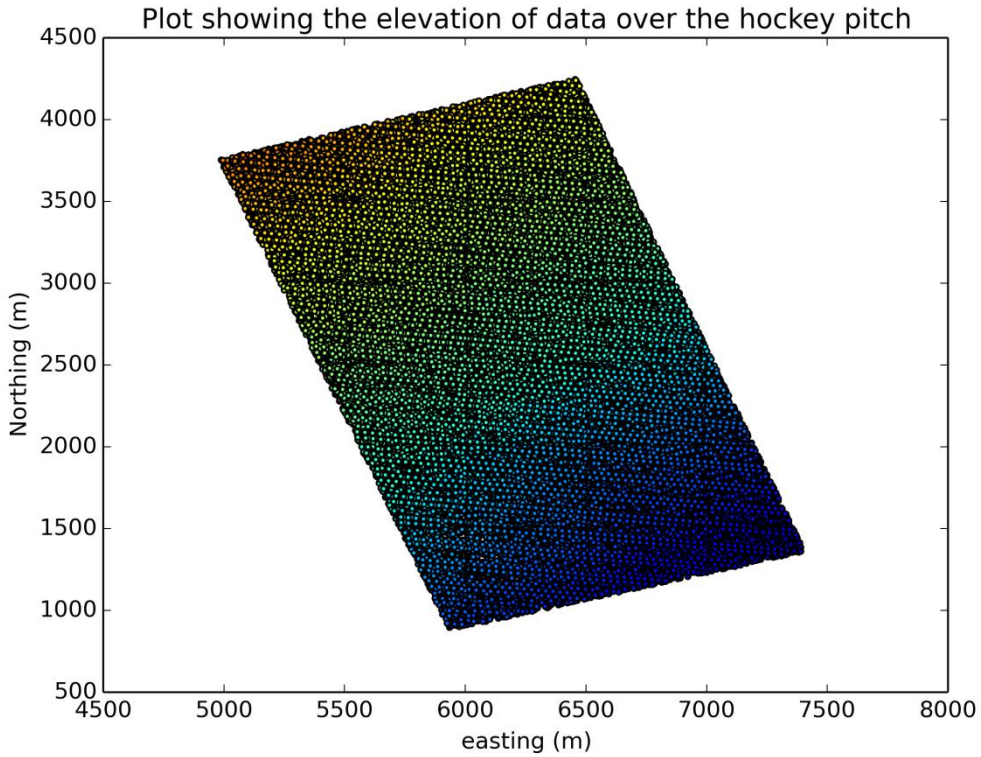

Figure 5-69 Map showing the elevation change over the hockey pitch. Easting and northing used for X and Y axes respectively, the data points coloured by elevation. Range of elevation change is 1.9 m.

The elevation over the hockey pitch shows a change in elevation of 1.9 metres over 30 metres, this gives a gradient of 2.1º. This is greater than expected but suggests the experimental methodology should use smaller grids of points instead of the whole hockey pitch. A 5 metre grid will be used to eliminate bias as a result of the slope.

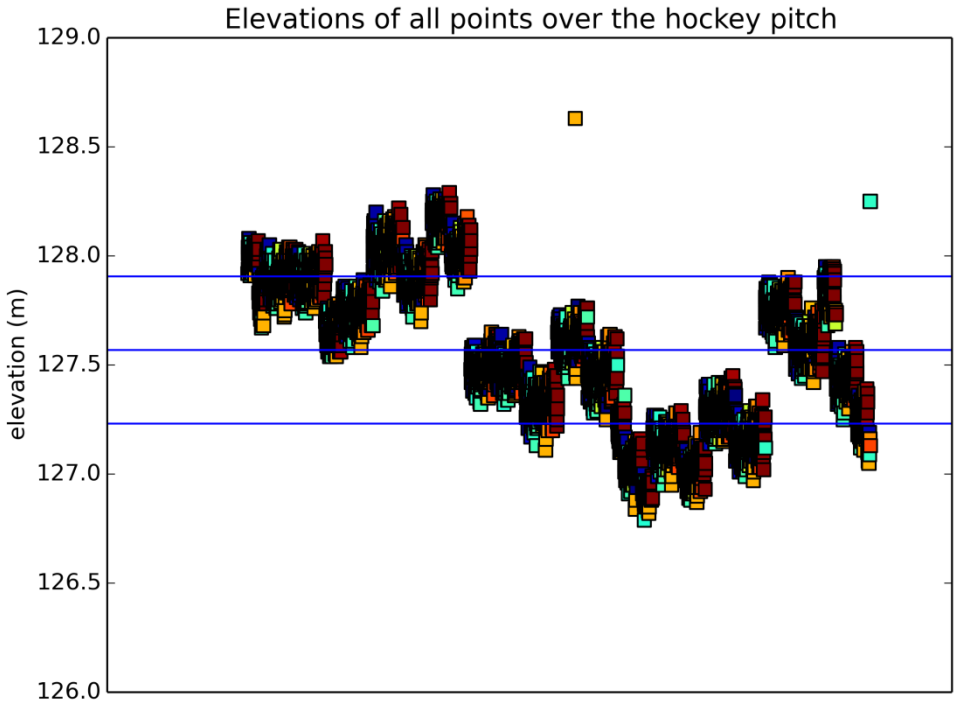

Figure 5-70 elevation of each point on the hockey pitch. Coloured by flighltline. The 3 horizontal bars represent the mean and 1 sigma confidence limits.

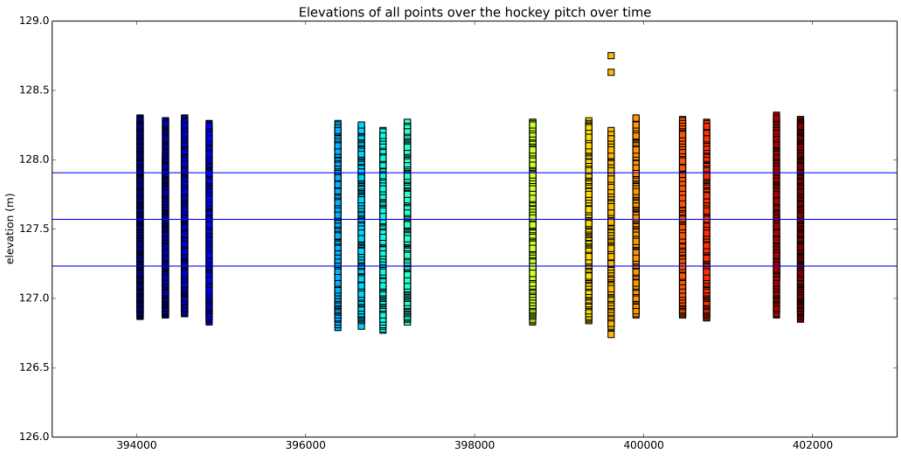

Figure 5-71 shows a scatter plot of elevation against GPS time. Each vertical cluster is a flight line and the spread of elevations shows the variation.

Figure 5-70 shows the variation in height of each point. This is demonstrating the outliers and variance within the dataset. More usefully, figure 5-71 groups these points by flight line. This grouping shows the variance within each flight line. The maximum and minimum values are different but more analysis is needed to suggest any difference in distribution. Violin plots provide a useful tool for this analysis, similar to a box and whisker plot but plotting a histogram of data along the spine of the plot.

Figure 5-72, figure 5-73, figure 5-74 and figure 5-75 show violin plots of individual 5-metre sections of flat hockey pitch. Each flight line over the area is shown as a plot of its distribution and quartiles. Figure 5-72 shows similar distributions of data showing a wide but bell shaped distribution for each line. The central quartiles (shown within the blue box) for each dataset show varying medians and dispersion of points. This variance in different flight lines can be seen across the four figures. Flight lines 12 and 15 are showing a bias towards recording lower elevations.

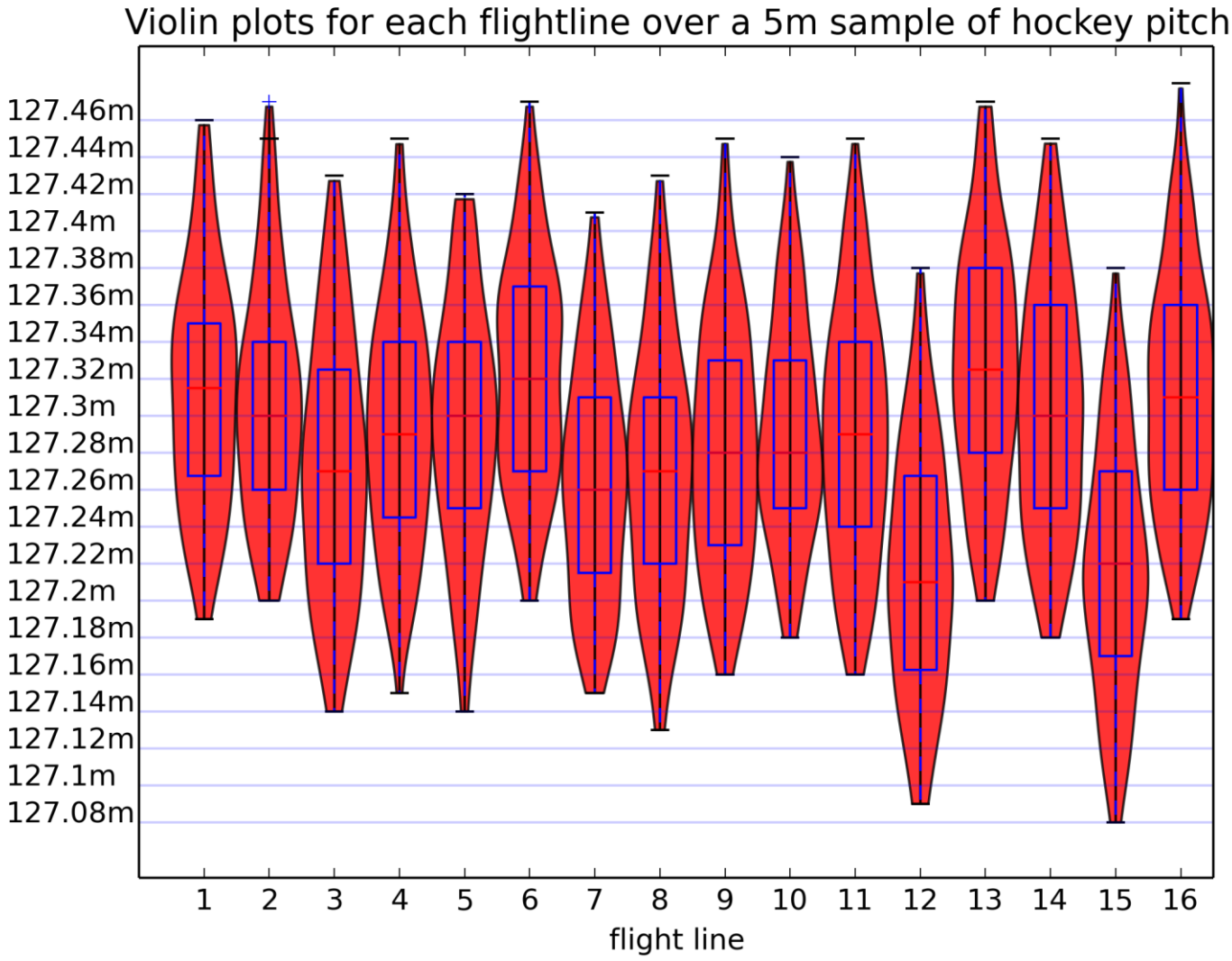

Figure 5-72 Violin plot showing a 5 metre sample of LiDAR data.

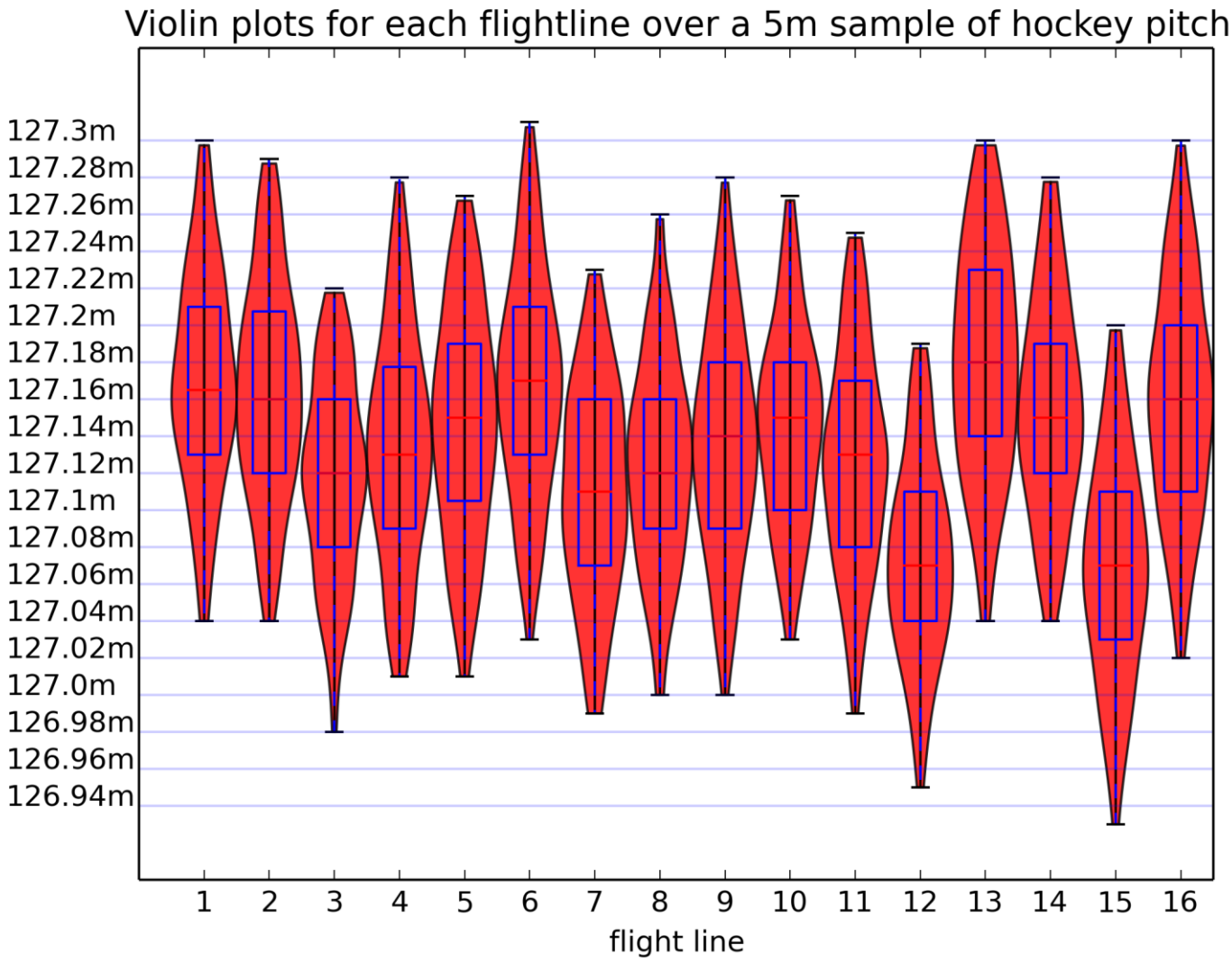

Figure 5-73 A Violin plot of another 5-metre area over the Hockey Pitch. Note the variance in extreme values

Figure 5-73 shows a separate 5-metre area of hockey pitch. Flight lines 12 and 15 show a bias towards lower elevations as with the other sample areas. There is a greater range of distributions between the flight lines. Line 13 shows as skew towards positive values whilst the others show a flat but symmetrical distribution with a strong tendency towards the mean. Line 13 shows a positive elevation bias.

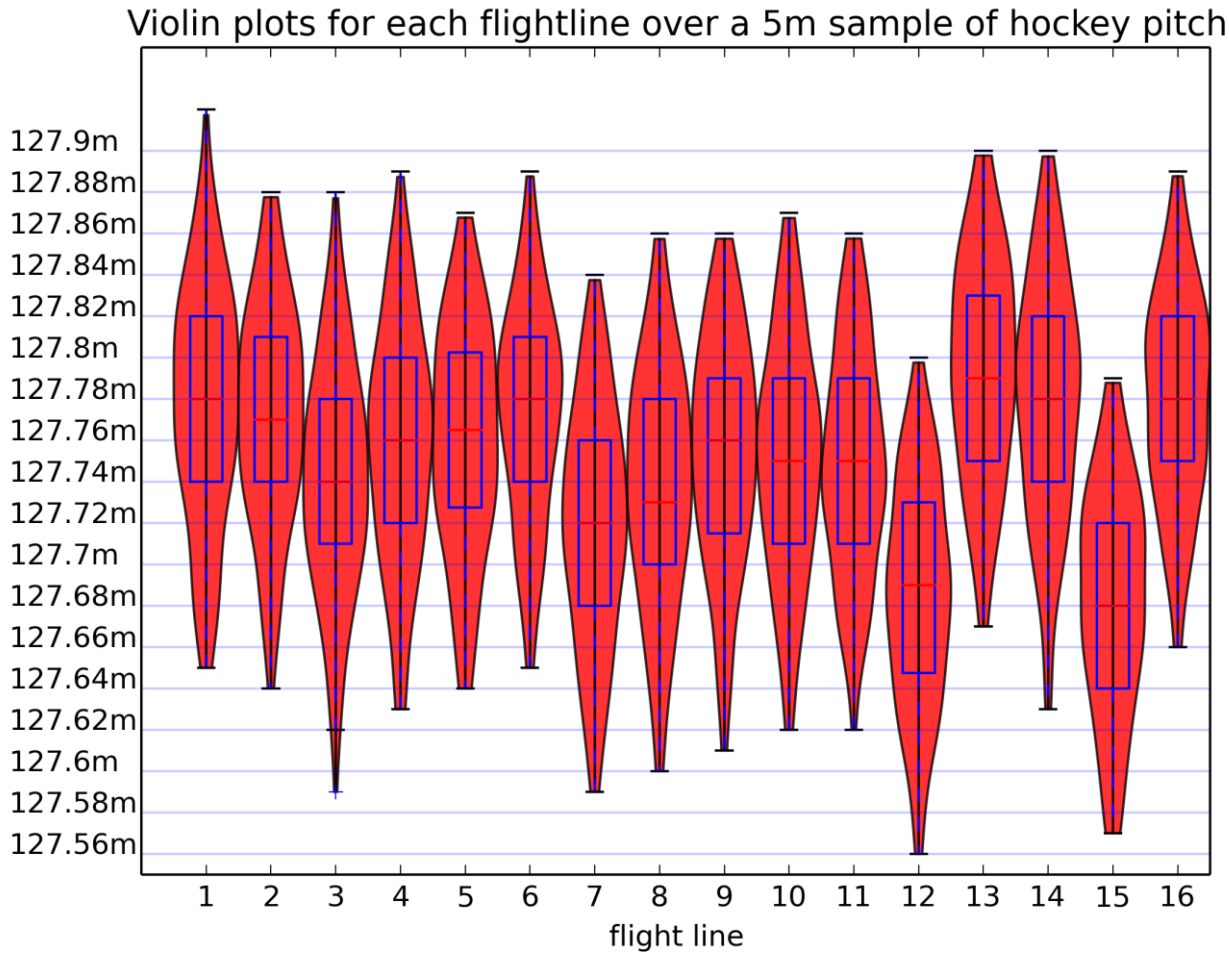

Figure 5-74 Violin plot over a 5-metre section of hockey pitch. The plots show significantly different characteristics and distributions

Flight lines 12 and 15 in figure 5-74 show a bias again, although this time flights 2 and 13 are showing a distinct positive bias. The distributions of each flight line are varied with differing skew values being clear. The central quartile plot of flight line 15 and 12 does not share any common elevations with fight line 13 or 15.

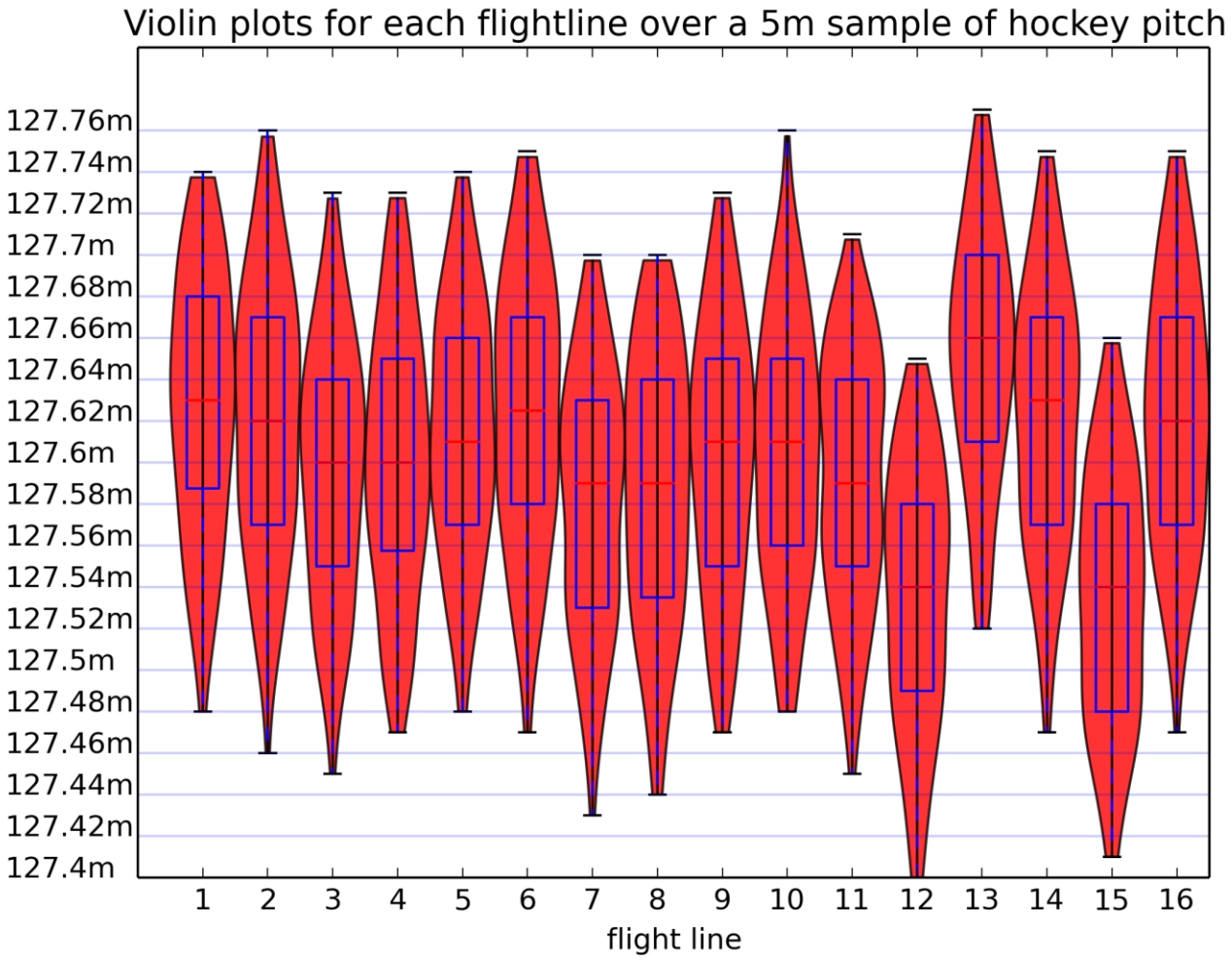

Figure 5-75 Violin plot over a 5-metre section of hockey pitch

Figure 5-75 shows the final violin plots for the hockey pitch sample areas. The four samples shows a consistent lack of repeatability with flight lines showing bias and differing distributions

The 5-metre sample size ensures that the area of the study is flat and that changes in elevation are not the primary cause of any deviations. To ensure the sample size is large, two separate 10 metre sections of hockey pitch is investigated and shown in figure 5-76 and figure 5-77.

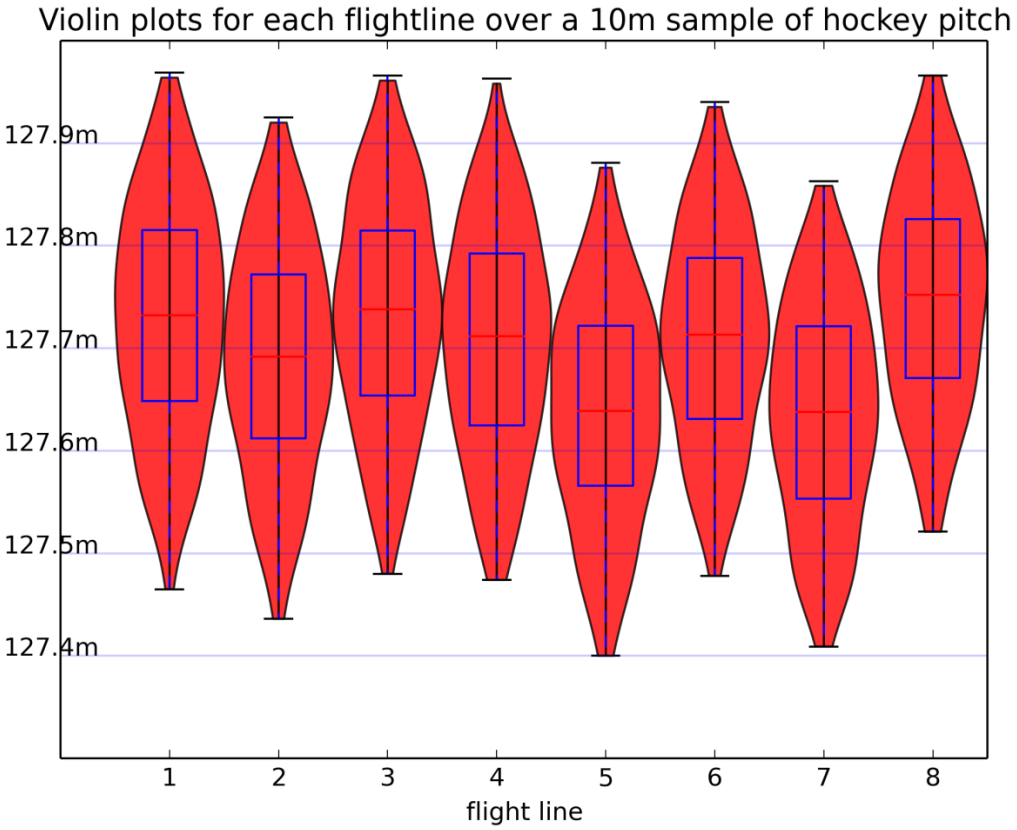

Figure 5-76 a Violin plot of a 10 area of Hockey Pitch

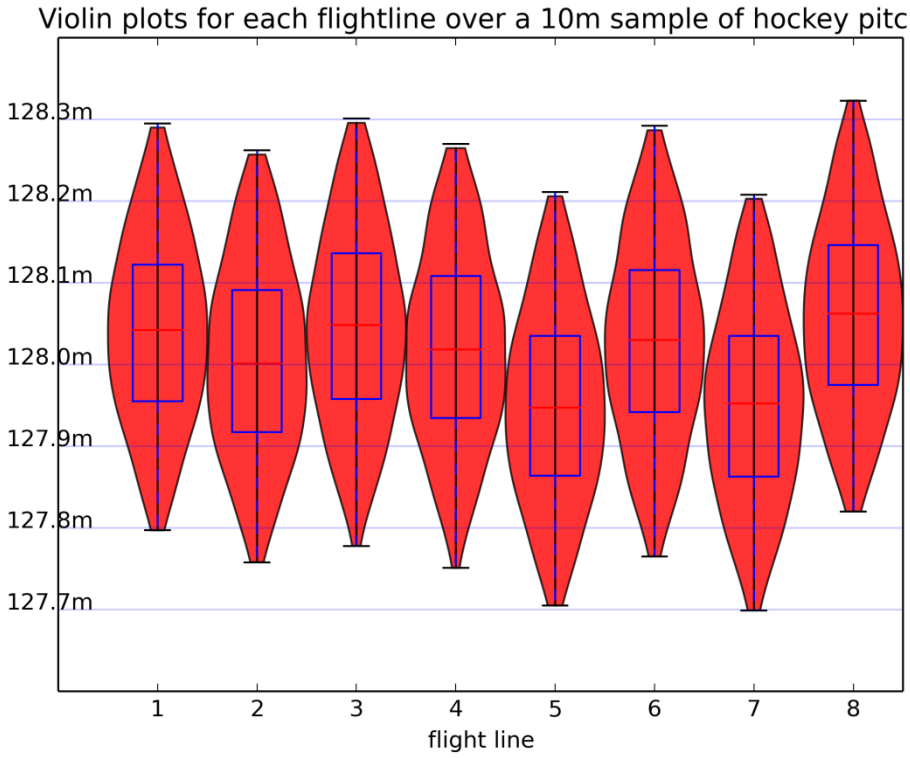

Figure 5-77 the second 10 metre hockey pitch area violin plot

The forest plots provide an interesting violin plot, shown in figure 5-78, whilst repetition and comparison with other areas is not possible due to the heterogeneous structure of forestry; it is possible to compare the overlapping flight lines for consistency in the representation of the environment.

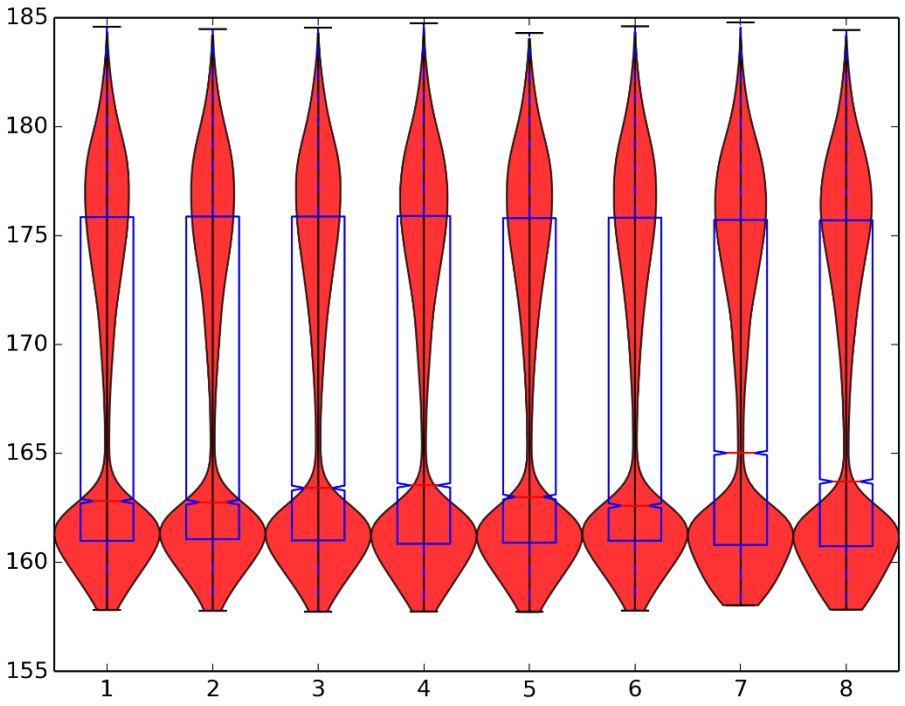

Figure 5-78 Violin plot showing the 8 overlapping flight lines of the forest plot

The plots show similar overall distributions with a range of canopy shots, fewer stem and understorey shots with a large bulge at lower elevations showing the ground and above ground cover. The mean is variable for each overlapping flight and suggests that the distribution although similar may be characterised as statistically dissimilar.

This chapter has presented the results of the study, these investigate the ability of a LiDAR system to define, characterise and reliably interpret the topography that is scanned. Whilst the results focus on simplifying forest characteristics to bring order and control to the experimental regime the results should be considered for both their impact on forestry but also the wider laser scanning applications.

6 Uncertainty Experiment Discussion

The chapter will draw on and interpret the table experiment results. The wider context will look at the suitability of LiDAR for detecting small objects, the options for increasing detection rates and look at LiDAR as a verifiable and objective measurement technique. Finally, the outcomes of this study will be used to look at the existing methods of defining a LiDAR scan and look at ways this could be improved.

6.1 Table Results

The table experiment results are interesting and do not conform to the expected outputs of the research. These results will be discussed in detail and explored within the literature framework.

The literature regarding point spacing and object detection is limited. An early review paper by Flood (2002) reviewed LiDAR post spacing in relation to FEMA mapping standards for flood modelling, LiDAR was found to comply with these standards, as such of the many recommendations made by the article, further investigation into small-scale point spacing was not one of them. An interesting paper by Hodgson *et al.,* (2005) investigating LiDAR derived elevations and terrain slope in leaf off conditions suggests that point spacing may be important but does not investigate further within the article the same research group and dataset was used by later studies. Chow and Hodgson (2007) used a point cloud with 2-metre spatial resolution covering the Piedmont area of South Carolina. The study down-sampled the LiDAR data in order to investigate the effects of DEM resolution on slope estimation. The study found that higher point spacing consistently and linearly underestimated slope angle. The study used a down-sampling approach of taking one in n number of points to simulate a lower point density. This does not account for the uneven point spacing characteristics found in laser scanning. A further study by Raber *et al*., (2007) using the South Carolina dataset used

by Chow and Hodgson investigated the impact of LiDAR post spacing on DEM accuracy for flood zone delineation. This study found that the results from hydraulic models had varying sensitivities and that flood stage values were typically insensitive to the DEM resolution whereas flood extent mapping was sensitive. The study once again simulates point spacing reductions using a down sampled technique of importing one in n points to reduce the resolution of the scan.

6.1.1 Likelihood of single tables detected

The likelihood of single table detection should be deterministic in nature; the factors should be calculable and be able to be determined prior to a survey (c.f. Barber 2007). The results achieved appear stochastic with a table's surface not showing any correlation with laser reflectivity. This places the scanner as the primary control on detection or omission.

There appear to be two mechanisms by which tables are not detected. First, that the table is insufficiently illuminated and secondly that the table falls within a scan pattern void. The latter essentially being a special case of insufficient illumination where no illumination occurs.

Footprint size was kept constant throughout the experiment, and its possible impact was tested using the theoretical models available as shown in figure 5-3 , the lack of laser illumination appears to be due to two factors, the irregular scan spacing and the dropouts from the laser returns. The irregular scan pattern has been investigated in figure 5-65 and figure 5-66; these studies show a cyclical (periodic) yet irregular pattern.

6.2 The effect of object spacing on detection

A primary purpose of laser scanning is to detect objects, these objects may be of specific interest (for example power line mapping) or of general interest (city modelling). It is of interest to determine if horizontal spacing affects the ability of a laser scanner to detect an object from its neighbours. Vertical spacing is well understood (Gelhar 2010), the hypothesis tested is whether objects become more difficult to detect as they move closer together. The detection of an object is distinct from its coalescence with neighbouring objects; an object that is detected is simply present. The ability to define the object as distinct from other objects is a function of the number of hits received by the object and the number of hits that characterise the landscape around the object; as such, a complex landscape may cause coalescence at lower densities.

The results from the table studies for the correlation of table spacing to detection are both interesting and difficult to interpret. The south-westerly flights show a clear positive correlation when looking at the number of undetected tables, thus the closer the spacing of the tables, the more difficult they are to measure the discrete objects using LiDAR data. This is juxtaposed by the results of the north-easterly flights, these show a strong negative correlation suggesting tables become easier to detect as they move closer together in a group. The overall trend when both flights are used together is consistent detection rates of less than 5% with the maximum level of omission found at the 1.5 metre separation. As such any correlation between detection and separation appears to be either too weak to be detected here or non-existent. The separation from one object to another is independent of the size of the object; it is this size and orientation of the individual object that appears to have an impact on detection.

6.3 Along-track laser point spacing

Laser scanning specifications assume the laser scanner to produce a regular pattern of laser returns. The expression of key variables in hertz implies an ordered and regular periodicity such that should an item oscillate at 50 Hz, it is expected that each cycle occurs every 0.02 seconds. The along-track laser point spacing recorded by a laser scanner over flat ground and at a constant speed does not support this hypothesis. The scan data shows that the line spacing varies with each scan. The speed is calculated from the 200 Hz trajectory and accelerations derived. To look at this the change in acceleration over time was investigated this change in acceleration is jerk. These values remain very low at between -0.05 and +0.05 m s^{-3} (the units are m s^{-3} as this is a change in the change of speed). As such, the variation in scan interval can be isolated from a change in speed.

The scan interval varies seemingly randomly. Whilst the sample size is small, the variation over a short period is clear and it is distinct between flight lines. The experimental design does not allow extended periods of observation. The observation period is limited to time periods where the platform ground speed is constant. As the aircraft had a variable ground speed (this is unavoidable and was kept as constant as possible) extended observation is not possible

The flight line from flight 6 (figure 5-65) shows no regular pattern, the maximum distance observed is 0.63 m and minimum 0.50 m, the standard deviation is 0.0283 m. The mean gap is 0.55 m. For flight 7, the gaps appear periodic, although show a maximum of 0.71 m a minimum of 0.46 m and average of 0.59 m, the standard deviation is 0.8 m. This is much more varied; the oscillation shows that the scan lines flip-flop between short distance and long distances apart. This is more akin to a mechanical or other deterministic reasoning. As the two graphs show very different results, it suggests either a pattern that has not been observed, temporary order to a more chaotic system seen in flight 7 or that the distances are random whilst governed by a scan frequency. The sample size was small in order to keep the ground

speed, attitude and acceleration variables constant. In order to test this further, an alternative experiment would be required. The experiment design would consider and constrain the required variables in order to only test the along track spacing. Such an experiment could make use of a ground-based experiment with a constant velocity platform used to mount the sensor. Such a design would allow for the observation of larger time periods resulting an increased number of observations allowing greater investigation into the causes.

6.4 Trajectory Information

The trajectory information stores the merged and filtered IMU and GNSS values; this provides the position of the sensor head and is the input to the point registration solution. When measuring the time the results show as a double precision float with four decimal places to denote the time, as a 200 Hz (0.005 seconds) measurement system, this provides sufficient precision to store the time values as numbers. When an integer value is encountered, (a whole second is reached) the data are stored as a rounded floating value with its decimal part rounded to zero. This is clearly wrong when viewed in terms of acceleration; the integer recording must be a generalisation as the results show a rounding up of the time to produce rapid periodic accelerations. This rounding error is the result of the Applanix software and all programs that use the Applanix application-programming interface to extract values from the trajectory file exhibit this behaviour. This rounding error appears in all the Applanix derived trajectory files investigated. The extent to which this causes a problem is unknown, it is clear however that the problem can be cascaded to the registration program.

6.4.1 Experimental Limitations

The experiment was designed to observe the coalescence of objects as the separation between objects decreased, this experimental objective was not fully investigated as the more intriguing and significant results of the experiment became clear during the exploratory data analysis. The effect of missing tables was unexpected and as such, the study changed direction to understand the cause of these omissions. Had the experiment been set up to detect this phenomena the experimental design would have looked at object reflectivity and object sizing as variables, instead these remained constant throughout the experiment.

The lack of multiple incident angles caused further limitations, due to unforeseen circumstances noted above with the two perpendicular flights that were not properly located over the target area of interest. This would have provided additional information on the effect of incident angle.

6.5 LiDAR Sampling

LiDAR is a sampling technique, most LiDAR surveys under sample the area of interest, the degree to which this is done is determined by the number of points emitted, the controls on the spacing of those points and the divergence of the beam. LiDAR is capable of oversampling and when two flight lines cover the same area of interest, a degree of oversampling is probable. This oversampling can provide redundancy to the single measurements taken by the LiDAR sensor.

6.5.1 Object characterisation through under sampling

When a survey under samples the area of interest it is important to be able to determine the pertinent properties of any object in the area of interest, these properties for topographic surveys would typically include presence, shape (height length and width for example). For forest applications, these may extend further to include properties such as canopy penetration, crown detection and ground accuracy.

In order to be able to under sample effectively, the relationship between the sampling strategy and the ability to extract the pertinent properties must be better understood. Ideally, the relationship should be understood to the point that object properties such as size, shape and material can be utilised to inform the required point density.

The most basic property of an object to detect for a survey is its absence or presence. This was tested through the experiments conducted. It is clear that not all objects are detected using a sampling strategy that theoretically allows for the objects of that size to be detected. The results for the table experiments were surprising; it was unexpected that any tables would be omitted at the point densities sampled. The tables were placed at near nadir scan angles and each had an object size greater than the predicted point spacing. Each table should have received two strikes that detected the presence of the table with each table theoretically receiving 2.115 strikes. When doubling the point density by adding the second flight this number doubles to 4.23 strikes per table. Whilst some tables did receive, two strikes per flight line and one received three under the final table configuration. In all cases except the final flight line for the final table configuration under half the tables received the expected number of hits.

Using both flights the expected number of strikes is in excess of four, some tables were omitted completely, this may be caused by the lack of pulse interactions caused by irregular spacing or by the return energies being too small to detect. The latter seems unlikely as the

same tables were observed under different table configurations. The irregular pulse spacing hypothesis is supported by the evidence presented in the results chapter, the random spacing between scan lines is a cause for concern when detecting small objects, or any linear objects that run perpendicular to the flight path. The along track detection is significantly more reliable as the pulses are not banded from the mirror movement and instead are spaced on time interval.

6.5.2 Achieving required point densities

It is common practice for aerial survey providers to deliver a survey according to a specified point density requirement. This can be achieved in two ways, flying lower and slower with high frequency equipment to scan at a given point density, alternatively the flights may be higher and faster but repeat over the survey area twice. There are advantages to approaches, the former providing higher pulse intensity, lower transmissivity effects and a more controlled scan pattern. The latter option has commercial benefits allowing pilots following linear objects to fly straighter lines keeping the area of interest within the swath (common for corridor mapping applications). It also allows the aircraft to be kept at a higher altitude giving the pilot a greater safety margin in the event of a malfunction and the higher flight path reduces noise and disturbance to residents in the flight path.

One of the criticisms of laser scanning is the lack of redundancy in the point measurements, when compared to photogrammetry where stereo pairs correlate to give a redundant image the single laser strike is unverified. By flying twice, the redundancy is increased with a separate flight covering the same area (although not always matching the same iFOV). This increased redundancy must be contrasted to the reduction in accuracy of individual points is reduced because of higher-flying heights. The inertial measurement units are accurate to a certain angular uncertainty, atmospheric effects become more pronounced and the intensity

of the resulting laser strike reduces making a return less likely and the digitisation of the pulse more difficult.

A major advantage of the two-flight strategy is the disruption of the ordered scan pattern, because the scan pattern is determined by mechanical controls for a single flight line the pattern of laser strikes must be ordered. Flying twice over the area is it exceptionally unlikely that the two overlapping flight patterns will match exactly with the resulting scan pattern appearing more of a stochastic pattern of hits distributed over the overlapping swaths. This increases the sampled area and decreases the risk of losing objects within the scan pattern.

The experiments have shown that single flight lines can suffer dropouts and omit objects and as such, a second flight does significantly increase the likelihood of object detection. With the data available, it is not possible to determine if a lower flying height would decrease the number of dropouts.

6.6 LiDAR Verifiability

For a LiDAR survey to be useful, it must show a true representation of the area of interest, whilst this representation will be abstracted from reality and presented at its captured survey scale, such a representation should still be accurate and repeatable. The verifiability of an experiment is important, the scientific method relies upon verifiability; the ability to repeat an experiment and observe the same results is paramount to understanding scientific principles.

Not only is the ability to repeat a set of observations and receive similar results important scientifically, it is important to many of the applied uses of LiDAR data in the fields of surveying, engineering and land management.

6.6.1 The Table Study and Verifiability

The table results present interesting verifiability questions. It is clear to see from the results that the tables are not uniformly observed, the tables show limited bias to detection based on arrangement or on surface type. The detection rates are spread randomly across the tables and as such, bias does not appear to be a factor. The results can be considered variable for each scan. Each scan misses a differing number of tables, but more importantly, equally sized objects are not equally detected.

The probability of detection of equally sized objects should be identical for a given scan. Either this variability is related to the object size being very close to the minimum mapping unit for the scan resolution or that an irregularity exists within the system that can cause omissions, such that localised resolutions vary significantly from the overall resolution.

The table study brings verifiability into question for the collected LiDAR data. The same tables with the same configurations are observed differently for the two over flights. In an applied context, this could mean missing tree crowns, archaeological features or engineering features such as power line structures, or pipelines.

6.6.2 Verifiability and Violin Plots

The violin plots provide an interesting and visual means of interpreting the LiDAR data, removing the spatial element to focus on a single and first order variable, elevation, has allowed the data to be investigate thoroughly. The results of the flat, hard and homogenous hockey pitch are of particular interest. This area should not present a challenge to the laser scanner; the near nadir laser strikes onto a flat hard surface should create very narrow error bands, the data shows a range in excess of 0.35 m, each flight shows a flat, wide but bell shaped distribution. The manufacturers stated accuracy is for a 0.15 m range. This value is

not expressed with a confidence estimate. Clearly, the performance of the system falls outside of the implied limits, only meeting the 99% confidence value. The mean values vary between each flight and taken in isolation would not show the true variability in single flight lines. It is known within the LiDAR industry that separate flights may have different constant offsets and are typically verified using ground control sites. Overlapping flight lines can be adjusted using a process known as strip adjustment, this is not routinely performed and relies upon the data to characterise the area overlapped in the same way. The table study suggests that for complex landscapes this may not be a good representation of the overlapping surfaces, this is because the laser characterises the micro-topography differently in overlapping flight lines the match is as much stochastic as it is elimination of systematic bias.

6.6.3 Verifiability and scale

The table study was conducted with the table arranged with a number of different separations, the point densities were varied by combining two flights together. A credible cause for the lack of verifiability is that the point densities captured were insufficient for the mapping scale. As such, objects were not represented correctly and the minimum mapping unit overestimated. The existing method of calculating point spacing in order to derive minimum mapping units (c.f. Barber 2007) is ineffective. Barber (2007) emphasises the probabilistic nature of this approach but the uncertainties are underestimated. There is little alternative work directly relating cartographic principles to point cloud based mapping. Given the primary purpose of most aerial laser surveys is mapping, often for a particular critical application this lack of work is clearly an area that needs further attention.

6.7 LiDAR point cloud descriptions

Point clouds are described using standardised terms; these are point spacing and point density. Point spacing is measured along track and across track; point density is given by the

number of points per unit of area. Both terms lack a rigorous definition and do not fully describe the point cloud. The results from this thesis show that currently the approaches to describing a point cloud do not adequately describe the survey characteristics of the point cloud.

Point density is simply defined as the number of points per unit of area (Baltsavias 1999). This definition is misleading for point clouds. The definition of a point is unclear, is this intended to be an emitted pulse of light or the alternative is the number of returned points. This eliminates the problems caused by low reflectivity surfaces and dropouts. It does reflect the number of points available to the end user for mapping and analysis purposes. The number of reflected returns is highly dependent on the complexity of the environment. This makes it difficult to plan to capture a given point density, it also makes point density correlated to the sensitivity of the digitisation technique.

Neither technique provides a wholly satisfactory measure and most importantly does not provide the user with an assurance of what features will and will not have been captured

Point spacing is an alternative approach. The point spacing is measured between points in the respective direction (along track or across track). The point spacing is a useful measure but alters with the scan angle for sinusoidal or saw tooth scan patterns. The along track spacing is closer at nadir than at zenith, conversely the across track spacing is closer at zenith as the mirror slows to change direction. This varied point spacing is accounted for using the nominal point spacing. Nominal point measures are deceptive, as they do not express the variability of the measure, just the average.

Point cloud descriptors should completely describe a point cloud such that two equal point clouds have equal attributes and detect features equally, a point cloud with the same descriptors as another should not differ significantly in the way that it surveys an area of

interest. Point spacing and point density both have their limits as discussed above. The limitations are primarily around describing the intra point-cloud variability.

Representation of laser footprints is a further factor in the measurement of point cloud descriptors and in the understanding of uncertainty of laser scanning. The point cloud represents each laser interaction as a point, a point is an infinitesimally small representation of an object; it has no area. The laser footprint conversely occupies a significant area and is complicated within that area by the distribution of light within that area. This is not accounted for in the existing point cloud measures, and point spacing and density measures assume an infinitesimally small area and measure from that point to the next point.

The basic premise of laser scanning is to illuminate an area of the laser this area is the footprint. This gives rise to the idea of measuring area illuminated. This is perhaps a better measure of resolution instead of point density; the area illuminated is directly related to the sampling resolution. As such, a measure of the percentage of a square metre area on the ground that is covered would give a view of the area sampled.

The area illuminated has potential as a measure, but it has downsides as well, the area illuminated alters between nadir and zenith, the measure per unit area also does not show the distribution within that measured area allowing multiple illuminations of the small area and sampling bias to go unreported. Further to this, the area illuminated can be extended by increasing the beam divergence. This wider footprint samples a larger area but does so with lower incident intensity (reducing the likelihood of a return) and reduces the precision as a larger area is sampled with only one measurement and reduces the accuracy, as the low intensity pulse is harder to digitise. The opposite value could be utilised to measure this effectively, teaming area illuminated with area unsurveyed, which is the “dark” areas of the scan would show the number of repeat observations. This information would allow for the user to understand the unsurveyed area from the surveyed area.

Demonstrating the difference between nadir and zenith values is difficult, whilst this could be established as an algorithm; this would not be intuitive to the end user. Box and whisker plots showing nadir, mean and zenith values may offer an intuitive visual and complete way of describing the data.

Point spacing as a measure has less flaws, it is the variability between zenith and nadir scans that cause the measure to be unrepresentative, the box and whisker display would again record the variance.

Existing point cloud measures give a false sense of confidence when attempting to map at a given scale, point spacing is not equal to minimum mapping unit and the new measures will better describe point clouds. Work needs to be done linking scanning resolution to mapping scale.

6.7.1 ALS and Mapping Scales

Linking point spacing to mapping scale is a more difficult concept; mapping scale is invariant of the landscape whereas laser surveying is dependent on topography and land cover. No clear guidance exists on mapping scales and the equivalent point cloud resolution required. The table studies have highlighted the need to represent objects as scale dependent entities. Whilst this study has collected, insufficient evidence to relate meaningful scale information to scan resolutions it has highlighted the need for future work on this topic.

The uncertainty experiments using LiDAR data are important and valuable experiments revealing a lot about LiDAR data. Previously assumed knowledge regarding point cloud characteristics have been tested and found to require further investigation, the nature of laser scanning using repeated passes to gather higher point densities has been investigated and the positives and negatives of that approach reviewed. The results of the experiment have

far ranging implications beyond the academic scope of this experiment, regular and reliable point cloud spacing is necessary for many applications.

6.8 Implications for Forestry

The results strongly suggest a need for further investigation into LiDAR remote sensing for object detection and recognition. In this study, the targets were regularly shaped simple objects that contained none of the complexity and variability of a real forest canopy. Nevertheless, the results can be extrapolated back to forest structure by understanding the additional uncertainty that would be present. The results show large uncertainties in the precise characterisation of objects by laser scanning that requires further investigation. This is an area of future study that should feed into the general guidance and standards that the users of laser scanning community should be aware of.

6.8.1 Tree Counting

Tree counting has a natural synergy to the object detection experiment. The approaches to tree counting include finding distinct local maxima, for example the Friedlander & Koch (2000) study, this approach filtered the canopy height model for local peaks using these peaks as crown locations. A tree crown is a complex shape that has a permeability to light as the laser pulse can miss the tree and continue to return a ground shot. The inability to successfully recognise regular hard objects suggests that a greater proportion of harder to determine objects would be missed. Local maxima results will have error associated with irregular scan pattern and irregular LiDAR return, geostatisical methods potentially have a greater source of error. Tesfamichael (2009) used a trained semivariogram approach to identifying trees. The error in the ALS point cloud could potentially over train the semivariogram or produce a large nugget effect as a result of the measurement errors being significant compared to the measured objects.

6.8.2 Tree Heights

Tree height studies have already identified significant errors with derived datasets, Takeda (2004) noted errors of 20 m in the DTM in comparison to true ground height. Whilst the data used for the table study did not have errors of that magnitude, it is a much higher resolution. The literature for forest measurement regularly states that the correct data is required in order to produce reliable results. Vosselman (2000) showed this with respect to ground filtering, Lim et al (2003) repeated this call and extended the errors to include missing crowns and missing structural information. Several authors have suggested that higher point density data would improve the results, such authors include Persson (2002), and Yu (2004) who both had under represented tree heights that were suggested to be caused by the point cloud missing the crown of the tree. The use of point density is a useful metric but the results show that point density is a poor predictor of the likelihood of an object to be detected.

6.8.3 ALS and Forestry

Interesting approaches to suppressed tree identification such as the Maltamo *et al.*, (2005) study using height profiles of the LiDAR data show a similar technique to the violin plots used in section 5.8. The violin plots showed a different profile for the overlapping areas of the same feature taken at nearly the same time. Holmgren and Perrson's (2004) study into species identification uses a shape fitting approach to identification. Using the table scans as an analogue to the study, the importance of repeatable and reliable laser scanning for species detection become clear.

Forests grow and change over time; as such, multi-temporal studies are important for monitoring and managing forest environments. Change detection in the form of growth, structural change and changing management practices may be masked by false positives shown from unrepeatable laser scans or true change masked due to the detection of false-negative (true difference obscured due to inaccuracies in the surveyed data) type artefacts in the data.

As forest studies become increasingly complex, investigating structure, growth and other factors, the need to understand the underlying data is greater than ever. Results from a study will always have error associated with them, understanding the magnitude of this error makes the results useful for estimation purposes.

This chapter has discussed the results in light of the existing scientific literature. It is clear that laser scanning has evolved to meet the needs of a number of disparate disciplines and applications. Whilst each discipline collects, processes and analyses the data specific to their needs, there is a lack of thorough investigation into the small-scale mechanics and observation patterns present within a laser system that may have compelling impacts on the work as a whole. The following chapter will look at the conclusions of this study, investigate the impacts that this may have and look towards the future with recommendations of how the laser scanning community and the research community can further enhance the laser scanning body of knowledge.

7 Conclusions, Impact and Recommendations

7.1 Conclusions

This study has reached the following conclusions; these conclusions show the need for careful consideration when specifying, acquiring, processing and analysing aerial laser survey data.

- Significant objects are not always detected during scans with a resolution significantly higher than the object size
- Illumination intensity appears to be a strong control on the detection of an object.
- LiDAR datasets are sensitive to small changes in the along and across track spacing even when configured to the same flight and sensor parameters as the comparison flight lines.

- Current LiDAR collection does not use standard measures for point cloud descriptors, nor does it take into account the variability that is possible within the scan tracks

7.2 Impact of Uncertainty Study

The uncertainty study has wide-ranging implications, both for the technical aspects of laser scanning and object detection and the procedural and industrial concerns regarding the effective procurement and specification of point cloud data and subsequent mapping and processing standards. Many applications require repeatable and reliable survey techniques, the omission of substantial features (table-sized objects) raises concerns over the ability to detect features for a number of applications. A number of applications are discussed below.

7.2.1 Forestry

Forestry applications will be considered further with the tree study; these applications seek to map and model a structurally complex three-dimensional environment using aerial laser data. The study shows that LiDAR data struggles to model structurally simple objects reliably; as such, environments that are more complex will need to be further investigated.

7.2.2 Geomorphology

Geomorphological mapping using ALS data includes applications for glacial environments, hydrology and flood mapping and modelling as well as geological applications. Many geomorphic features are expressed as subtle perturbations in the landscape and may be linear sinuous features. Eroded features and small micro-topographic expressions may be missed because of laser scanning at a resolution previously believed to be adequate.

7.2.3 Archaeology

Archaeological applications for ALS fall into prospection and documentation studies. Prospection relies on exposing micro-topography and subtle features in the landscape. Barber (2007) provides advice on this application; the table study shows this advice needs reviewing in light of the findings of this study.

7.2.4 Engineering

Safety critical applications can arise from the use of ALS for engineering, notably power line engineering has pioneered the use of ALS for engineering studies; such applications include vegetation infringement studies, looking for locally clustered vegetation growth that can cause significant impacts to power line reliability. Other applications include power line sag modelling; this requires high-resolution models of power line conductors and insulators. These applications are clearly safety critical and a better understanding of the data is required to understand what is detected and omitted within these niche applications.

The applications above use ALS as a convenient, rapid and effective method of collecting data, whilst ALS does provide much of the data required to inform the research questions, further understanding the uncertainty of the data will enhance these applications and ensure suitable data is collected and ensure informed decisions are made.

7.3 Recommendations

There are several themes that run through the conclusions; these require both further academic research and engagement by the aerial laser scanning community.

The key areas for the focus of academic research are:

- Investigate the characteristics of laser footprint interactions in simple and complex environments in order to better determine the factors controlling reflection.
- Design and conduct an experiment that isolates the laser scanning system from its navigation components to investigate irregular point cloud spacing.
- Investigate the processes behind the lack of verifiability within laser point clouds

The laser scanning community should collaborate to build a standard way of working for the following:

- A common convention on the comparison of laser point clouds such that two point clouds can be described in a similar way. These should link to the mechanism of laser scanning. Point density and point spacing are ill thought out and poor descriptors of point cloud resolution
- Work towards a common mapping standard that directly relates the point cloud descriptors to minimum mapping unit, resolution and mapping scale.

These recommendations are based upon the investigation and analysis work conducted in this study, the study has considered data from two major LiDAR system manufacturers and looked at simplifying complex forestry problems into simple shape investigations.

8 Reference:

Aguiar, E. (2010)

http://the.honoluluadvertiser.com/article/2010/Apr/06/ln/hawaii4060354.html - accessed 05/05/2012

Aguilar, F. J., Mills, J. P., Delgado, J., Aguilar, M. A., Negreiros, J. G., & Pérez, J. L. (2010). Modelling vertical error in LiDAR-derived digital elevation models. *ISPRS Journal of Photogrammetry and Remote Sensing*, *65*(1), 103-110.

Amable, G. S., Devereux, B. J., Cockerell, T., and Renshaw, G. (2004). Analysis of interaction patterns between vegetation canopies and small footprint, high-density, airborne LiDAR. In *Proceedings of the 20th International Society for Photogrammetry and Remote Sensing Congress*, Istanbul, July 2004.

Anderson, K., Bennie, J., & Wetherelt, A. (2010). Laser scanning of fine scale pattern along a hydrological gradient in a peatland ecosystem. *Landscape ecology*, *25*(3), 477-492.

Axelsson, P. (1999) Processing of laser scanner data – algorithms and applications. *ISPRS Journal of Photogrammetry and Remote Sensing* 54 (2-3) 138 - 147

Baltsavias, E.P. (1999). Airborne laser scanning: Basic relations and formulas. ISPRS Journal of Photogrammetry and Remote Sensing. 54 199-214

Barber, D. (2007). 3D Laser Scanning for Heritage, Advice and Guidance to Users on Laser Scanning in Archaeology and Architecture. English Heritage Publishing.

Barclay HJ, Goodman D (2000) Conversion of total to projected leaf area index in conifers. *Canadian Journal of Botany* 78:447–454

Barrett, F, McRoberts, RE, Tomppo, E, Cienciala, E. and Waser, L.T. (2016) A questionnaire-based review of the operational use of remotely sensed data by national forest inventories. *Remote Sensing of Environment*, *174*: 279-289.

Boba, M., Ussyshkin, V., Slater, M., Sitar, M., and Szameitat, W. (2008). Impact of an optimized position and orientation system on the final accuracy of LiDAR data. *The International Archives of the Photogrammetry, Remote Sensing and Spatial Information Sciences,* 37, 241-245.

Bortolot, Z. J., and Wynne, R. H. (2005). Estimating forest biomass using small footprint LiDAR data: An individual tree-based approach that incorporates training data. *ISPRS Journal of Photogrammetry and Remote Sensing*, 59(6), 342-360.

Brandtberg, T. Warner, T.A., Landenberger, R.E. and McGraw, J.B. (2003) Detection and analysis of individual leaf-off tree crowns in small footprint, high sampling density lidar data from the eastern deciduous forest in North America. *Remote Sensing of Environment*. 85 290-294

Brokaw, N.V.L. and Lent, L.A. (1999) Vertical Structure. In Hunter, M.L. (ed) Maintaining Biodiversity in Forest Ecosystems. Cambridge University Press (379-399)

Butcher 2011 – LiDAR news article http://www.lidarnews.com/content/view/8611/)

Campbell, J. B. (2007). Introduction to remote sensing 4th edition. Guilford Press.

Challis, K. (2006). Airborne laser altimetry in alluviated landscapes. *Archaeological Prospection*, 13(2), 103-127.

Chase, A. F., Chase, D. Z., Weishampel, J. F., Drake, J. B., Shrestha, R. L., Slatton, K. C. and Carter, W. E. (2011). Airborne LiDAR, archaeology, and the ancient Maya landscape at Caracol, Belize. *Journal of Archaeological Science*,38 (2), 387-398.

Chasmer, L., Hopkinson, C., and Treitz, P. (2006) Investigating laser pulse penetration through a conifer canopy by integrating airborne and terrestrial lidar. *Canadian Journal of Remote Sensing,* 32 (2) 116-125

Chason, J. W., Baldocchi, D. D., & Huston, M. A. (1991). A comparison of direct and indirect methods for estimating forest canopy leaf area. *Agricultural and Forest Meteorology*, *57*(1), 107-128.

Chen, J., Ustin, S. L., Suchanek, T. H., Bond, B. J., Brosofske, K. D., & Falk, M. (2004). Net ecosystem exchanges of carbon, water, and energy in young and old-growth Douglas-fir forests. *Ecosystems*, *7*(5), 534-544.Chow, T. E., & Hodgson, M. E. (2009). Effects of lidar post-spacing and DEM resolution to mean slope estimation. *International Journal of Geographical Information Science*, *23*(10), 1277-1295.

Chu, H. J., Chen, R. A., Tseng, Y. H., & Wang, C. K. (2014). Identifying LiDAR sample uncertainty on terrain features from DEM simulation. *Geomorphology*, *204*, 325-333.

Coops, N. C., Hilker, T., Wulder, M. A., St-Onge, B., Newnham, G., Siggins, A., & Trofymow, J. T. (2007). Estimating canopy structure of Douglas-fir forest stands from discrete-return LiDAR. *Trees*, *21*(3), 295-310.

Devereux, B., Amable, G., Crow, P., and Cliff, A. (2005). The potential of airborne lidar for detection of archaeological features under woodland canopies. *Antiquity*, 79(305), 648-660

Donoghue, D. N., Watt, P. J., Cox, N. J., and Wilson, J. (2007). Remote sensing of species mixtures in conifer plantations using LiDAR height and intensity data. *Remote Sensing of Environment*, 110(4), 509-522.

Dubayah, R. O., and Drake, J. B. (2000). Lidar remote sensing for forestry. *Journal of Forestry*, 98(6), 44-46.

El-Shiemy, N. (2009) Georeferencing component of LiDAR systems. In Shan, J. and Toth, C.K. (2009) Topographic Laser Ranging and Scanning: Principles and Processing pp. 195-214 CRC Press

Exelisvis (2014) https://www.exelisvis.com/Portals/0/helparticles/IntroRS/landsat_band_placement.png page accessed 09/10/2014

Federal Office of Topography, Swisstopo (2012) http://www.swisstopo.admin.ch/internet/swisstopo/en/home/products/height.html - accessed 18/02/2013

Filin, S., and Pfeifer, N. (2006). Segmentation of airborne laser scanning data using a slope adaptive neighborhood. *ISPRS journal of Photogrammetry and Remote Sensing*, 60(2), 71-80.

Fisher, P. F., & Tate, N. J. (2006). Causes and consequences of error in digital elevation models. *Progress in Physical Geography*, *30*(4), 467-489.

Flood, M. (2002). Product definitions and guidelines for use in specifying lidar deliverables. *Photogrammetric engineering and remote sensing*, *68*(12).

Forestry Commission (2012) "Management of multifunctional forests (MULTIFOR)" accessed 09/01/2012

Franklin JF, Spies TA, Van Pelt R, Carey A, Thornburgh D, Burg DR, indenmayer D (2002) Disturbances and the structural development of natural forest ecosystems with some implications for silviculture. *Forest Ecology Management* 155:399–423

French, J. R. (2003). Airborne LiDAR in support of geomorphological and hydraulic modelling. *Earth surface processes and landforms*, *28*(3), 321-335.

Friedlaender, H. and Koch, B. (2000) First experience in the application of laser scanner data for the assessment of vertical and horizontal forest structures. *International Archives of Photogrammetry and Remote Sensing*. V XXXIII p 693

Gaveau, D. and Hill, R. (2003) Quantifying canopy height underestimation by laser pulse penetration in small footprint airborne laser scanning data. *Canadian Journal of Remote Sensing*, 29, 650-657

Gaulton, R., and Malthus, T. J. (2010). LiDAR mapping of canopy gaps in continuous cover forests: A comparison of canopy height model and point cloud based techniques. *International Journal of Remote Sensing*, 31(5), 1193-1211.

Gelhar, B. (2010) Benefits of a discrete return and full waveform airborne LiDAR system. European LiDAR Mapping Forum, The Hague, Holland. 1st December 2010

Goodwin, N.R., Coops, N.C., and Culvenor, D.S. (2006) Assessment of Forest Structure with airborne LiDAR and the effects of platform altitude. *Remote Sensing of Environment*. 103 (2) 140-152

Gower ST, Norman JM (1991) Rapid estimation of leaf area index in conifer and broad-leaf plantations. *Ecology* 72:1896–1900

Hall, S. A., Burke, I. C., Box, D. O., Kaufmann, M. R., & Stoker, J. M. (2005). Estimating stand structure using discrete-return lidar: an example from low density, fire prone ponderosa pine forests. *Forest Ecology and Management*, *208*(1), 189-209.

Harding, D. J., Lefsky, M.A., Parke, C.G., and Blair, J.B. (2001) Laser altimeter canopy height profiles. Methods and Validation for closed canopy, broadleaf forests. *Remote Sensing of the Environment*. 76 (3) 283 -297

Harding, D. (2009) Pulsed laser altimeter ranging techniques and implications for terrain mapping. In Shan, J. and Toth, C.K. (2009) Topographic Laser Ranging and Scanning: Principles and Processing pp. 173 - 194 CRC Press

Hardy, A. J., Barr, S. L., Mills, J. P., & Miller, P. E. (2012). Characterising soil moisture in transport corridor environments using airborne LIDAR and CASI data. *Hydrological Processes*, *26*(13), 1925-1936.

Hill, R. A., and Broughton, R. K. (2009). Mapping the understorey of deciduous woodland from leaf-on and leaf-off airborne LiDAR data: A case study in lowland Britain. *ISPRS Journal of Photogrammetry and Remote Sensing*, 64(2), 223-233.

Hodgson, M. E., Jensen, J., Raber, G., Tullis, J., Davis, B. A., Thompson, G., & Schuckman, K. (2005). An evaluation of lidar-derived elevation and terrain slope in leaf-off conditions. *Photogrammetric Engineering & Remote Sensing*, *71*(7), 817-823.

Höfle, B., and Pfeifer, N. (2007). Correction of laser scanning intensity data: Data and model-driven approaches. *ISPRS Journal of Photogrammetry and Remote Sensing*, 62(6), 415-433.

Hofton, M. A., Rocchio, L., Blair, J.B., and Dubayah, R. (2002) Validation of vegetation canopy LiDAR sub-canopy topography measurements for a dense tropical forest. *Journal of Geodynamics*, 34 (3-4) 491-502

Holmgren, J. And Perrson, A. (2004) Identifying species of individual trees using airborne laser scanning*, Remote Sensing of Environment* 90 415-423

Hyyppa, J., Hyyppa, H.,Yu, X., Kaartinen, H., Kukko, A., and Holopainen, M., (2009) Forest Inventory using Small-Footprint Airborne LiDAR. . In Shan,J. and Toth, C.K. (2009) Topographic Laser Ranging and Scanning: Principles and Processing pp.335-370 CRC Press

Ishii, H. T., Tanabe, S. I., and Hiura, T. (2004). Exploring the relationships among canopy structure, stand productivity, and biodiversity of temperate forest ecosystems. *Forest Science*, 50(3), 342-355.

JNCC and Defra (on behalf of the Four Countries' Biodiversity Group). 2012. UK Post-2010 July 2012.available from http://jncc.defra.gov.uk/pdf/UK_Post2010_Bio-Fwork.pdf. accessed 23/01/2013

Kaasalainen, S., Kaasalainen, M., Mielonen, T., Suomalainen, J., Peltoniemi, J. I., and Naranen, J. (2006). Optical properties of snow in backscatter. *Journal of Glaciology*, 52(179), 574-584.

Kaasalainen, S., and Rautiainen, M. (2005). Hot spot reflectance signatures of common boreal lichens. *Journal of geophysical research*, 110(D20), D20102.

Kalogirou, V. (2006) Simulations of Discrete-return LiDAR signal from conifer stands for forestry applications. MSc thesis (University of London MSc in Remote Sensing), University College London.

Kim, S., McGaughey, R. J., Andersen, H. E., & Schreuder, G. (2009). Tree species differentiation using intensity data derived from leaf-on and leaf-off airborne laser scanner data. *Remote Sensing of Environment*, *113*(8), 1575-1586.

Knight, D. T. (1996). Rapid development of tightly-coupled GPS/INS systems. In Position Location and Navigation Symposium, 1996., IEEE 1996(pp. 300-305). IEEE.

Kobler, A. Pfeifer, N., Ogrinc, P. Todorovski, L. Ostir, K. And Dzeroski, S. (2007) Repetitive interpolation: A robust algorithm for DTM generation from Aerial Laser Scanner data in forested terrain. *Remote Sensing of Environment* 108 9-23

Landy, J (2011) Sub-canopy terrain modelling for archaeological prospecting in forested areas through multiple-echo discrete-pulse laser ranging: a case study from Chopwell Wood, Tyne & Wear, Durham. Msc Thesis Durham university.

Lefsky, M., Cohen, W. Acker, S., Parker, G. Spies, T. and Harding, D. (1999) LiDAR remote sensing of canopy structure and biophysical properties if Douglas-fir, western hemlock forests. *Remote Sensing of Environment*, 70 339-361

Liang, X., Hyyppä, J., and Matikainen, L. (2007). Deciduous-coniferous tree classification using difference between first and last pulse laser signatures.International Archives of Photogrammetry, *Remote Sensing and Spatial Information Sciences*, 36(3/W52).

Lillesand, T. M., Kiefer, R. W., & Chipman, J. W. (2007). *Remote sensing and image interpretation* (No. Ed. 6). John Wiley & Sons Ltd.

Lim, K. Treitz, P. Wulder, M., St-Onge, B. and Flood, M. (2003) LiDAR remote sensing of forest structure. *Progress in Physical Geography* 27 (1) 88-106

Luscombe, D. J., Anderson, K., Gatis, N., Wetherelt, A., Grand-Clement, E., & Brazier, R. E. (2014). What does airborne LiDAR really measure in upland ecosystems?. *Ecohydrology*.

MacKinnon A (2003) West-coast temperate old-growth forests. Forest Chronicles 79:475–484

Maltamo, M., Packalen, P., Yu, X., Eerikainen, K., Hyyppa, J., and Pitkanen, J., (2005) Identifying and quantifying structural characteristics of heterogenous boreal forests using laser scanner data. *Forest Ecology and Management* 216 41-50

Means, J., Acker, S., Harding, D., Blair, J. Lefsky, M. Cohen, W., Harmon, M., and McKee, A. (1999) use of large footprint scanning airborne lidar to estimate forest stand characteristics in the western cascades, Oregon. *Remote Sensing of Environment*. 67 298-308

Michez, A., Piégay, H., Toromanoff, F., Brogna, D., Bonnet, S., Lejeune, P., & Claessens, H. (2013). LiDAR derived ecological integrity indicators for riparian zones: Application to the Houille river in Southern Belgium/Northern France. *Ecological Indicators*, *34*, 627-640.

Moafipoor, S., Grejner-Brzezinska, D. A., and Toth, C. K. (2004). Tightly coupled GPS/INS integration based on GPS carrier phase velocity update. In ION NTM January 2004 San Diego, CA.

Moffiet, T., Mengerssen, K., Witte, C., King, R., and Denham, R. (2005) Airborne laser scanning: Exploratory data analysis indicates potential variables for the classification of individual trees or forest stands according to species. *ISPRS Journal of photogrammetry and Remote Sensing*. 59 289-309

Morsdorf, F., Meier, E., Kötz, B., Itten, K. I., Dobbertin, M., and Allgöwer, B. (2004). LIDAR-based geometric reconstruction of boreal type forest stands at single tree level for forest and wildland fire management. *Remote Sensing of Environment*, 92(3), 353-362.

Naesset, E. (1997) Determination of mean tree height of forest stands using airborne laser scanner data. *ISPRS journal of Photogrammetry and Remote Sensing*. 52 49-56

Naesset, E. (2002) predicting forest stand characteristics with airborne scanning laser using a practical two-stage procedure and field data. *Remote Sensing of Environment*. 80 80-89

Naesset, E. (2004) Effects of different flying altitudes on biophysical stand properties estimated from canopy height and density measured with a small footprint airborne scanning laser. *Remote Sensing of Environment*. 91 (2) 243 – 255

Næsset, E., and Økland, T. (2002). Estimating tree height and tree crown properties using airborne scanning laser in a boreal nature reserve. *Remote Sensing of Environment*, 79(1), 105-115.

Neal J, Bates P.D., Fewtrell T, Hunter N, Wilson MD, Horritt MS (2009) Distributed whole city water level measurements from the Carlisle 2005 urban flood event and comparison with hydraulic model simulations, *Journal of Hydrology*, 368, 42-55

Neal, J., Schumann, G., Fewtrell, T., Budimir, M., Bates, P. and Mason, D. (2011), Evaluating a new LISFLOOD-FP formulation with data from the summer 2007 floods in Tewkesbury, UK. *Journal of Flood Risk Management*, 4: 88–95

Nelson, R., Krabill, W., and MacLean, G. (1984). Determining forest canopy characteristics using airborne laser data. *Remote Sensing of Environment*,15(3), 201-212.

Nelson, R. Krabill, W. and Tonelli, J. (1988) Estimating forest biomass and volume using airborne laser data. *Remote Sensing of Environment*. 15 201-212

Optech Incorporated (2004) ALTM 3100 Hardware Training Manual Level 1.

Optech Incorporated (2006) Airborne Laser Terrain Mapper ALTM3100 EA Operations Manual. P5

Ørka, H. O., Næsset, E., and Bollandsås, O. M. (2009). Classifying species of individual trees by intensity and structure features derived from airborne laser scanner data. *Remote Sensing of Environment*, 113(6), 1163-1174.

Parker GG, HarmonME, LefskyMA, Chen JQ, Van Pelt R,Weis SB, Thomas SC, Winner WE, Shaw DC, Franklin JF (2004) Three-dimensional structure of an old-growth Pseudotsuga-Tsuga canopy and its implications for radiation balance microclimate and gas exchange. *Ecosystems* 7:440–453

Persson, A. Holmgren, J. and Soderman, U. (2002) Detecting and measuring individual trees using an airborne laser scanner. *Photogrammetric Engineering and Remote Sensing*. 68 (9) 925-932

Persson, Å., Holmgren, J., and Söderman, U. (2006, February). Identification of tree species of individual trees by combining very high-resolution laser data with multi-spectral images. In *Proceedings of International Workshop 3D Remote Sensing in Forestry*, Vienna, February (pp. 91-96).

Petrie, G. and Toth, C.K. (2009) Airborne and Spaceborne Laser Profilers and Scanners In Shan, J. and Toth, C.K. (2009) Topographic Laser Ranging and Scanning: Principles and Processing pp. 44-48 CRC Press

Pfeifer, N. and Mandlburger, G. (2009) LiDAR data filtering and DTM generation. . In Shan,J. and Toth, C.K. (2009) Topographic Laser Ranging and Scanning: Principles and Processing pp. 307-334 CRC Press

Pitkänen, J., Maltamo, M., Hyyppä, J., and Yu, X. (2004). Adaptive methods for individual tree detection on airborne laser based canopy height model.International *Archives of Photogrammetry, Remote Sensing and Spatial Information Sciences*, 36(8), 187-191.

Pouliot, D.A., King, D.J., Bell, F.W., and Pitt, D.G. (2002) Automated tree crown detection and delineation in high resolution digital camera imagery of coniferous forest regeneration. *Remote Sensing of Environment* 82 322-334

Raber, G. T., Jensen, J. R., Hodgson, M. E., Tullis, J. A., Davis, B. A., & Berglund, J. (2007). Impact of LiDAR nominal post-spacing on DEM accuracy and flood zone delineation. *Photogrammetric engineering & remote sensing*, *73*(7), 793-804.

Reitberger, J., Krzystek, P., and Heurich, M. (2006) full-waveform analysis of small-footprint airborne laser scanning data in the Bavarian forest national park for tree species classification. *International Workshop 3D Remote Sensing in Forestry Proceedings*. Vienna, February 14-15 2006, pp, 218-227

Ritchie, J.C., Evans, D.L., Jacobs, D., Everitt, J.H., and Weltz, M.A. (1993) Measuring canopy structure with an airborne laser altimeter. Transactions of ASAE 36 1235-1238

Rhoads, A. G., Hamburg, S. P., Fahey, T. J., Siccama, T. G., & Kobe, R. (2004). Comparing direct and indirect methods of assessing canopy structure in a northern hardwood forest. *Canadian Journal of Forest Research*, *34*(3), 584-591.

Roe, G. (2010) LiDAR being used in Haiti Relief Effort. http://blog.lidarnews.com/lidar-being-used-in-haiti-relief-effort. accessed 23/01/2010

Scherzinger, B. and Hutton, J. (2006) Applanix In-Fusion Technology Explained. White paper accessed http://www.applanix.com/media/downloads/articles_papers/Applanix%20IN-Fusion.pdf 20/8/12

Scherzinger, B. M., and Woolven, S. (1996, September). POS/MV-handling GPS outages with tightly coupled inertial/GPS integration. In OCEANS'96. MTS/IEEE. *Prospects for the 21st Century. Conference Proceedings* (Vol. 1, pp. 422-428). IEEE

Schreier, H., Lougheed, J., Tucker, C., and Leckie, D. (1985). Automated measurements of terrain reflection and height variations using an airborne infrared laser system. *International Journal of Remote Sensing*, 6(1), 101-113.

Schwarz K. P., Chapman, M. A., Cannon, M. W., and Gong, P. (1993). An integrated INS/GPS approach to the georeferencing of remotely sensed data. *Photogrammetric engineering and remote sensing*, 59(11), 1667-1674.

Sithole, G. And Vosselman, G. (2004) Experimental comparison of filter algorithms for bare-earth extraction from airborne laser scanning point clouds. *ISPRS Journal of photogrammetry and Remote Sensing* 59 (1) 85-101

Stilla, U. And Jutzi, B. (2009) Waveform analysis fir small-footprint pulsed laser systems. In Shan,J. And Toth, C.K. (2009) Topographic Laser Ranging and Scanning: Principles and Processing pp.215-234 CRC Press

Suratno, A., Seielstad, C., and Queen, L. (2009). Tree species identification in mixed coniferous forest using airborne laser scanning. *ISPRS Journal of Photogrammetry and Remote Sensing*, 64(6), 683-693.

Takeda, H. (2004) Ground surface estimation in dense forest. *The International Archives of Photogrammetry, Remote Sensing and Spatial information Sciences 35 Part b3* 1016-1023

Tesfamichael, S.G., Ahmed, F., Van Aardt, J.A.N., and Blakeway, F. (2009) A semi-variogram approach for estimating stems per hectare in Eucalyptus grandis plantations using discrete-return lidar height data. *Journal of Forest Ecology and Management.* 258 1188-1199

Trimble (2007) The first global satellite navigation system. Pp151

Ussyshkin, R. V., and Smith, B. (2006). Performance analysis of ALTM 3100EA: Instrument specifications and accuracy of lidar data. *In ISPRS Commission I Symposium, Paris; Proceedings, part B*

Ussyshkin, V., Boba, M., and Sitar, M. (2008). Performance Characterization of an Airborne Lidar System: Bridging System Specifications and Expected Performance. *The International Archives of the Photogrammetry, Remote Sensing and Spatial Information Sciences*, 37.

Ussyshkin, R. V., and Smith, R. B. (2007, May). A new approach for assessing lidar data accuracy for corridor mapping applications. In *Conference Proceedings, the 5th International Symposium on Mobile Mapping Technology.*

Usshykin, R.V., Ravi, R., Ilnicki, M., and Pokorny, M. (2009) Mitigating the impact of the laser footprint size on airborne LiDAR data accuracy. ASPRS 2009 annual conference Baltimore, Maryland. March 2009

Ussyshkin V, Theriault L. (2011) Airborne Lidar: Advances in Discrete Return Technology for 3D Vegetation Mapping. Remote Sensing. 3(3):416-434.

Ussyshkin, R. V., Theriault, L., Sitar, M., and Kou, T. (2011). Advantages of Airborne Lidar Technology in Power Line Asset Management. In *Multi-Platform/Multi-Sensor Remote Sensing and Mapping (M2RSM), 2011 International Workshop* on (pp. 1-5). IEEE.

Van Pelt, R., & Nadkarni, N. M. (2004). Horizontal and vertical distribution of canopy structural elements of Pseudotsuga menziesii forests in the Pacific Northwest. *Forest Science*, *50*, 326-341.

Villikka, M., Maltamo, M., Packalén, P., Vehmas, M., and Hyyppä, J. (2007). Alternatives for predicting tree-level stem volume of Norway spruce using airborne laser scanner data. *The photogrammetric journal of Finland*, 20(2), 33-42.

Vosselman, G. (2000) Slope based filtering of laser altimetry data. *International Archives of Photogrammetry and Remote Sensing* 33 (b3/2) 935-942

Wagner, W., Ullrich, A., Melzer, T., Briese, C., and Kraus, K. (2004) From single pulse to full waveform airborne laser scanners: Potential and Practical Challenges. In International Archives of Photogrammetry, *Remote Sensing and spatial information sciences* (2004) 35 part B3, 201-206

Wagner, W., Ullrich, A., Ducic, V., Melzer, T., and Studnicka, N. (2006) Gaussian decomposition and calibration of a novel small-footprint full-waveform digitising airborne laser scanner. *ISPRS Journal of Photogrammetry and Remote Sensing*. 60 100-112

Wehr, A. (2009) LiDAR systems and calibration. In Shan, J. and Toth, C.K (eds). (2009) Topographic Laser Ranging and Scanning: Principles and Processing pp. 129 – 172 CRC Press

Wehr, A. and Lohr, U. (1999) Airborne laser scanning – an introduction and overview. *ISPRS Journal of Photogrammetry and Remote Sensing*. 54 68-82

Wikipedia (2013) http://en.wikipedia.org/wiki/National_LIDAR_Dataset - accessed 25/01/12

Yu, X., Hyyppa, J. Kaartinen, H., and Maltamo, M. (2004) Automatic detection of harvested trees and determination of forest growth using airborne laser scanning. *Remote Sensing of Environment*. 90 451-462

Zimble, D. A., Evans, D.L., Carlson, G.C., Parker, R.C., Grado, S.C., and Gerard, P.D. (2003) Characterizing vertical forest structure using small footprint airborne LiDAR. *Remote Sensing of Environment* 87 (2-3) 171-182